EPITHELIAL EXPRESSED B7-H4 DRIVES DIFFERENTIAL IMMUNOTHERAPY RESPONSE IN MURINE AND HUMAN BREAST CANCER

By

Elizabeth C. Wescott

Dissertation
Submitted to the Faculty of the
Graduate School of Vanderbilt University
in partial fulfillment of the requirements
for the degree of

DOCTOR OF PHILOSOPHY
in
Molecular Pathology and Immunology
August 9, 2024
Nashville, Tennessee

Approved:

Ann Richmond, Ph.D. (Chair)

Justin M. Balko, Pharm.D., Ph.D. (Advisor)

Mary Philip, M.D., Ph.D.

Vivian Weiss, M.D., Ph.D.

John Wilson, Ph.D.

Dedication

To my two daughters, you can do anything you set your mind to

and

To my husband, you have sacrificed to support my goal.

Acknowledgements

I have been so blessed during my time at Vanderbilt by an incredibly collaborative and supportive research environment. Dr. Justin Balko has been a wonderful mentor who has worked with me to identify my strengths and overcome my weaknesses. Dr. Susan Opalenik has been the best help with my many experimental and technical questions during the 5+ years I've sat across from her in main lab. Dr. Ann Hanna has shared her macrophage and tumor-immune study experience and greatly improved my experimental designs and hypotheses. My fellow former and current graduate student lab-mates – Dr. Margaret Axelrod, Dr. Brandie Taylor, Xiaopeng Sun, Julia Steele, Jacey Marshall, and Reilly Fankhauser – have always provided a sounding board and offered to help during mouse sac days. Dr. Axelrod in particular was an amazing welcome to me into the lab as my rotation mentor and helped me figure out how to work with T cells. Finally, Dr. Catherine Fahey and Dr. Erica Carballo have been wonderful colleagues and shared their medical knowledge with me.

I've been blessed to have two junior students to mentor and work with – Juliana Bronzini and Annie Murray – both of whom have helped tremendously in performing experiments and giving me valuable experience as a mentor and teacher. They have informed my desire to pursue teaching more formally as a possible career option.

To my friends who I've met through the IGP – Dr. Jennifer Shuman, Dr. Gabriella Robertson, Dr. Katie Robertson, and Kathryn Butcher – thank you for coming to my seminars, sharing your science knowledge in other disciplines, and becoming great friends even outside Vanderbilt. The collaborative community at Vanderbilt – professors, staff, and other colleagues – has continued to support one of my main reasons for choosing to come to Vanderbilt for my graduate studies.

My community outside of Vanderbilt has been the reason I kept up with my PhD studies even after going through a pandemic and becoming a parent. My church community has been a

solid source of prayer and community, especially in motherhood. My parents have always pushed me to succeed, teaching me to love science from a young age, giving me a plethora of opportunities to cultivate that love as I grew up in high school, and supporting me through a fabulous education at Davidson College. My mom in particular got her own advanced degree – Juris Doctor – during my time at Vanderbilt and motivated me to persevere through the most difficult parts of graduate school.

Finally, to my husband, Evan, who moved to Nashville after I started at Vanderbilt to marry me and start our life here together, I would never have been able to finish my studies without you. You have sacrificed for my schedule and my experience and for our daughters more times than I can even count. This PhD has been a team effort and I'm so proud to have you by my side as I complete it.

Table of Contents

LIST OF FIGURES

Chapter I: INTRODUCTION

Breast cancer subtypes and standards of care

Breast cancer (BC) is the leading cause of new cancer cases among women and the second leading cause of cancer related deaths in women[1]. It is a heterogeneous disease that can be classified into several subtypes based on the molecular profiling of the tumor cells. Breast cancer treatment and outcome largely depends on tumor subtype. BC can be divided into two histological or four molecular subtypes based on whether the cancer cells are invasive and the expression or lack thereof of specific hormone receptors and proteins, respectively. About 25% of breast cancers are preinvasive and classified as ductal carcinoma in situ (DCIS – about 80%) or lobular carcinoma in situ (LCIS – about 20%) depending on whether the cells are found in the milk ducts or lobular units (**Figure 1.1**). The remaining 75% of breast cancers are invasive ductal carcinoma (IDC) or invasive lobular carcinoma (ILC) with IDC making up the majority of invasive BC.

Invasive BC is further classified to molecular subtypes. These subtypes have different biological features and clinical behaviors, which have significant implications for diagnosis, treatment, and prognosis. Broadly, BC can be divided into luminal and basal categories based on the expression of epithelial and mesenchymal markers and additional cellular markers. BC can also be divided into three common breast cancer subtypes including hormone receptor-positive (HR+), HER2-amplified (HER2+), and triple-negative breast cancer (TNBC) (**Figure 1.1**).

Hormone receptor-positive breast cancer, also known as estrogen receptor-positive (ER+) and/or progesterone receptor-positive (PR+), is the most common subtype, accounting for approximately 70% of all breast cancer cases[2]. These cancers are also referred to as luminal breast cancer and can be further divided into luminal A and luminal B subtypes.

Luminal breast cancer is characterized by the expression of luminal/epithelial markers, such as cytokeratin 8 (CK8) and cytokeratin 18 (CK18), and have a well-differentiated morphology, with cells arranged in a glandular pattern[3]. These tumors express high levels of ER and/or PR, which promote cell growth and proliferation in response to estrogen and progesterone. ER+ breast cancers (Luminal A) are usually slow-growing and have a favorable prognosis, as they are responsive to hormonal therapies such as tamoxifen and aromatase inhibitors (**Figure 1.2**). However, Luminal B cancers that express PR are characterized by a high proliferative rate and poorer prognosis[3]. Luminal breast cancers are associated with mutations or alterations in genes involving estrogen signaling, such as ER and GATA3[4].

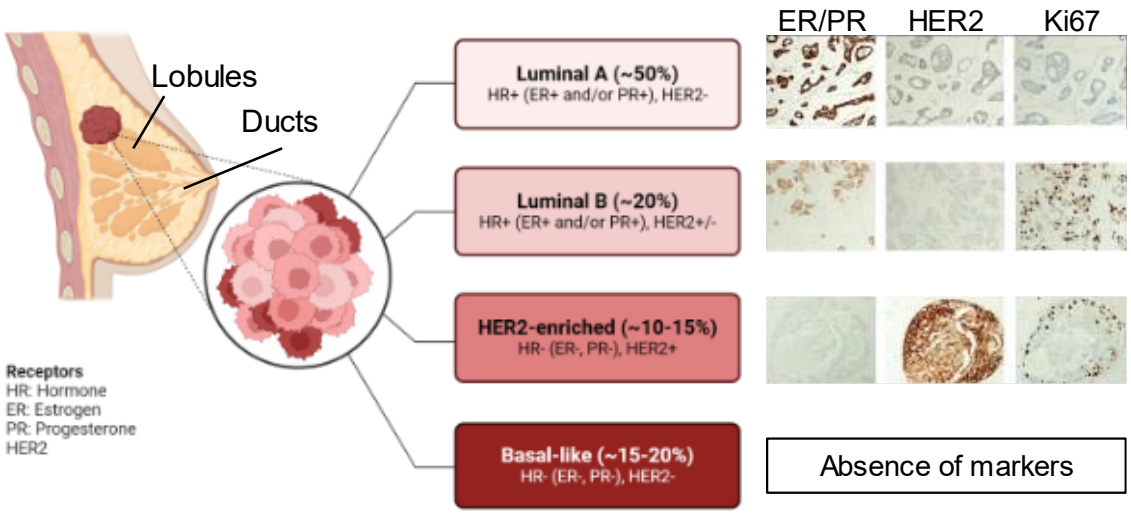

Figure I.1. **Breast cancer histological and molecular subtypes.** Figure adapted from Sarvari *et al.* 2022 and Lee *et al.* 2020. Figure made using Biorender.com[5,6].

HER2-amplified (HER2+) breast cancer is characterized by the overexpression or amplification of the HER2 gene, which encodes a cell surface receptor that promotes cell growth and survival. HER2+ tumors account for approximately 15-20% of all breast cancer cases[7]. These tumors are often aggressive and have a poor prognosis, as they are resistant to hormonal therapies. However, the development of targeted therapies such as trastuzumab and pertuzumab has significantly improved outcomes for HER2+ breast cancer patients.

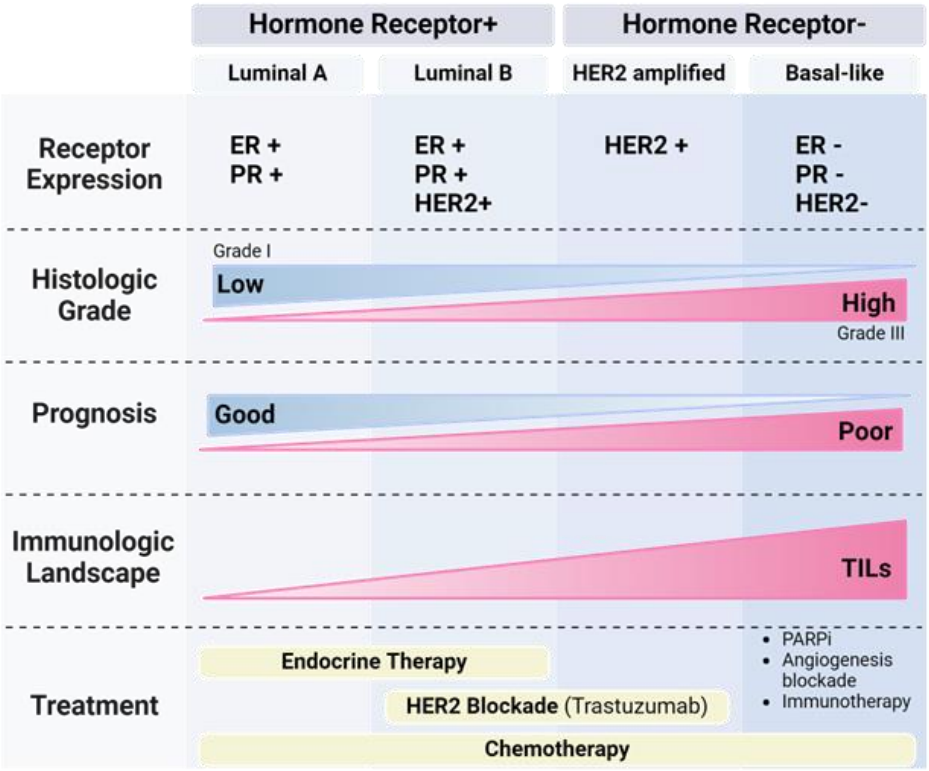

Figure I.2. **Breast cancer treatment and prognosis is informed by hormone receptor status.** ER-, PR-, and HER2- BC is called triple-negative breast cancer (TNBC) and lacks specific targeted therapies. Figure made using Biorender.com.

Triple-negative breast cancer (also referred to as basal-like breast cancer) is a subtype that lacks expression of ER and PR, and lacks HER2 amplification and activating mutations, accounting for approximately 10-15% of all breast cancer cases[8]. TNBC tumors are highly heterogeneous, are characterized by the expression of basal cell markers such as cytokeratin 5 (CK5), cytokeratin 17 (CK17), and epidermal growth factor receptor (EGFR), and can be further classified into different molecular subtypes based on gene expression profiling[8,9]. Basal tumors also exhibit high expression of mesenchymal markers, such as vimentin and N-cadherin[10]. TNBC is often aggressive, with a higher risk of recurrence and metastasis, and a poorer prognosis compared to other subtypes[9]. TNBC patients do not benefit from hormonal or targeted therapies, and chemotherapy remains the mainstay of treatment. These tumors are

typically more immunogenic, and as such have been a focus of experimental immunotherapies (**Figure 1.2**).

The formation of these breast cancer subtypes is a complex process involving multiple genetic and epigenetic alterations. For example, the development of ER+ breast cancer is associated with mutations or alterations in the genes encoding ER and/or PR, as well as other genes involved in estrogen signaling pathways[11]. Similarly, HER2+ breast cancer is associated with amplification of the HER2 gene, as well as mutations or alterations in other genes involved in HER2 signaling pathways[12]. In contrast, TNBC is associated with mutations or alterations in genes involved in DNA repair pathways, cell cycle regulation, and other cellular processes including mutations to the BRCA1/2 genes[4,13].

Genetic mutations, like those in BRCA1/2, have been identified as one of the major causes of breast cancer. Mutations in these genes can lead to a loss of protein function, which can increase the risk of breast and ovarian cancer. It is estimated that women with a BRCA1 or BRCA2 mutation have a 60-85% lifetime risk of developing breast cancer, compared to a 12% risk in the general population[14]. In addition, mutations in other genes, such as TP53, PTEN, and PALB2, have also been linked to an increased risk of breast cancer[15]. TP53 is a tumor suppressor gene that helps to prevent the development of cancer by regulating cell growth and division. Mutations in TP53 can lead to a loss of this regulatory function, increasing the risk of breast and other types of cancer. TP53 mutations are relatively rare in the general population but are more common in individuals with a family history of breast cancer[16].

PTEN is another tumor suppressor gene that helps to prevent the development of cancer by regulating cell growth and division. Mutations in PTEN can also lead to an increased risk of breast cancer, as well as other types of cancer such as endometrial and thyroid cancer[16]. PALB2 is a gene that helps to repair DNA damage in cells. Mutations in PALB2 can lead to an increased risk of breast cancer, as well as an increased risk of ovarian and pancreatic cancer[16].

The molecular subtype of BC and/or the genetic mutation status can both determine treatment strategy. Immune infiltration can also be a prognostic marker, particularly for novel therapeutic combinations of chemotherapy and immunotherapies (as in TNBC), which will be discussed further below.

The tumor-immune microenvironment (TIME)

Cancer cells and tumor cells are constantly interfacing so as to overcome the other. The cancer immunity cycle begins when cancer cells die and release antigens (**Figure 1.3**). This is often initiated through chemotherapy. Antigen presenting cells (APCs) such as dendritic cells pick up antigens released by dying cancer cells and bring them to the lymph nodes to present to T cells. When they are activated, the T cells traffic back to the tumor as cytotoxic T lymphocytes that are clonally expanded to the cancer antigens. Once the T cells recognize the cancer cells through MHC, they kill the cancer cells through cytokine release, granzymes, and recruiting additional immune cells such as proinflammatory macrophages.

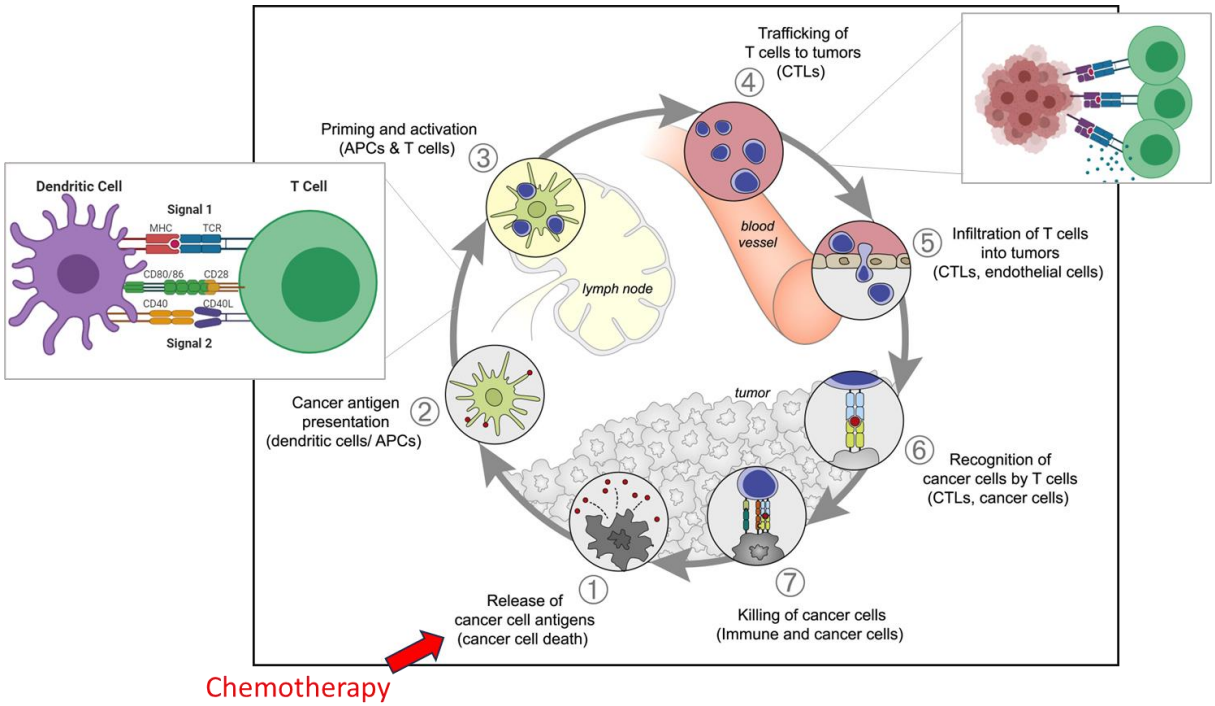

Figure I.3. **The cancer immunity cycle**. Figure adapted from Chen and Mellman, 2013[17].

The tumor microenvironment (TME) is a complex network of cells and extracellular matrix consisting of fibroblasts, immune cells, endothelial cells, and other stromal components. The tumor-immune microenvironment (TIME) is a subset of the TME that includes immune cells and their interactions with tumor cells. In breast cancer, the TIME can promote or inhibit cancer progression. Tumor infiltrating lymphocytes (TILs) have been shown to be a prognostic factor in breast cancer, in which higher levels of TILs are associated with better outcomes[18–21]. These TILs can include CD4+ T cells, CD8+ cytotoxic T cells, B cells, and myeloid cells that initiate antitumor immunity. However, the TIME can also contain pro-tumor immune cells such as regulatory T cells (Tregs) and myeloid-derived suppressor cells (MDSCs).

Differences in the TIME between BC subtypes

Breast cancer subtypes have variation in the amount of immune infiltration. HR+ cancers, which are the most common, tend to have low levels of immune infiltration. HER2+ breast cancer tends to have higher levels of TILs compared to HR+ cancers and thus may be more responsive to immunotherapies. TNBC is characterized by typically high levels of immune infiltration and expression of checkpoint molecules, like PD-L1. However, in some of these tumors, the TIME is immunosuppressive, with high levels of MDSCs and Tregs. Figure 1.2 summarizes the increasing abundance of TILs from HR+ cancers to TNBC. In all three subtypes of BC, immune abundance was a prognostic factor for neoadjuvant chemotherapy, and was associated with survival in HER2+ and TNBC[18]. The degree of TIL infiltration has been hypothesized to reflect the level of tumor mutation burden (TMB), which is higher in TNBC and HER2+ cancers[22].

In additional to TILs, PD-L1 expression can be used as a prognostic marker in some BCs. As PD-L1 expression is often influenced by the abundance of TILs, testing for both is underway in some cases[22–24]. Immune abundance and/or PD-L1 expression in the TIME has strong influence on the success of immunotherapies. As TNBC lacks therapeutic targets, has

unmet clinical need, and tends to have higher levels of TILs in some cases, so it has been the focus of immunotherapies[25].

An introduction to immune checkpoint ligands

Immune checkpoint inhibitors (ICI), including anti-PD-1/anti-PD-L1 monoclonal antibodies, have become a staple in the clinical treatment of many cancer types[26]. The immune system is highly regulated to promote protective responses against pathogens and cancer, while also inhibiting adverse inflammation and autoimmunity. Effector lymphocytes of the immune system therefore express immunosuppressive proteins, such as CTLA-4 and PD-1, that bind to their respective ligands, CD80/86 and PD-L1 to inhibit exacerbated inflammation. Cancer cells and other cells in the tumor microenvironment can express T cell co-inhibitory molecules of the B7 family, like PD-L1, to evade or suppress adaptive immunity. Together, these proteins work to downregulate inflammation and induce an immunosuppressive environment in tumors[27–30].

Many types of immune cells infiltrate tumors, including T cells and myeloid cells, to induce a proinflammatory, anti-tumor response. However, tumor cells or other microenvironmental cells expressing PD-L1 or other co-inhibitory ligands, can engage infiltrating T cells and suppress T cell activation[28,30]. Therefore, infiltrating lymphocytes in PD-L1$^+$ tumors are likely unable to eradicate the tumor. Currently approved ICIs target the immune system by preventing inhibitory interactions between these suppressive cells and infiltrating lymphocytes, to reinvigorate a proinflammatory response[30,31].

ICI has seen broad success in several cancer types, including breast cancer[32,33]. Breast cancer remains one of the leading causes of new cancer diagnoses and cancer-related deaths[34]. Furthermore, triple negative breast cancer (TNBC) is one of the more difficult subtypes to treat and as such is a candidate for novel cancer therapies, like immunotherapy[35]. TNBC patients have been the focus of immunotherapy treatment due to abundant tumor infiltrating immune cells, high tumor mutation burden, and their lack of target-specific therapies compared

to other breast cancer subtypes. Many patients have had favorable outcomes with anti-PD-1/anti-PD-L1 modalities[32,36–42]. As such, pembrolizumab is now approved in combination with neoadjuvant chemotherapy (NAC) in early-stage, high-risk TNBC regardless of PD-L1 status, and in combination with chemotherapy patients with metastatic PD-L1+ TNBC tumors[32,37,41,43–46]. However, a gap in knowledge persists in predicting those patients most likely to respond to ICI therapy.

There are very few usable clinical biomarkers to identify responders versus non-responders. For example, many breast cancer cells or infiltrating immune cells do not express PD-L1, and those that do still fail to respond to PD-1/PD-L1-targeted ICI. Since immune evasion is a hallmark of cancer, this suggests the action of alternative inhibitory pathways in many breast cancers and the potential to identify additional tumor biomarkers to predict response to ICI[47]. One potential mechanism of resistance is the presence of additional immune checkpoint ligands that may override the PD-1/L1 pathway.

The role of alternate immune checkpoint ligands in breast cancer

In additional to PD-L1, alternative immune checkpoint ligands, including B7-H3, B7-H4, and B7-H4/VISTA, have emerged as important players in breast cancer by suppressing antitumor immune responses. Like other members of the B7 family, these ligands are transmembrane proteins that bind to cognate receptors. B7-H3 is expressed on various cells, including tumor cells and immune cells, and its overexpression has been associated with poor prognosis and resistance to chemotherapy in breast cancer[48,49]. B7-H4 is expressed in breast cancer cells (among other cancer types) and tumor-infiltrating immune cells and has been shown to inhibit T cell responses and promote tumor growth and metastasis[50–53]. B7-H5 is a immune checkpoint molecule that is expressed on immune cells and can suppress T cell responses in breast cancer[54,55].

The expression of alternate immune checkpoint ligands in breast cancer is regulated by various signaling pathways, including the PI3K/AKT/mTOR and NF-κB pathways. These

pathways are frequently dysregulated in breast cancer, leading to the upregulation of alternative immune checkpoint molecules[56]. As such, some targeted therapies, such as PI3K inhibitors have been tested in clinical trials to sensitize tumors to ICI.

The blockade of alternative immune checkpoint ligands has emerged as a promising therapeutic strategy in breast cancer. Preclinical studies have shown that the blockade of these molecules can induce antitumor immune responses and improve outcomes in breast cancer models[57,58]. However, further research is needed to evaluate the safety and efficacy of these therapies in clinical trials. One of the immune checkpoint ligands that is of particular interest to the field of BC therapeutics is B7-H4. Unlike other ligands, B7-H4 is almost exclusively expressed on tumor cells vs. healthy breast cells, and recent research suggests it could be a biomarker of therapy response or the target for novel immunotherapies[58]. The following section will discuss this molecule in detail, while the discussion includes current clinical trials targeting B7-H4 in breast cancer.

An introduction to B7-H4

B7-H4 (encoded by *VTCN1*) is an immune checkpoint ligand in the CD28/B7 family of molecules characterized by sequence similarity to other B7 family proteins and is expressed in several human tumor types, including breast cancer[59–61,57,62,50,63,51]. It is a type I transmembrane protein of 297 amino acids. It has a single N-terminal extracellular domain and a very short two-amino acid C-terminal intracellular domain, that lacks any known signaling motifs[50]. The extracellular domain consists of two immunoglobulin-like domains, IgV and IgC, that are connected by a flexible hinge region. The IgV domain is responsible for binding to its yet unidentified receptor. The human and mouse orthologs share about 90% homology, particularly in the IgV binding domain, suggesting this molecule is highly conserved.

B7-H4 and PD-L1 (Programmed-death-ligand-1) are both members of the B7 family of co-stimulatory and co-inhibitory molecules and share a similar structure. PD-L1 is also a transmembrane protein with the IgV and IgC extracellular domains. The IgV domain of PD-L1

binds to its receptor PD-1 (Programmed-death-1) and exerts inhibitory effects on T cells. The intracellular domain of PD-L1 contains a signaling motif that interacts with the cytoplasmic tail of PD-L1, thus leading to inhibition of T cell activation[64]. The lack of signaling motifs in the B7-H4 intracellular domain raises questions about its binding partner and putative functions.

The initial discovery of B7-H4 was accompanied by functional studies of the molecule. Both initial papers published side by side in *Cell Immunity* show inhibition of activated T cells and suppression of IL-2 function *in vitro*[50,62]. B7-H4 was found to be expressed on B cells and macrophages. It was later found to be expressed in several cancers, particularly breast, ovarian, and lung cancer. Several studies have suggested that B7-H4 has a co-inhibitory role on tumor lymphocytes[52,59,61,63,65,66]. Its receptor has not yet been identified but is thought to be expressed on activated, but not resting, T lymphocytes based on initial published functional studies[50,62,65]. B7-H4 expression is associated with “immune cold” TNBC tumors that lack infiltrating and activated immune cells and is correlated with worse patient outcome[57,61,63,67,68]. In contrast, PD-L1 is often expressed on highly immunogenic tumors[59,69–71]. Furthermore, published literature has shown an inverse correlation between breast tumors expressing B7-H4 and PD-L1, though no mechanism for this reciprocal pattern has been established[59,61,67]. We sought to understand the expression and regulation of B7-H4 in breast cancers to determine whether it could be a mechanism of immune suppression and therefore a mechanism of resistance to current immunotherapies.

Study aims and hypothesis

Patients with early-stage TNBC are eligible to receive neoadjuvant anti-PD-1 (pembrolizumab) with neoadjuvant chemotherapy[32,37,44]. Additionally, patients with late-stage/metastatic TNBC have also shown response to anti-PD-1 treatment with chemotherapy[24,36]. However, currently available ICIs are ineffective in subsets of patients with no identifiable biomarker to distinguish these patients from those that respond robustly. Because of the proposed immunosuppressive function of B7-H4 within the TIME and because

immune evasion is a hallmark of cancer, we propose the function of alternative checkpoint ligands as a potential mechanism of immunotherapy resistance in breast cancers. In the present study, we aimed to identify mechanisms driving B7-H4 expression and regulation in breast cancer. We also designed murine *in vivo* tumor models to test whether manipulation of B7-H4 status influenced therapy response to ICIs. Finally, we assessed available clinical trial data by B7-H4 status to determine any association with B7-H4 expression and resistance to currently available ICIs. Specifically, in Chapter III, we established B7-H4 is preferentially expressed on epithelial cell types in immune cold tumors. In Chapter IV, we tested whether B7-H4 overexpression induced ICI resistance and explored a paradoxical phenotype of resistance in murine tumors but lack of association in human BC. Finally, in Chapter V, we identified that B7-H4 was regulated by PI3K signaling, unlike PD-L1, which is regulated by IFN and we explore potential mechanisms for B7-H4 inhibition of immune cells based on our findings *in vivo*. These studies have exposed important differences between murine and human tumors regarding B7-H4 biology and have implications for the field in identifying appropriate therapeutic targets for patients resistant to ICIs.

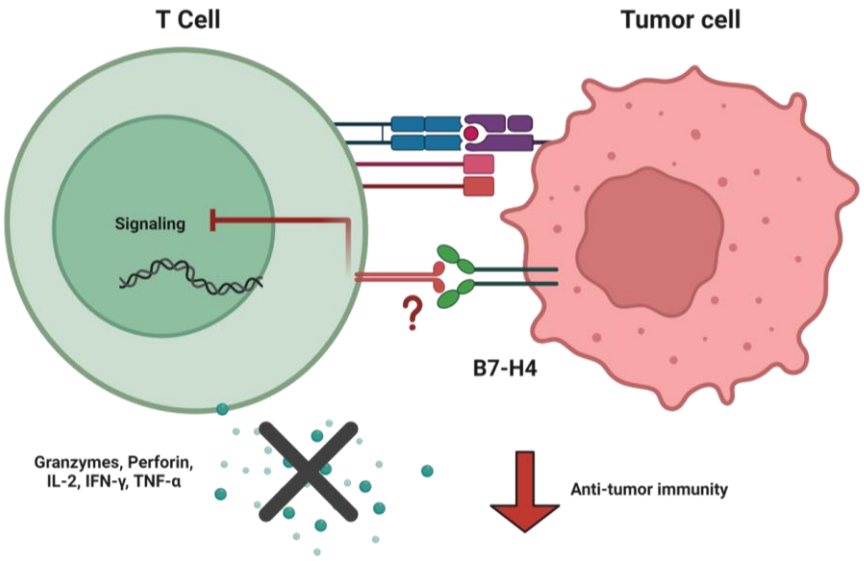

Figure I.4. **Hypothesis for B7-H4 function within the tumor microenvironment.** B7-H4 binds to an as yet unknown receptor, leading to downregulation of proinflammatory signaling and reduced anti-tumor immunity.

Chapter II: MATERIALS AND METHODS

Patient samples

Clinical specimens used for characterization of B7-H4 expression were surgically resected tumor samples collected retrospectively from 77 patients with TNBC and residual disease after neoadjuvant chemotherapy, diagnosed and treated at the Instituto Nacional de Enfermedades Neoplásicas under INEN 10-018 and 348 patients with ER+HER2- and TNBC diagnosed and treated at VUMC under NCT00899301 and NCT00651976. We assessed B7-H4 correlation with survival in 91 patients (with B7H4 mIF data) from the TBCRC 043 clinical trial[72] (NCT03206203) and in 151 patients (with reverse phase protein array, RPPA, data) in the ISPY2 clinical trial[43] (NCT01042379). For TBCRC043 trial 106 patients with metastatic TNBC were randomized into two groups receiving carboplatin or carboplatin + atezolizumab, however only 91 had viable samples for biomarker analysis of B7-H4 and were included in the analysis. For the I-SPY2 trial dataset, 151 patients were assessed that had accompanying reverse phase protein array (RPPA) expression data and randomized into paclitaxel control treatment (n = 85) or paclitaxel + pembrolizumab treatment (n = 66). Of the 151 patients, 62 were HR-negative and 89 were HR-positive.

Cell lines and tissue culture

Murine mammary cancer cell lines EMT6 and E0771 were obtained from ATCC. EMT6 cells were grown in DMEM/F12 (Gibco) supplemented with 10% fetal bovine serum (FBS) (Life Technologies). Murine B7-H4+ cell lines were generated using retroviral transduction with the pBabe-puro plasmid (Addgene). Positive cells were collected by fluorescence activated cell sorting to obtain a pure positive population. Cell expression was regularly validated by flow cytometry.

Human breast cancer cell lines MDA-MB-468 (DMEM + 10% fetal bovine serum; FBS) were obtained from ATCC. MMTV-neu cells (DMEM-F12 + 10% FBS + EGF 20 ng/mL + Hydrocortisone 0.5 µg/mL + Insulin 10 µg/mL) were derived from a spontaneous tumor within the FVB/N-Tg (MMTV-neu) 202 Mul/J mouse. All cells were routinely tested for mycoplasma contamination. Cells were treated with 50nM trametinib (SelleckChem) or 1µM buparlisib (SelleckChem).

Viral transduction

Murine B7-H4 (Genecopoeia) was cloned into pBabe-puro (Addgene) vector by restriction digest. Retroviral particles were produced by transfecting Phoenix packaging cells using Lipofectamine 3000 (Life Technologies). Target cells were transduced in the presence of polybrene and selected by puromycin resistance. pBabe-puro was a gift from Hartmut Land & Jay Morgenstern & Bob Weinberg (Addgene plasmid #1764; http://n2t.net/addgene:1764 ; RRID:Addgene_1764)[73].

Immunoblotting

Cells were lysed in 1× RIPA buffer (0.1% SDS detergent, 50 mM Tris pH 7.4, 150 mM NaCl, 1.0% NP-40, 0.5% deoxycholic acid, 1 mM EDTA, 1 mM EGTA, 5 mM sodium pyrophosphate, 50 mM NaF, 10 mM b-glycerophosphate) with added phosphatase inhibitors (PhosSTOP, Roche) and protease inhibitors (cOmplete, Roche). Lysates were sonicated and incubated on ice for 15 min before centrifugation at 13,000 × g for 10 min at 4 °C. Protein concentrations of the lysates were determined by BCA assay (Thermo). Samples were separated on NuPage 4%-12% BisTris gels (Invitrogen) and transferred to nitrocellulose membranes. Membranes were blocked with 5% nonfat dry milk or 5% BSA in tris-buffered saline (TBS) with 0.1% Tween-20 for 1 h at room temperature and then incubated overnight at 4 °C with the appropriate antibody in blocking buffer as indicated. Following incubation with appropriate horseradish peroxidase-conjugated secondary antibodies, proteins were visualized using an enhanced

chemiluminescence detection system (Thermo). This study was performed using the following antibodies: Vinculin from Santa Cruz (#73614), and ERK1/2 (#9102), p-ERK1/2 (#4370), AKT (#2920), p-AKT (#4060), and B7-H4 (#14572) all of which were purchased from Cell Signaling Technologies.

Flow cytometry

Cancer cells were washed in phosphate-buffered saline (PBS) and harvested with TrypLE (Life Technologies) for 10 min at 37 °C. Dissociated cells were washed once in PBS and incubated with respective flow antibodies at 4 °C for 20 min in the dark for surface staining and 30 minutes for intracellular staining. Flow cytometry of cancer cells was performed using the following antibodies: B7-H4 (BioLegend #103132, 1:100 dilution), EpCAM (BioLegend #118216,1:2000 dilution), and CD44 (BioLegend #103028, 1:1500 dilution). Flow cytometry of tumor dissociates was performed using the following antibodies: CD45 (BioLegend #109822), TCRB (Invitrogen #48-5961-82), CD8 (Invitrogen #MA5-16759), FOXP3 (Invitrogen #12-5775-82), CD44 (BioLegend #103036), PD-1 (BioLegend #135241), Granzyme B (Invitrogen #35-8898-82), Nkp46 (BioLegend #137637), CD11b (BioLegend #101263), F4/80 (BioLegend #123120), CD206 (BioLegend #141721), Arg1 (Invitrogen #12-3697-82), and Nos2 (Invitrogen #58-5920-82). Zombie Violet (Thermo) or dye EF780 (eBioscience #65-0865-14) was used as viability dyes for dead cell exclusion. Samples were analyzed on an Attune NxT flow cytometer (Life Technologies) or CyTEK Aurora and analyzed by FlowJo Version 10.

Mice

All mice were housed at the Vanderbilt University Medical Center vivarium, which is accredited by the Association for Assessment and Accreditation of Laboratory Animal Care International (AAALAC). Mouse procedures and studies were approved by the Vanderbilt Division of Animal Care and Institutional Animal Care and Use Committee (IACUC). C57BL/6J and BALB/c mice were purchased from Envigo (Indianapolis, IN) and allowed to acclimatize for at least one week

before tumor implantation and experimentation. For all experiments, 6- to 8-week-old female mice with 100-200 mm^3 tumors were stratified into specific treatment groups.

Tumor implantation and treatment strategy

For mammary tumor models, 5 x 10^4 EMT6 were orthotopically injected into the fourth left mammary fat pad of female BALB/c mice. 1 x 10^6 MMTV-neu (epithelial or mesenchymal) cells were injected into the fourth left mammary fat pad of female NUDE mice. Cells were tested for mycoplasma contamination prior to each experiment using the e-Myco Mycoplasma PCR Detection Kir (LiliF Diagnostics). Following the establishment of tumors (~100-200mm^3) mice were stratified prior to therapy administration. BALB/c mice were treated via intraperitoneal (IP) injection with isotype IgG1 control (BioXcell, clone BE0083) or anti-PD-L1 (Genentech, clone 6E11) dosing at 200µg for the first treatment and 100µg for two subsequent treatments at one-week intervals. For chemotherapy experiments, tumors were treated with paclitaxel (200ug or 400ug) or doxorubicin (200ug or 100ug) once weekly for four weeks. Drug was administered either via intravenous or intraperitoneal routes as indicated in figure legends. For tumor growth analysis, tumors were measured 2-3 times weekly with calipers, and volume was calculated in mm^3 using the formula (length x width x width/2). Mice were humanely euthanized at defined end points or when the tumor volume reached 2000mm^3 or tumor ulceration.

Tumor dissociation and immune cell isolation

EMT6 tumors were harvested from mice at either 500mm^3 or one-week post-treatment as indicated in figure legends and dissociated using the Mouse Tumor Dissociation Kit (Miltenyi Biotec) according to manufacturer's specifications with the gentleMACs Octo dissociator (Miltenyi Biotec) default tumor protocol (40 minutes at 37°C under constant agitation). The dissociate was then passed through a 70µm filter, washed with 20-30mL of PBS, and ACK lysed. The single cell suspension was then subjected immediately to antibody staining for flow

cytometry as described above, or cell sorting by magnetic bead isolation. Dead cells were excluded using the Dead Cell Removal Kit (Miltenyi Biotec). Additional cell isolation was performed using CD45 (TIL) mouse microbeads (Miltenyi Biotec).

RNA isolation

After dissociation and CD45+ cell isolation, RNA was harvested from mouse tumor immune cells using the Maxwell 16 automated workstation (Promega) and the LEV simplyRNA Cells Kit (Promega). RNA concentration was determined by spectrophotometry (NanoDrop2000, Thermo Fisher Scientific).

NanoString gene expression analysis

Gene expression profiles of tumor-infiltrating immune cells from either untreated or anti-PD-L1 treated B7H4+ or parental EMT6 tumors were assessed using the nanoString Mouse Pan-cancer Immunology panel (770 genes) according to the manufacturer's specifications. CD45 TIL bead sorted tumor dissociates were used for RNA preparation, and 100 ng of total RNA was used for input into nCounter hybridizations. Raw RCC files were processed using nanoString nSolver to generate data frame for further data analysis. The raw count data was first batch corrected using ComBat-Seq [PMID: 33015620]. Low quality genes or samples were further filtered using negative control beads and a normalization factor is created using positive control bead and housekeeping genes to normalize the entire dataset. After normalization, the data were log transformed. PCA was performed to observe general clustering pattern and ensure no strong batch effect is present. Differential gene expression analysis was performed using Wilcox test with multiple-test correction p value generated. Function gene sets were directly obtained from nanoString mouse Pan-cancer immunology panel. Gene set score was calculated using a z-score sum of all the genes within the set.

Single-cell RNA sequencing

MMTV-neu cells were harvested directly from cell culture and prepared for single cell RNA sequencing. Each sample (targeting 15,000 cells per sample) was processed for single-cell 5′ RNA sequencing utilizing the 10x Chromium system. Libraries were prepared following the manufacturer's protocol. The libraries were sequenced using NovaSeq 6000 with 150 bp paired-end reads. RTA (v.2.4.11; Illumina) was used for base calling. Data was analyzed in R using the filtered h5 gene matrices in the Seurat package. In brief, samples were subset to include cells with >200 but <3,000 unique transcripts to exclude probable non-cellular RNA reads and doublets. Cells with >15% of reads coming from mitochondrial transcripts were also excluded as probable dying cells. Normalization, scaling, dimensional reduction, and unsupervised clustering were also performed using Seurat. Cells were classified as mesenchymal or epithelial based on *Epcam* expression.

Immunohistochemistry (IHC) and multiplexed immunofluorescence (mIF)

Formalin-fixed paraffin-embedded (FFPE) tissue sections were cut at 4 μM and deparaffinized. Antigen retrieval was performed with citrate buffer pH 6. Endogenous peroxidase was blocked, and protein block was applied. Sections were then incubated with the primary antibodies (B7H4 AF2154 R&D Systems at 1:600, CD45 ab10558 Abcam at 1:2500, B7H4 D1M8I Cell Signaling 1:200, pan-Cytokeratin AE1/AE3 Biocare at 1:600, EpCAM ab71916 Abcam 1:500, CD44 ab157107 Abcam 1:1000, CD8 144B Statlab) overnight at 4°C. For chromogenic IHC, visualization system was Envision (Agilent Technologies, Santa Clara, CA), DAB as the chromogen (Agilent Technologies) and hematoxylin was applied as the counterstain. For multiplex fluorescence IHC, sections were then incubated with the secondary antibody and TSA reagent applied according to manufacturer's recommendations in a cyclic manner. Breast cancer with known B7H4 expression was used as a positive control.

Image analysis and quantification

Whole slide images were digitally acquired using an AxioScan Z1 slide scanner (Carl Zeiss) at 20x. Automated quantification was performed via pathologist-supervised machine learning algorithm using QuPath software[74]. Tumor areas were manually annotated to exclude extensive necrosis present in most samples. For chromogenic IHC, color deconvolution to separate hematoxylin and DAB. Cell segmentation was determined on the hematoxylin. Positive cell detection algorithm according to the cell DAB OD mean was used to calculate percent of positive tumor cells and H-score. For fluorescence IHC, cell segmentation was determined on DAPI. Object classifiers were trained on annotated training regions from control tissue and tumor samples to define cellular phenotypes. Single cell data including sample ID, xy coordinate, cell phenotype, and B7H4 intensity were exported from QuPath to calculate B7H4 intensity for each cell phenotype in R.

Reverse phase protein array (RPPA)

RPPA was performed as described previously[75–77]. Briefly, lysates were prepared and printed in triplicate spots (approx. 10nL per spot) onto nitrocellulose coated slides (Grace Biolabs, Bend, OR, USA) using a Quanterix 2470 Arrayer (Quanterix, Billerica, MA, USA). Standard curves of control cell lysates were included for quality assurance purposes. Antibodies used on the RPPA were validated before use by confirming the presence of a single band at the appropriate molecular weight with a panel of control cell lysates using conventional western blotting. Immunostaining was performed by probing each slide with one primary antibody targeting the protein of interest. Biotinylated goat anti-rabbit IgG (H+L) (1:7,500, Vector Laboratories Inc, Burlingame, CA) or rabbit anti-mouse IgG (1:10, DakoCytomation, Carpinteria, CA, USA) were used as secondary antibodies. Signal amplification was performed using a tyramide-based avidin/biotin amplification system (DakoCytomation, Carpinteria, CA, USA) followed by streptavidin-conjugated IRDye 680 (LI-COR, Lincoln, NE, USA) for visualization. Negative

controls were stained with secondary antibody alone. Total protein was measured using Sypro Ruby protein blot staining per manufacturer's instructions (Molecular Probes, Eugene, OR, USA). RPPA data was generated directly from images acquired using a Tecan PowerScanner (Tecan, Mannedorf, Switzerland) and analyzed with MicroVigene software Version 5.1.0.0 (Vigenetech, Carlisle, MA, USA). Total protein intensities for each sample were calculated by averaging the Sypro staining intensity of the three replicate spots. For each sample/endpoint the final signal intensity was calculated by: 1) subtraction of negative control spot intensity from primary antibody spot intensity, 2) averaging the resulting net intensities for the three replicate spots, and 3) dividing by the total protein intensity value for each sample. For the present study, anti-human-B7-H4 (clone D1M8I) XP from Cell Signaling (#14572) was used.

Chapter III: B7-H4 IS PREFERENTIALLY EXPRESSED ON EPITHELIAL CELLS[1]

Introduction

B7-H4 has been associated with immunologically cold tumors in contrast to PD-L1, which is often expressed in immunologically hot tumors[57,61,67,68]. B7-H4 has also been associated with TNBC subtypes, but the broader pattern of expression in BC subtypes is unknown[63]. Furthermore, published literature has shown an inverse correlation between breast tumors expressing B7-H4 and PD-L1, though no mechanism for this reciprocal pattern has been established[59,61,67]. Currently, TNBC patients with or without PD-L1 expression are eligible to receive anti-PD-1 neoadjuvant therapies after several clinical trials showed improved benefit in both the early and advanced settings[32,37,44,78]. PD-L1-positive patients have overall better responses to these therapies in the advanced setting based on clinical trials[24,36,78–80]. We sought to understand the expression and regulation of B7-H4 in breast cancers to determine whether it could be a mechanism of immune suppression and therefore a mechanism of resistance to current immunotherapies.

As mentioned previously, BC can be divided into luminal and basal cancers based on the expression of epithelial and mesenchymal markers among other cellular markers[2,3,81]. A great majority of breast cancers arise from gene mutations in epithelial cells[82]. Understanding the epithelial or mesenchymal properties of BC can be crucial to understanding cancer development and progression. Epithelial cells are a major component of the body's tissues and organs, lining the surfaces of organs and serving as a barrier between the body's internal and

[1] This chapter is adapted in part from Wescott, E.C.*, Sun, X., Gonzalez-Ericsson, P.I., Hanna, A., Taylor, B.C., Sanchez, V., Bronzini, J., Opalenik, S.R., Sanders, M.E., Wulfkuhle, J., Gallagher, R.I., Gomez, H., Isaacs, C., Bharti, V., Wilson, J.T., Ballinger, T.J., Santa-Maria, C.A., Shah, P.D., Dees, E.C., Lehmann, B.D., Abramson, V.G., Hirst, G.L., Brown-Swigart, L., van ‘t Veer, L.J., Esserman, L.J., Petricoin, E.F., Pietenpol, J.A., Balko, J.M. (2024). Epithelial expressed B7-H4 drives differential immunotherapy response in murine and human breast cancer. *Cancer Research Communications*; 4 (4): 1120-1134.

external environments. These cells are characterized by their tightly packed arrangement, with cells adhering to one another via specialized structures called tight junctions. Epithelial cells are also polarized, with distinct apical and basal surfaces that perform different functions within the tissue. These cells are involved in a wide range of biological processes, including absorption, secretion, and protection against environmental stresses[83–85]. Mesenchymal cells are a more loosely organized group of cells that include fibroblasts, osteoblasts, chondrocytes, and other cell types. These cells are characterized by their ability to move and migrate, and they play a critical role in tissue repair and regeneration. Mesenchymal cells are also involved in the formation of connective tissue, bone, and cartilage, and they are important for maintaining the structural integrity of tissues and organs[83,84,86].

Mesenchymal cells and the epithelial-to-mesenchymal transition also have implications in cancer metastasis[83–85,87–89]. Epithelial cells undergo genetic and epigenetic changes that cause them to lose their normal functions and become cancerous. This process, known as epithelial-mesenchymal transition (EMT), involves a loss of the tight junctions that normally hold epithelial cells together, allowing cells to become more motile and invasive. Mesenchymal cells are also involved in the early stages of tumor formation, particularly in the development of the tumor microenvironment (TME)[90]. They provide structural support and can promote angiogenesis. Additionally, in murine mammary tumors, mesenchymal cancer cells were shown to assemble an immunosuppressive TME and thus have implications for immunotherapy resistance[84]. As mentioned above, the different BC subtypes have a wide range of typical immune infiltration patterns with vast heterogeneity even within subtypes. Furthermore, immune infiltration has been shown to be a predictor of immunotherapy response in BC[91–93].

These prior findings expose several gaps in the field, particularly in B7-H4 biology. First, which tumors have the highest B7-H4 expression of the subtypes? Second, is B7-H4 regulated by similar cell signaling mechanisms as PD-L1? Third, does B7-H4 expression negatively correlate with immune infiltration in human TNBC and murine mammary cancer tumors, as has

been previously shown? Thus, for the first aim of our study, we sought to uncover the broader mechanisms of B7-H4 expression in BC with the goal of identifying which patients are likely to have B7-H4+ tumor cells and future implications to therapeutic response. We also sought any phenotype cellular markers that could be predictive of B7-H4 expression in BC subtypes and identified strong correlations with epithelial vs. mesenchymal cell phenotype. These findings have implications in identifying biomarkers for BC patient response or resistance to ICI therapies.

Results

B7-H4 is expressed in immunologically cold breast tumors

We sought to confirm prior findings of B7-H4 association with immunologically cold tumors and characterized TNBC samples post-neoadjuvant chemotherapy (NAC) treated patients that had residual disease according to the distribution of infiltrating CD8+ T cells. Four groups – immune desert (ID), margin-restricted (MR), stromal-restricted (SR), and fully inflamed (FI) – were defined according to previously published metrics[61,94] (**Figure 3.1A**). The ID and MR tumors (those exhibiting the most immunologically cold phenotypes and associated with worse outcomes) had the highest level of tumor B7-H4 expression (**Figure 3.1B-C**), though in contrast to prior findings[61,95], B7-H4 was also present in FI tumors, possibly due to the selective or direct molecular effects of NAC in this cohort. As has been previously shown, FI and SR tumors demonstrated improved outcomes after surgery (**Figure 3.1D**). Regardless of microenvironment type, B7-H4 expression was associated with worse recurrence-free (RFS) and overall survival (OS) in these post-NAC TNBC samples (**Figure 3.2**).

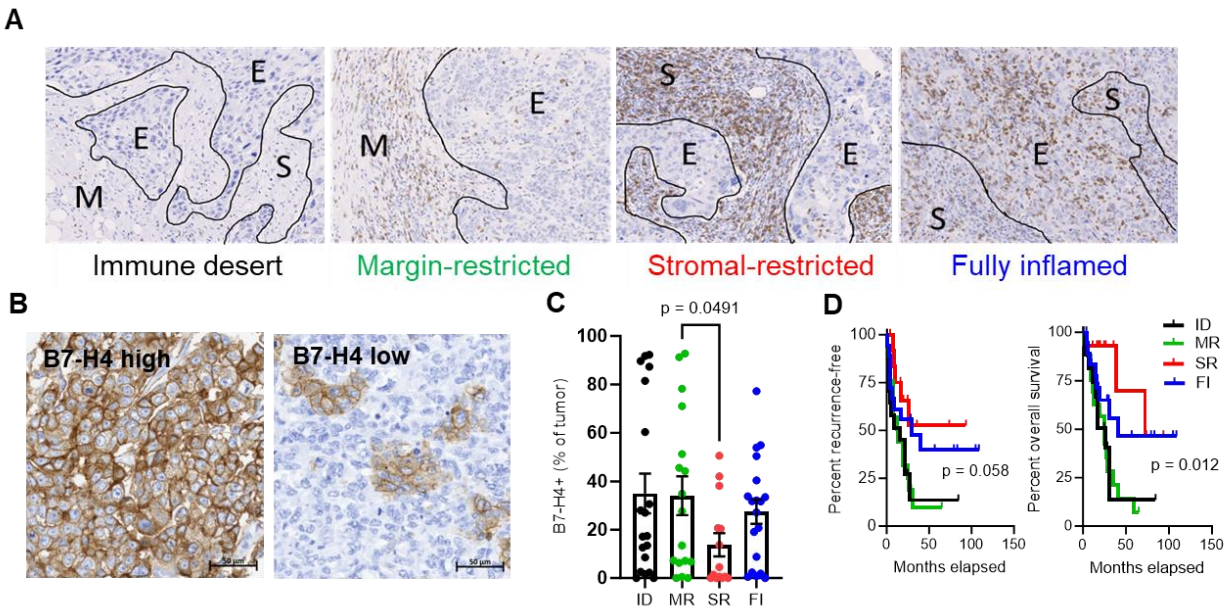

Figure III.1. **B7-H4 is associated with immune cold tumors.** (A) Representative TNBC samples (residual disease, post-neoadjuvant chemotherapy) categorized based on CD8 T cell infiltration and localization into Immune Desert (ID), Margin-restricted (MR), stromal-restricted (SR), and fully inflamed (FI). (B) B7-H4 is heterogeneously expressed in TNBC. (C) ID and MR tumors have the highest level of B7-H4 expression (n=69: ID: 19, MR: 17, SR: 14, FI: 19). MR and SR tumors were analyzed by unpaired-t test. (D) MR and ID tumors also have worse recurrence-free and overall survival (n=69). Data were analyzed by Mantel-Cox test.

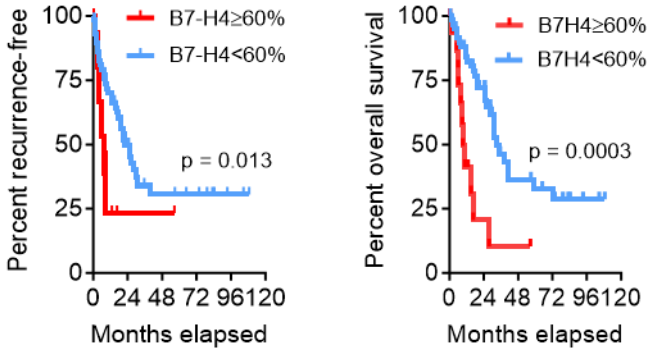

Figure III.2. **B7-H4 is associated worse survival.** B7-H4 expression directly correlates with worse outcomes in patients (n=77; >60%: 16, <60%: 51). Data were analyzed by Mantel-Cox test.

Although B7-H4 has been shown to be associated with more immunologically cold tumors, other cancer cell features associated with MR and B7-H4 status have not been

evaluated at the protein level. Thus, we chose MR (B7-H4 high) and SR (B7-H4 low) tumors, as well as FI tumors, and evaluated the protein expression of immune markers in the CD8+/cytotoxic T cell and pan-cytokeratin/tumor cell compartments using Nanostring GeoMX Digital Spatial Profiling (DSP). Samples were stained with a multiplexed immunofluorescence panel containing pan-cytokeratin (panCK), CD3, CD8, and DAPI to distinguish tumor cell and T cell regions (**Figure 3.3A**). Gating for the CD3+ and panCK+ compartments was used to extract detection antibody barcodes specifically in these cells. We compared protein expression in tumor cell regions only in MR and SR samples; ID tumors were not evaluated since they contain insufficient immune content, and FI tumors were excluded from the analysis as the dispersion of immune cells in the tumor-rich regions limited specificity of the intended gating procedure (i.e., the juxtaposition of immune cells and tumor cells limited interpretability - data not shown).

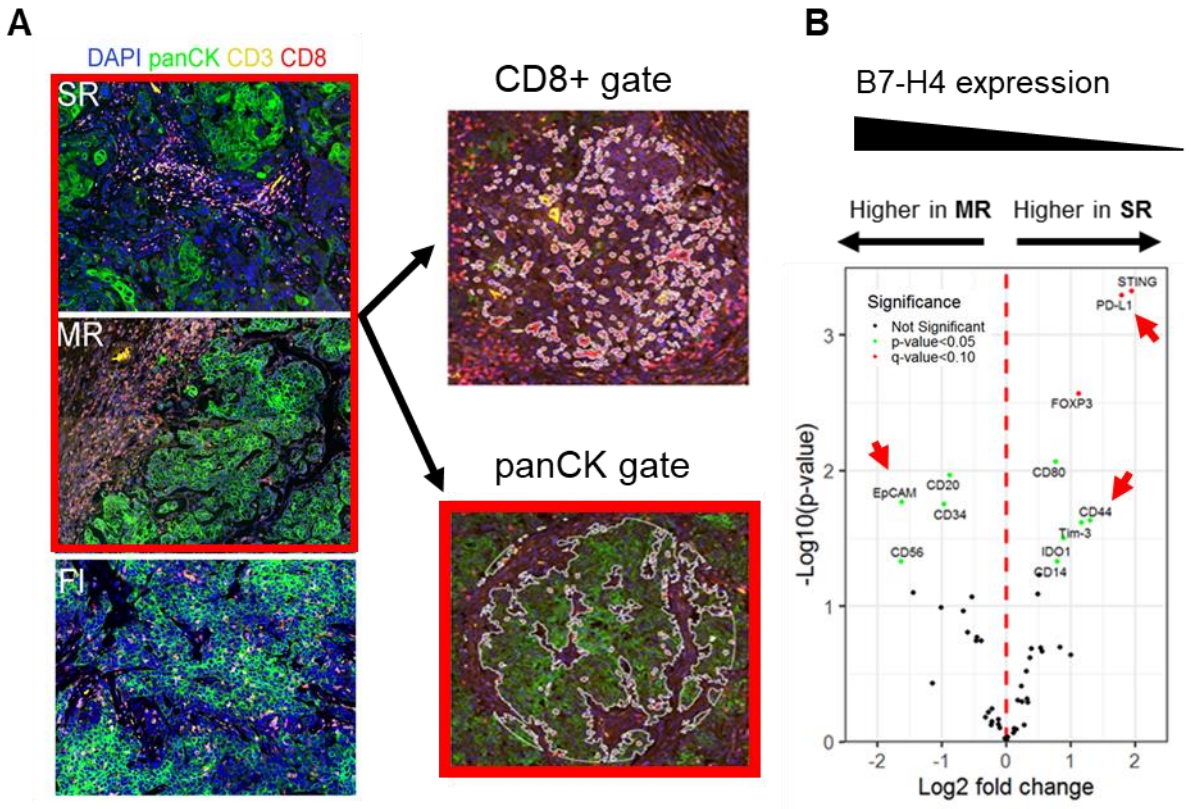

Figure III.3. **B7-H4+ tumors are associated with EpCAM expression.** (A) TNBC samples stained with immunofluorescent markers for DAPI, panCK, CD3, and CD8 to identify regions of interest (ROI) for Nanostring GeoMX Digital Spatial Profiling (DSP). MR and SR panCK+ ROIs were selected and differential protein expression between tumor samples is shown. (B) Within the panCK gated cells, MR tumors had higher EpCAM expression. SR tumors had higher CD44

expression, as well as higher PD-L1. Data shown are log2 fold change of differentially expressed genes. ($p < 0.05$, $q < 0.10$, data analyzed using R.)

Although B7-H4 was not a validated detection marker in the GeoMX panel, B7-H4 expression in the tumor cells was independently validated by immunohistochemistry (IHC) (**Figure 3.1B-C**). The SR samples had higher PD-L1 which was expected due to greater infiltrating immune cells and a more inflammatory microenvironment (**Figure 3.3B**). Interestingly, these samples also had higher upregulation of the mesenchymal marker CD44 compared to MR tumors, which had higher EpCAM (epithelial status) expression (**Figure 3.3G**). As our MR tumors had the higher B7-H4 expression, we explored further correlations between epithelial cell markers and B7-H4 expression in breast cancer.

B7-H4 expression is associated with epithelial vs. mesenchymal cell status

We examined over 60 breast cancer cell lines from the Cancer Cell Line Encyclopedia (CCLE)[96,97] and observed strong positive correlations with markers of epithelial cell status and B7-H4 (**Figure 3.4A**). Interestingly, other checkpoint ligands of the B7-family had an inverse relationship and were strongly associated with markers of mesenchymal cell status (**Figure 3.4A**). Additionally, epithelial-to-mesenchymal transition (EMT) transcription factors correlated with lower levels of *VTCN1* expression in these same cell lines (**Figure 3.4B**). *VTCN1* expression was higher when EMT-associated genes had low expression and vice-versa (**Figure 3.4B**). These data suggest that B7-H4 is associated with, and could be regulated by, EMT in tumors.

We next screened several murine and human cell lines to identify a model of B7-H4 expression and perform perturbations to understand the mechanism of expression (**Figure 3.5A-B**). The MMTV-neu mammary tumor cell line had the highest B7-H4 expression and we used this cell line for future experiments[98,99]. This cell line was derived from an FVB/n transgenic mouse with the activated rat *neu* oncogene under control of the mouse mammary tumor virus

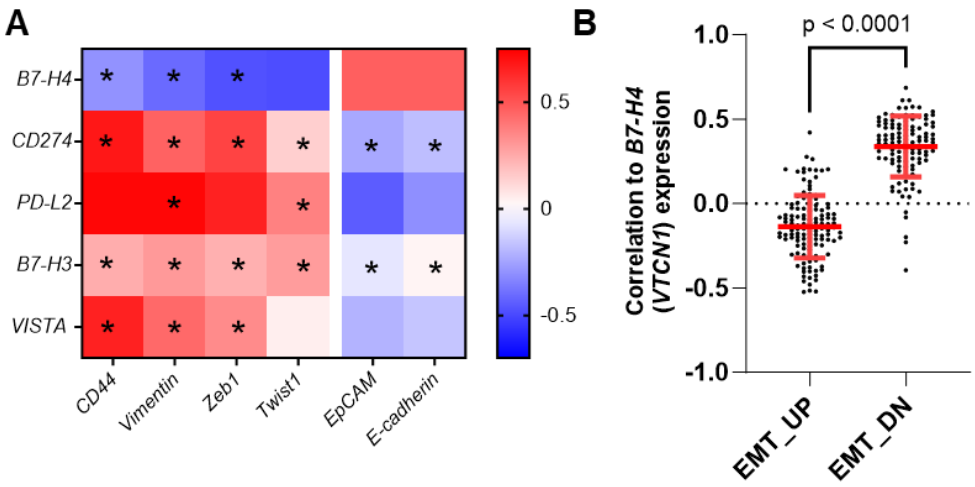

Figure III.4. **B7-H4 (*VTCN1*) is highly correlated with epithelial gene markers in mouse and human cells unlike other checkpoint ligands.** (A) In human breast cancer cell lines (CCLE), B7-H4 is the only checkpoint ligand positively correlated with epithelial markers and negatively correlated with mesenchymal markers. Data shown are spearman correlations between genes. Significant correlations ($p < 0.05$) are indicated by asterisk. (B) Genes downregulated during EMT are positively correlated with *VTCN1* in human cell lines (CCLE).

(MMTV) promoter leading to early onset of oncogene expression in the mammary epithelium and spontaneous tumor formation[98]. In one additional murine cell line (MMTV-NIC, also derived from a spontaneous tumor from an FVB/n transgenic mouse with a bicistronic transcript of *neu*-IRES-Cre under transcriptional control of the MMTV promoter[100,101]) and the human MDA-MB-468s (a TNBC patient-derived cell line), epithelial cells (EpCAM+) expressed B7-H4 (**Figure 3.5B**).

The MMTV-neu cell line consists of epithelial-like and mesenchymal-like cell populations when assessed by morphology and protein expression (**Figure 3.6A-C**). We were able to sort these two populations by fluorescence activated cell sorting (FACS) into single cell derived populations. Because of the correlation between B7-H4 and epithelial cell status, we were curious whether these cells were undergoing EMT or MET (mesenchymal-to-epithelial transition) and whether we could connect B7-H4 expression to EMT gene regulation. However, we established these cells were distinct and not actively undergoing EMT by following their phenotype over more than 20 consecutive passages. (**Figure 3.7**). After these cells were

established as distinct populations, we observed that epithelial cells maintained B7-H4 expression (**Figure 3.6B-C**).

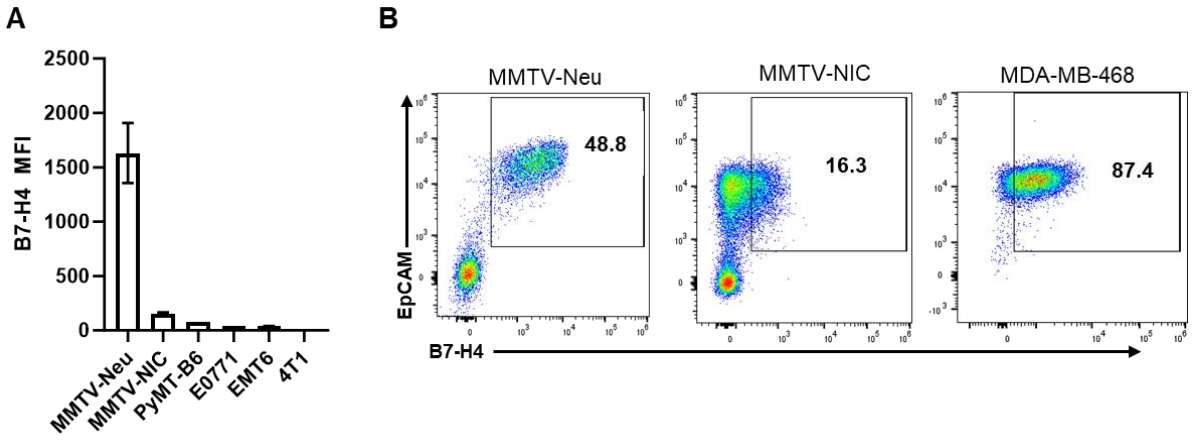

Figure III.5. **Several murine and human cell lines express B7-H4.** (A) Murine cancer cell lines express B7-H4. The MMTV-neu cell line has the highest B7-H4 expression. (B) B7-H4 is only expressed on epithelial EpCAM+ cells in murine and human cell lines.

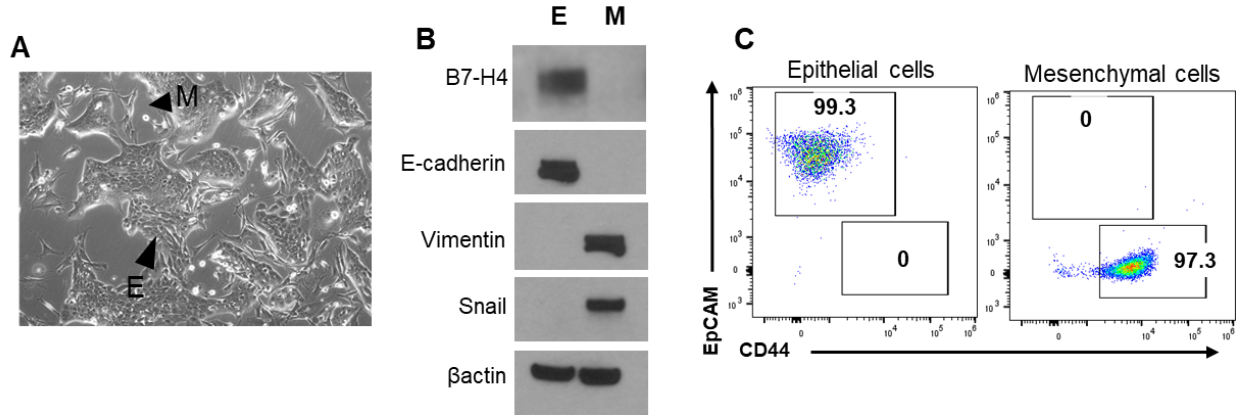

Figure III.6. **MMTV-neu cells consist of epithelial and mesenchymal-like cell populations.** (A) The MMTV-neu cell line with highest B7-H4 levels is comprised of phenotypically epithelial-like (abbreviated E) and mesenchymal-like (M) cells. (B) In MMTV-neu cells, the CD44+ M cells do not express B7-H4 but all the EpCAM+ E cells do. (C) MMTV-neu E and M cells express hallmark markers.

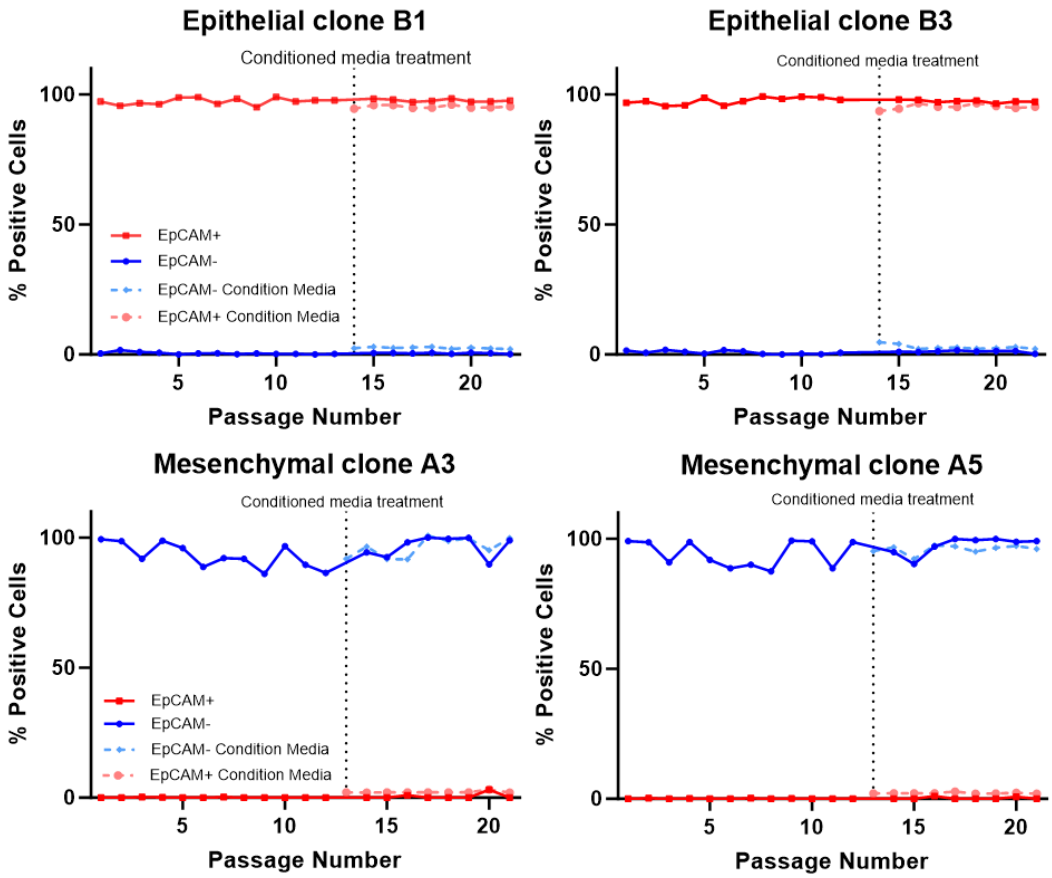

Figure III.7. **MMTV-neu epithelial and mesenchymal cells did not undergo EMT or MET.** Single cell-derived clones were isolated from parental, heterogeneous MMTV-neu cells by FACS single-cell limiting dilutions. 16 epithelial and 10 mesenchymal single-cell clones were passaged independently for over 20 passages. After 13 passages, conditioned media from the alternate cell line was collected, filtered, and applied to a passage of each single-cell clone. Independent clones or clones treated with conditioned media did not undergo epithelial-to-mesenchymal or mesenchymal-to-epithelial transition *in vitro*. Two representative clones from each cell line are shown.

We also performed single cell RNA sequencing on the heterogeneous MMTV-neu cell line and observed *Epcam* expression correlated with *Vtcn1* expression on the single cell level, but *Vtcn1* was not co-expressed with *Snai1*, a mesenchymal marker (**Figure 3.8A**). To validate the identified association of B7-H4 in epithelial cancer cells in human tumors, we stained primary ER+HER2- and TNBC tumors for B7-H4, EpCAM, and CD44 by mIF. Once again, B7-H4 was more frequently co-expressed with EpCAM on tumor cells compared to CD44 on tumor cells (**Figure 3.8B**). In summary, we established B7-H4 as a preferential marker of epithelial cell

status, rather than mesenchymal cell status. Additionally, we determined B7-H4 expression was associated with EMT/MET, however we could not confirm EMT in our murine cell line model of B7-H4.

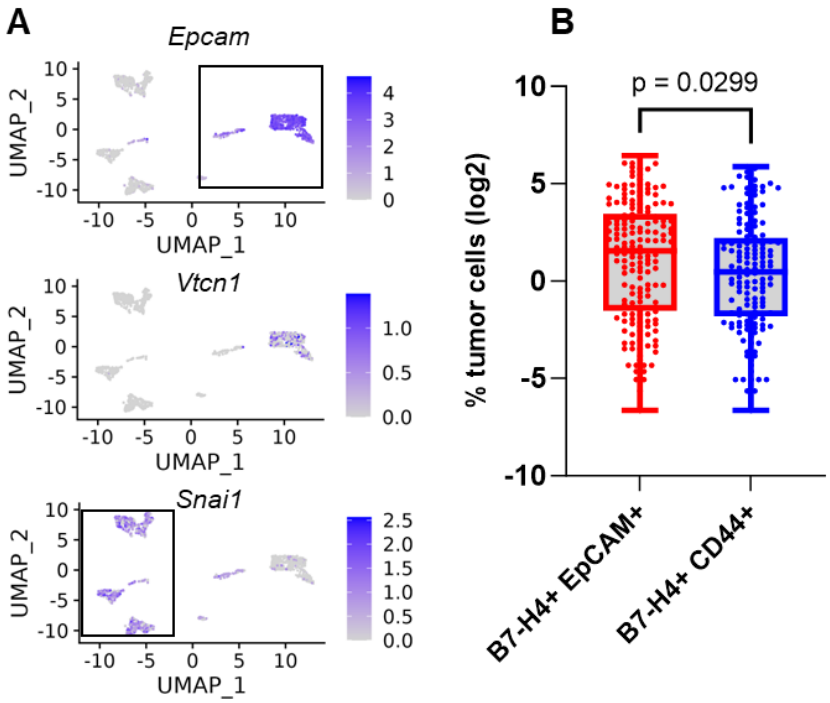

Figure III.8. **MMTV-neu and TNBC EpCAM+ cells preferentially express B7-H4.** (A) Single cell RNA sequencing of the heterogenous MMTV-neu cells confirms Vtcn1 is solely expressed in the epithelial cell population. (B) A cohort of human tumors including both TNBC and ER+HER2- were stained for B7-H4, EpCAM, and CD44 by mIF. Data shown are log2 of % B7-H4+ tumor cells and include 132 samples with >1% B7-H4 expression. (Paired t-test of transformed data)

Only MMTV-neu epithelial cells form tumors

We were interested in whether the epithelial and mesenchymal cell populations of the MMTV-neu cell line were equally tumorigenic and thus whether B7-H4 expression affected survival in this murine model. To that end, we injected NUDE female mice orthotopically with purified MMTV-neu epithelial and mesenchymal cell and measured tumor growth (**Figure 3.9A**). The epithelial cell tumors grew reliably and quickly within NUDE mice. At first, we observed no

growth of the mesenchymal cell tumors. However, after >50 days, we observed two mice injected with MMTV-neu mesenchymal cells form tumors. We followed these tumors up to 150 days post injection and then harvested them.

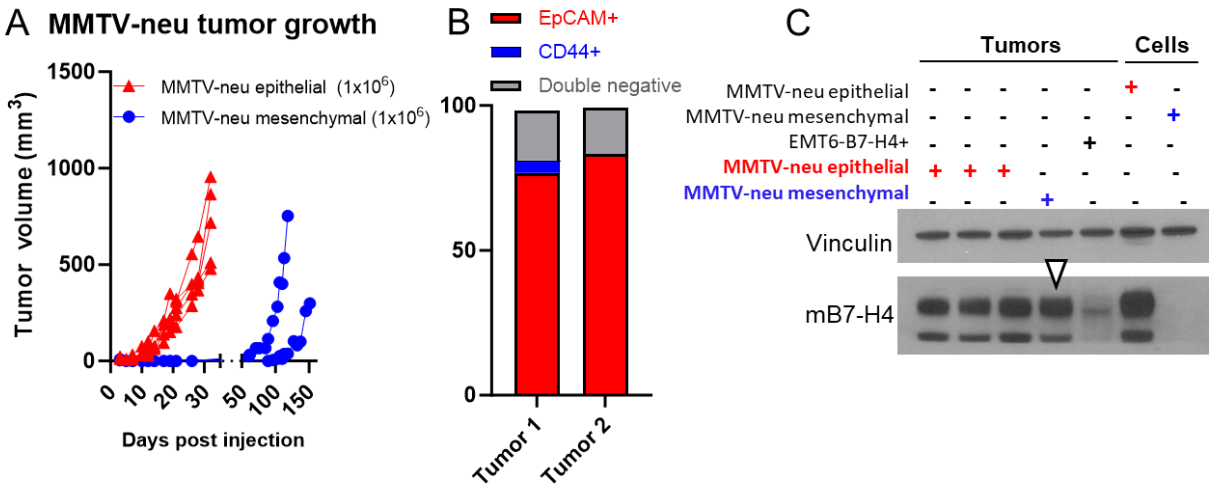

Figure III.9. **MMTV-neu epithelial cells reliably form tumors and mesenchymal cells undergo MET *in vivo*.** (A) MMTV-neu cells were injected as indicated above into NUDE mice. 5/5 epithelial tumors formed and after >50 days, 2/5 mesenchymal tumors formed. (B) Tumor dissociate was assessed by flow cytometry for the presence of EpCAM and CD44 expression on CD45- tumor cells. These tumors were predominantly EpCAM+. (C) One of the mesenchymal tumors was harvested and probed for B7-H4 tumor expression (white arrow). This tumor acquired B7-H4 expression *in vivo*. Control samples included MMTV-neu epithelial tumor protein, EMT6-B7-H4+ tumor protein (a transduced tumor model), and the MMTV-neu epithelial and mesenchymal cells.

We next wondered whether the mesenchymal cells had undergone mesenchymal-to-epithelial transition (MET) *in vivo* and that is why they were able to develop into tumors. To that end, we first assessed dissociated tumors by flow cytometry for the epithelial marker EpCAM and the mesenchymal marker CD44 on CD45- tumor cells. Both tumors predominately expressed EpCAM on the CD45- cell fraction, suggesting MET had occurred (**Figure 3.9B**). We also harvested protein from one mouse that formed a mesenchymal tumor and probed for B7-H4 expression, as B7-H4 was a marker on the MMTV-neu epithelial cells but not mesenchymal

cells. Surprisingly, these tumors were B7-H4+ suggesting they had acquired epithelial-like characteristics *in vivo* that were not present in tissue culture conditions (**Figure 3.9C**).

To determine whether this was a rare spontaneous tumor event deriving from the NUDE mouse or most likely a tumor formed from the orthotopically injected FVB/n mesenchymal cells, we stained CD45+ and CD45- cells within the tumor dissociates for MHC Class I expression (called H2D in mice), as a marker of cell haplotype. Our NUDE mice express H2Dd. FVB/n mice express H2Dq. Thus, a NUDE mouse spontaneous tumor would have tumor cells that express H2Dd while an orthotopic tumor would have cells from the FVB/n, or H2Dq, background. Antibody staining revealed CD45- (tumor) cells were H2Dq positive but H2Dd negative (**Figure 3.10**). CD45+ cells were H2Dd positive (infiltrating in from NUDE lymph). Our H2Dq antibody was cross-reactive for several haplotypes but our H2Dd antibody was reactive only for H2Dd and H2Db haplotypes. Therefore, we concluded these tumors derived from the FVB/n mesenchymal cells not from a spontaneous tumor within the mammary fat pad.

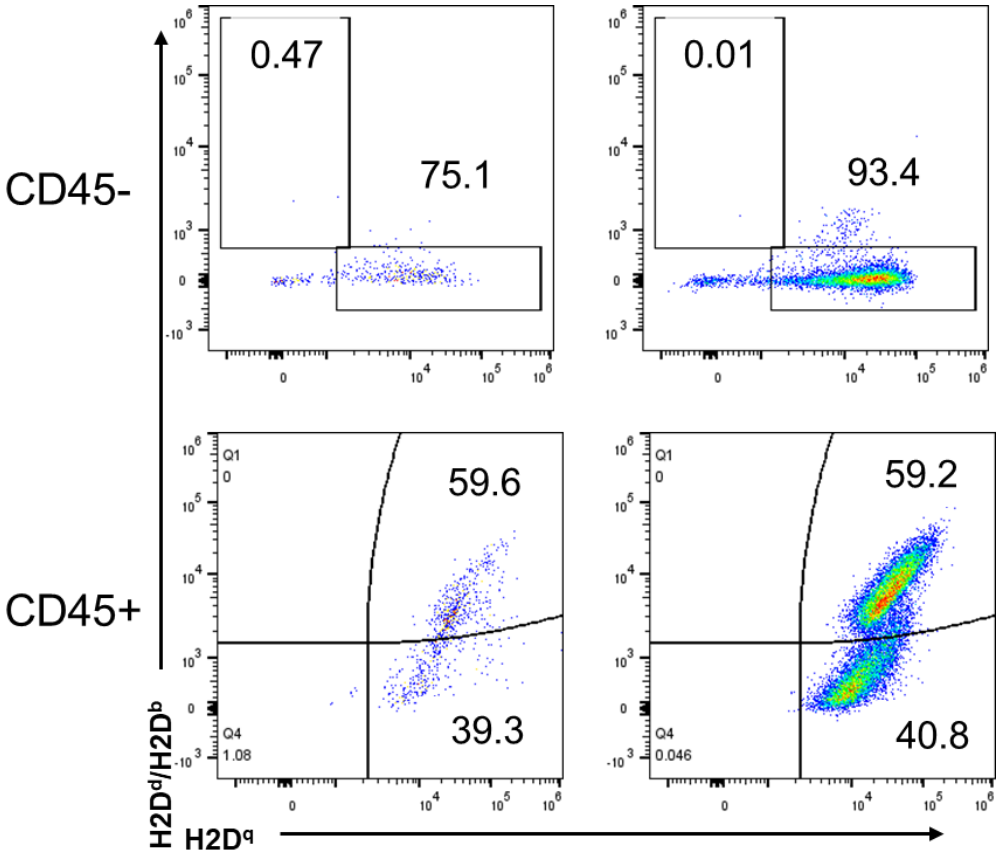

Figure III.10. **Tumors formed from FVB/n mesenchymal cells not from spontaneous tumors in the NUDE mouse background.** Flow cytometry was performed using an H2Dd/H2Db antibody in PE and a Pan-H2 antibody that reacts with H2Dq in APC. CD45- cells were predominantly H2Dq positive (FVB/n haplotype). CD45+ immune cells within the tumor expressed both H2Dd (NUDE haplotype) and H2Dq.

In summary, we observed 2 instances of mesenchymal cells forming tumors *in vivo* out of 15 NUDE mice. These experiments were repeated in syngeneic FVB/n mice with no mesenchymal tumors forming. This suggests such proposed mesenchymal-to-epithelial transition is an extremely rare event, likely arising from a couple cells acquiring epithelial characteristics. Of the tumors that formed, mesenchymal cells had transitioned to express B7-H4, comparable to the levels in epithelial cell injected tumors.

Discussion

The current study has uncovered novel associations of B7-H4 tumor cell expression with epithelial cell status. We were able to validate this finding across a variety of human BC and murine mammary cancer cell lines. Additionally, we validated that B7-H4 is more highly expressed in immune-cold TMEs, in contrast to PD-L1. All of these data suggest a potential novel mechanism for B7-H4 regulation that is distinct from PD-L1, to which the ligand is commonly compared. Interestingly, while others observed inverse expression patterns between B7-H4 and PD-L1 on a per tumor basis, we observed no inverse expression of the two ligands on a per tumor cell basis within tumors (**Supplementary Figure 1**, see Appendix I). This does not rule out similar regulatory mechanisms, but it does rule out any suppressive effect of PD-L1 on B7-H4 within the same tumor cell. Instead, PD-L1+ tumors tend to be more inflamed than B7-H4+ tumors, and PD-L1 can often be expressed on immune cells within the tumor stroma. Therefore, between breast tumors, there may be a preference for PD-L1 expression over B7-H4 expression indicated by the immune infiltration or lack thereof, but within tumors or tumor cells, there is no inhibitory effect of the two checkpoint ligands that we observed (i.e., no direct

reciprocal regulation). Stated another way, B7-H4 expression could be inhibiting tumor immunogenicity while tumor immunogenicity could be promoting PD-L1 expression, thus resulting in a reciprocal pattern of expression between tumors.

In the post-neoadjuvant chemotherapy TNBC cohort, we observed vast heterogeneity in tumor immune cell infiltration even within one subtype of BC. Our data support published literature that immune infiltration is a predictor of therapeutic response because tumors with higher B7-H4 expression (and lower immune infiltration) had worse outcomes in our cohort[18–20]. This could be driven by the lack of immunogenicity or the presence of B7-H4 or both. This provokes additional experiments to test the functionality of B7-H4 directly *in vivo*, which will be described in later chapters.

Additionally, we observed a unique phenomenon in the MMTV-neu mouse tumor model. The cell line in our hands was comprised of an epithelial and mesenchymal population, in which only the epithelial cells expressed B7-H4. Because this cell line was passaged many times in the lab, we tested whether the cells were constantly going through EMT to maintain that heterogenous phenotype *in vitro*. Despite passaging these cells separately for over 3 months *in vitro*, we did not observe EMT or the converse, MET. Thus, the orthotopic cell line did in fact consist of both epithelial and mesenchymal cells at the time of initial harvest and establishment. However, interestingly, we did observe only the epithelial cell phenotype was able to grow tumors over an extended amount of time *in vivo*. It was not completely unexpected that the epithelial cell fraction was more tumorigenic, as most BC arises from epithelial cell genetic mutations (inherited or spontaneous) within the breast. EMT is a more common event in cancer metastasis, but MET must occur as the metastases establish at distant sites. Surprisingly, the mesenchymal cell phenotype was able to transition to epithelial cells *in vivo* when it could not *in vitro.* This suggests the need to additional stimulatory factors found in the TME. We tested TGFβ, known to be a potent inducer of EMT, *in vitro* but found it was insufficient to induce transition. Further solidifying the association of B7-H4 with epithelial cell status, we observed

acquired B7-H4 expression in tumor cells that had transitioned from mesenchymal to epithelial phenotype.

We wanted to confirm that mesenchymal-to-epithelial transition *in vivo* was a rare event arising from transition of just one or a couple cells injected orthotopically. To do this, we attempted an experiment in which we retrovirally transduced epithelial or mesenchymal MMTV-neu cancer cells with individual barcode-containing vectors. We pooled this labeled cell population and injected the mice with either labeled epithelial or mesenchymal cancer cells. Should tumors arise from the mesenchymal cells, we would be able to trace back the tumor cells by their individual barcodes. We hypothesized that the epithelial tumors would arise from heterogeneous cells injected into the mammary fat pad that formed a tumor, but mesenchymal tumors would arise from only a couple mesenchymal cells that underwent mesenchymal-to-epithelial transition. Unfortunately, no mesenchymal tumors grew during this experiment (n = 10 NUDE mice and n = 10 FVB/n mice). This experiment, however, would be an important contribution to the field of mammary tumor models as we could identify which mesenchymal cells transition to tumor-sustaining epithelial cells and how those mesenchymal cells could gain B7-H4 expression *in vivo*.

Collectively, these experiments show a strong association of B7-H4 with epithelial cell status within TNBC tumors, MMTV-neu murine cancer cells, and MDA-MB-468 human BC cells. We have also phenotypically characterized the MMTV-neu orthotopic tumor cell line in our hands to further explore B7-H4 and EMT/MET biology.

Chapter IV: B7-H4 INDUCES DIFFERENTIAL RESISTANCE TO IMMUNOTHERAPY IN MURINE AND HUMAN BREAST CANCERS[2]

Introduction

While the introduction of neoadjuvant anti-PD-1 immunotherapy (pembrolizumab) has improved pathological complete response (pCR) and overall response for TNBC patients, there are still 25-40% of patients who do not benefit[32,37,41,78,102]. While several underlying mechanisms may be at play, as mentioned in Chapter I, our hypothesis for some patient resistance to ICI is the presence of alternate immune checkpoint ligand B7-H4. B7-H4 is highly expressed in many breast cancers, particularly TNBC, and could be inducing immunosuppressive functions *in vivo* that counteract anti-PD-1/PD-L1 immune activation. To test this, we designed a mouse model with B7-H4 overexpression in EMT6 mammary cancer cells (that emulate basal-like BC) and assessed tumor resistance to ICI as well as changes to the immune cell gene expression profile. These data provide insight to potential mechanisms of B7-H4 function *in vivo* that can be explored for further study. Additionally, we analyzed two human ICI clinical trial datasets, in which HR+ and TNBC patients were treated with neoadjuvant anti-PD-1 or anti-PD-L1. For both cohorts, we have B7-H4 protein expression data and survival data. These experiments address gaps in knowledge in the field of B7-H4 signaling *in vivo* particularly in the context of ICI treatment in BC patients.

---

[2] This chapter is adapted in part from Wescott, E.C.*, Sun, X., Gonzalez-Ericsson, P.I., Hanna, A., Taylor, B.C., Sanchez, V., Bronzini, J., Opalenik, S.R., Sanders, M.E., Wulfkuhle, J., Gallagher, R.I., Gomez, H., Isaacs, C., Bharti, V., Wilson, J.T., Ballinger, T.J., Santa-Maria, C.A., Shah, P.D., Dees, E.C., Lehmann, B.D., Abramson, V.G., Hirst, G.L., Brown-Swigart, L., van ‘t Veer, L.J., Esserman, L.J., Petricoin, E.F., Pietenpol, J.A., Balko, J.M. (2024). Epithelial expressed B7-H4 drives differential immunotherapy response in murine and human breast cancer. *Cancer Research Communications*; 4 (4): 1120-1134.

Results

B7-H4 expression induces moderate resistance to single-agent anti-PD-L1 immunotherapy in mice

Currently, patients with TNBC (early stage and advanced) are eligible for pembrolizumab therapy[32,37]. We wanted to assess whether B7-H4 was acting as a mechanism of tumor resistance to immune checkpoint inhibitors (ICIs), specifically the anti-PD-1/L1 axis, and could be a potential biomarker of a lack of patient response to ICIs. We overexpressed murine B7-H4 in EMT6 cells, a mesenchymal basal-like murine model that does not express B7-H4 (**Figure 4.1A**). Compared to MMTV-neu cells that endogenously express B7-H4, the level of enforced expression is slightly higher in this tumor model. These tumors maintain high levels of B7-H4 *in vivo* (**Figure 4.1B**). As our lab has previously shown, EMT6 tumors are sensitive to treatment with anti-PD-L1[103]. We treated EMT6-B7-H4+ and parental (vector alone control) tumors with anti-PD-L1 (Genentech, Clone 6E11) (**Figure 4.1C**). Compared to parental EMT6 controls, EMT6-B7-H4+ tumors had moderate resistance to anti-PD-L1 treatment (**Figure 4.1D**). This model is heterogeneously responsive to anti-PD-L1 immunotherapy and even systematically treated, genetically matched mice can demonstrate intrinsic resistance, acquired resistance, or complete response, classified based on the tumor growth curves (**Figure 4.1E**). Fewer mice with EMT6-B7-H4+ tumors completely cleared their tumors and more mice had intrinsic resistance compared to the EMT6 control cohort (**Figure 4.1F**).

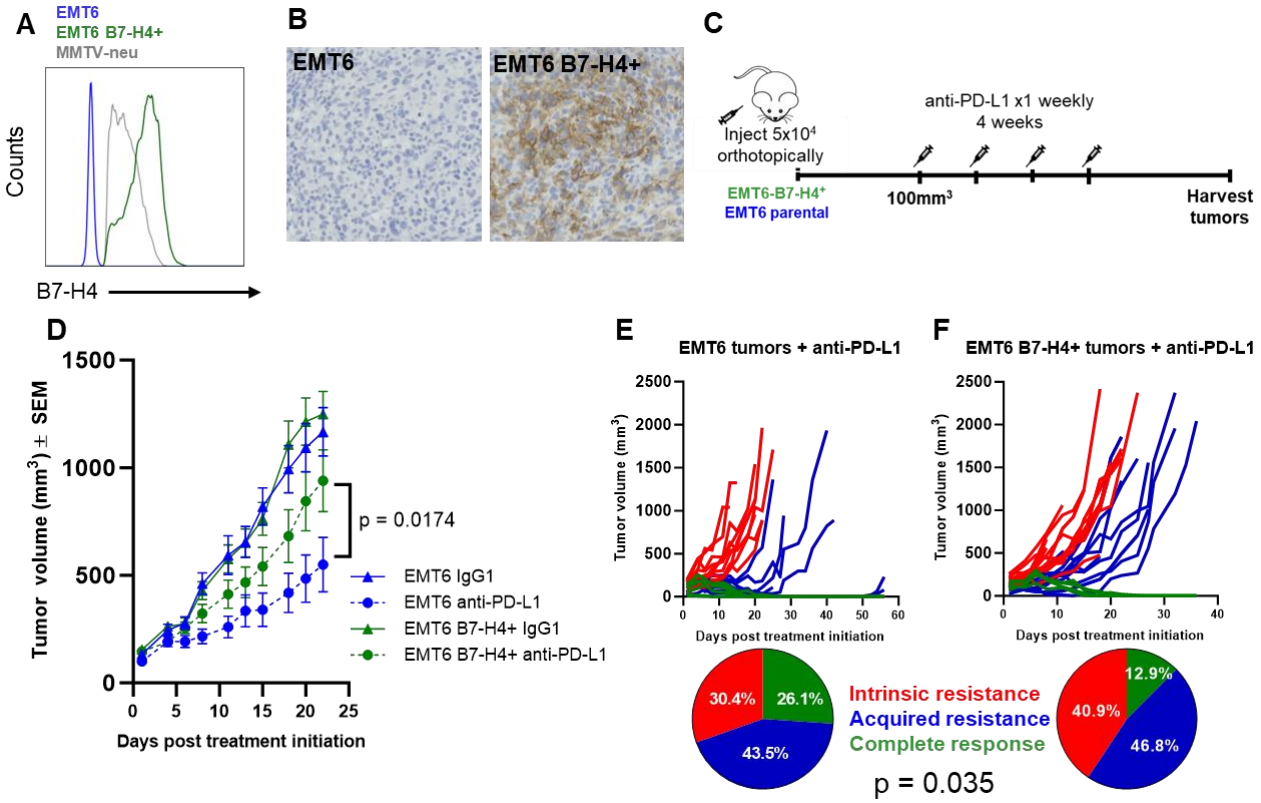

Figure IV.1. **Overexpression of B7-H4 in the EMT6 murine model induced resistance to anti-PD-L1 ICI.** (A) EMT6 cells were virally transduced with the pBabe-B7-H4 retroviral vector and overexpress exogenous murine B7-H4. (B) EMT6 B7-H4+ tumors maintain high B7-H4 expression *in vivo* assessed by IHC. (C) Animals were orthotopically injected with EMT6 cells ± B7-H4 and treated 1x per week with anti-PD-L1 at 200 ug (first dose) or 100ug (subsequent doses) for 4 weeks, after tumors reached 100mm3. (D) EMT6 B7-H4+ tumors are significantly resistant to anti-PD-L1 immunotherapy compared to control tumors. Data were analyzed by One-way ANOVA of individual AUC values with Tukey's post-hoc test for multiple comparisons between EMT6 anti-PD-L1 and EMT6 B7-H4+ anti-PD-L1 treated groups (p = 0.0174, EMT6 Isotype n = 21, EMT6 anti-PD-L1 n = 23, EMT6 B7-H4+ Isotype n = 21, EMT6 B7-H4+ anti-PD-L1 n = 23. Data were collected from a total of 3 independent experiments.). (E-F) When tumor response is categorized into three groups, EMT6 B7-H4+ tumors have overall greater intrinsic resistance to treatment and reduced complete response compared to EMT6 control tumors (p = 0.035, Chi-square = 6.683, df = 2, n = 23 mice for EMT6 parental tumors and n = 31 mice for B7-H4 tumors).

B7-H4 has also been reported to be expressed on some macrophage populations[104–107]. We wanted to assess whether the phenotype of ICI resistance was driven by tumor B7-H4 expression or immune cell B7-H4 expression. We stained tumor sections by mIF to identify

CD45+ and B7-H4+. We found (CD45-) tumor cells made up nearly all B7-H4+ cells *in vivo* (**Figure 4.2A-B**).

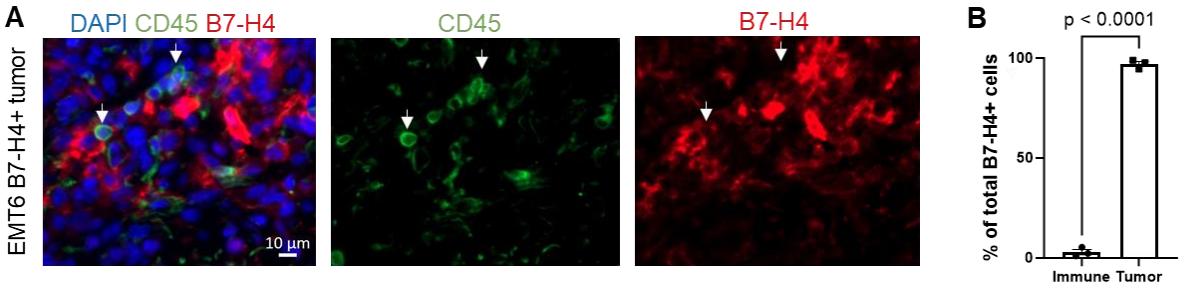

Figure IV.2. **B7-H4+ cells are tumor cells.** (A) EMT6 B7-H4+ tumors were stained by multiplexed immunofluorescence. B7-H4 is expressed on CD45- tumor cells in vivo. Representative image shown. Scale bar 10µm. (B) Quantification of (A), n = 3 mice. Data analyzed by unpaired t-test. Data were analyzed in GraphPad Prism v10.

In the BALB/c model, we did not identify any B7-H4 positive immune cells within the tumor. We found no additional B7-H4+ CD45+ immune cells in additional organs in the BALB/c mouse (**Figure 4.3A**). Interestingly, we did observe CD45+ B7-H4+ cells in C57BL/6 spleens and intestine (**Figure 4.3A-D**). Based on morphological phenotype and the location within the tissue, these are likely B7-H4+ macrophages. Together, these data suggest B7-H4 tumor cell expression in EMT6 tumors contributes to immunotherapy resistance by altering tumor susceptibility to ICI, and as a side observation, notes a possible and interesting strain-specific difference in B7-H4 expression between BALB/c and C57BL/6 mice which could be important to others in the field for future mechanistic studies in pre-clinical models.

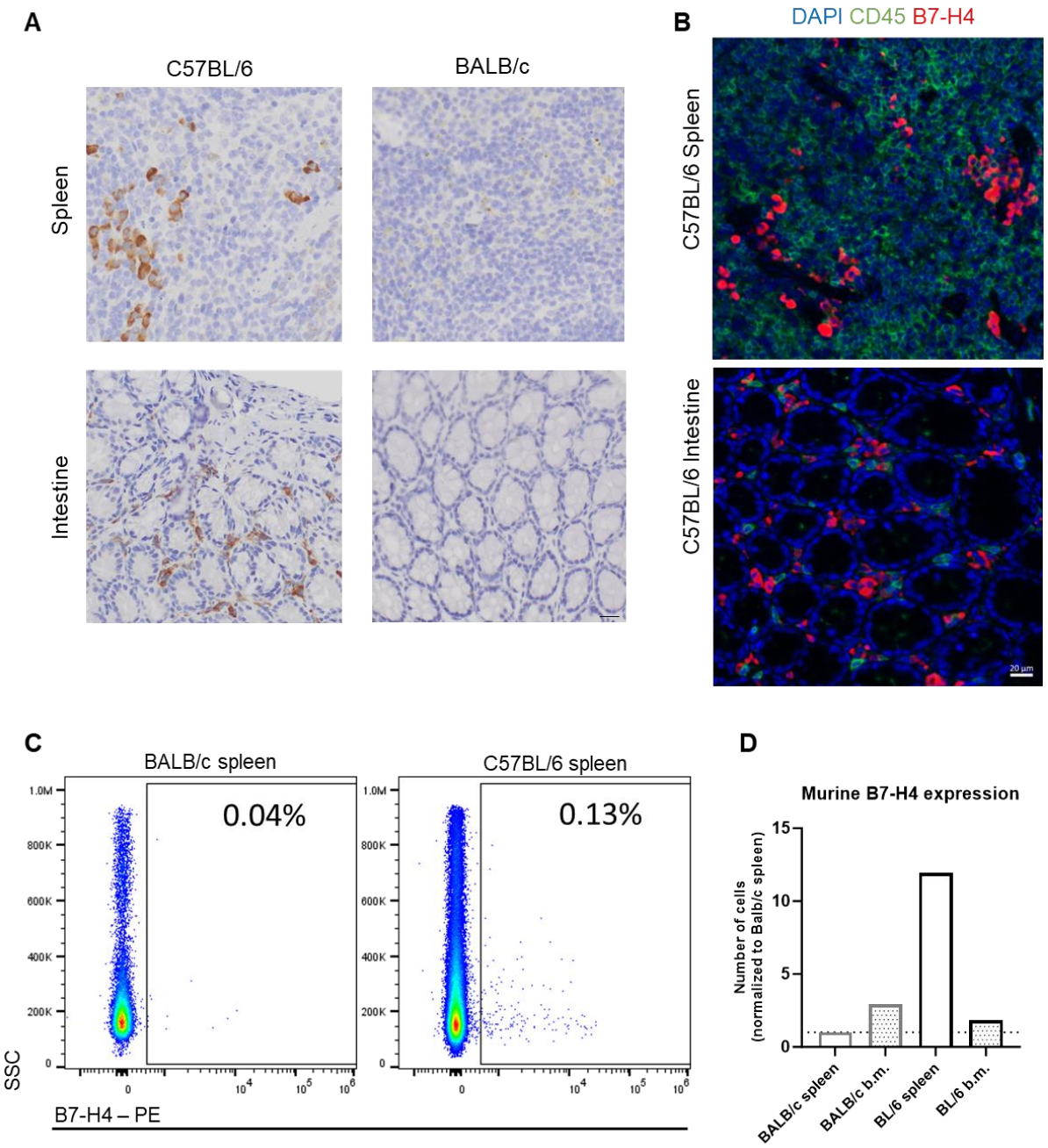

Figure IV.3. **B7-H4 was expressed on some tissue immune cells in the C57BL/6 model, but not the BALB/c model. (**A) Formalin-fixed, paraffin-embedded sections of BALB/c and C57BL/6 mice were stained for B7-H4, CD45, and DAPI using multiplexed immunofluorescence, or B7-H4 by IHC. CD45+ B7-H4+ cells were observed in spleen and intestine in C57BL/6 mice but not BALB/c mice. (B) Based on morphological characterization, these are likely macrophages. BALB/c spleen, intestine, and other healthy tissues examined (lymph node, fat pad, lung) had no B7-H4+ immune cells. Scale bar 20µm. (C) Flow cytometry of B7-H4+ cells are not present in the BALB/c spleen but are in the C57BL/6 spleen, similar to our findings by

mIF. (D) Representation of flow cytometry scatter plots. B7-H4+ immune cells were only found in the C57BL/6 spleen, not bone marrow (b.m.)

Anti-PD-L1 treatment did not induce a pro-inflammatory immune response in B7-H4+ tumors

B7-H4 is more highly expressed in immune cold human breast tumors, and B7-H4+ tumors in mice were less responsive to anti-PD-L1 therapy. Therefore, we asked how the amount and functional status of tumor infiltrating lymphocytes and myeloid cells were impacted by B7-H4 expression with or without treatment with ICI. When we assessed infiltrating immune cells ($CD45^+$) in our tumor model, we found similar populations of T cells and myeloid cells regardless of B7-H4 status (**Supplementary Figure 2**). We next performed Nanostring gene expression analysis using the Mouse Pan-Cancer Immune Panel of 770 genes to identify markers of functional changes in the tumor immune microenvironment. We wanted to test whether B7-H4 exerts an immunosuppressive effect in the context of immunotherapy-induced activation that could explain the lack of response to anti-PD-L1 in our tumor model. We compared sorted CD45+ tumor immune cells between EMT6 tumors with and without B7-H4 overexpression seven days post-treatment with anti-PD-L1. In the EMT6 control tumors, we saw an increase in transcriptomic markers of immune cell activation after anti-PD-L1 treatment compared to isotype treated tumors (**Figure 4.5A**). Many of these proinflammatory genes are expected in antitumor immunity including *Gzma*, *Gzmb*, *Prf1*, *Ifng*, and *Cxcl9/10* (**Supplementary Table 1**).

We further compared functional immune gene sets and observed markers of an immune-activated environment after anti-PD-L1 treatment (**Figure 4.5B**). In contrast, B7-H4+ tumors did not have the same markers of immune activation with anti-PD-L1 treatment (**Figure 4.5C-D**). While there are some markers of T cell activity including *Zap70* and *Lck*, these samples lack the upregulation of pro-inflammatory genes found in the EMT6 treated tumors (**Supplementary Table 2**). Additionally, B7-H4+ tumors in the isotype group have high expression of immunosuppressive genes including *Tgfbr1* (TGF-β receptor), *Cd33*, and *CD68*

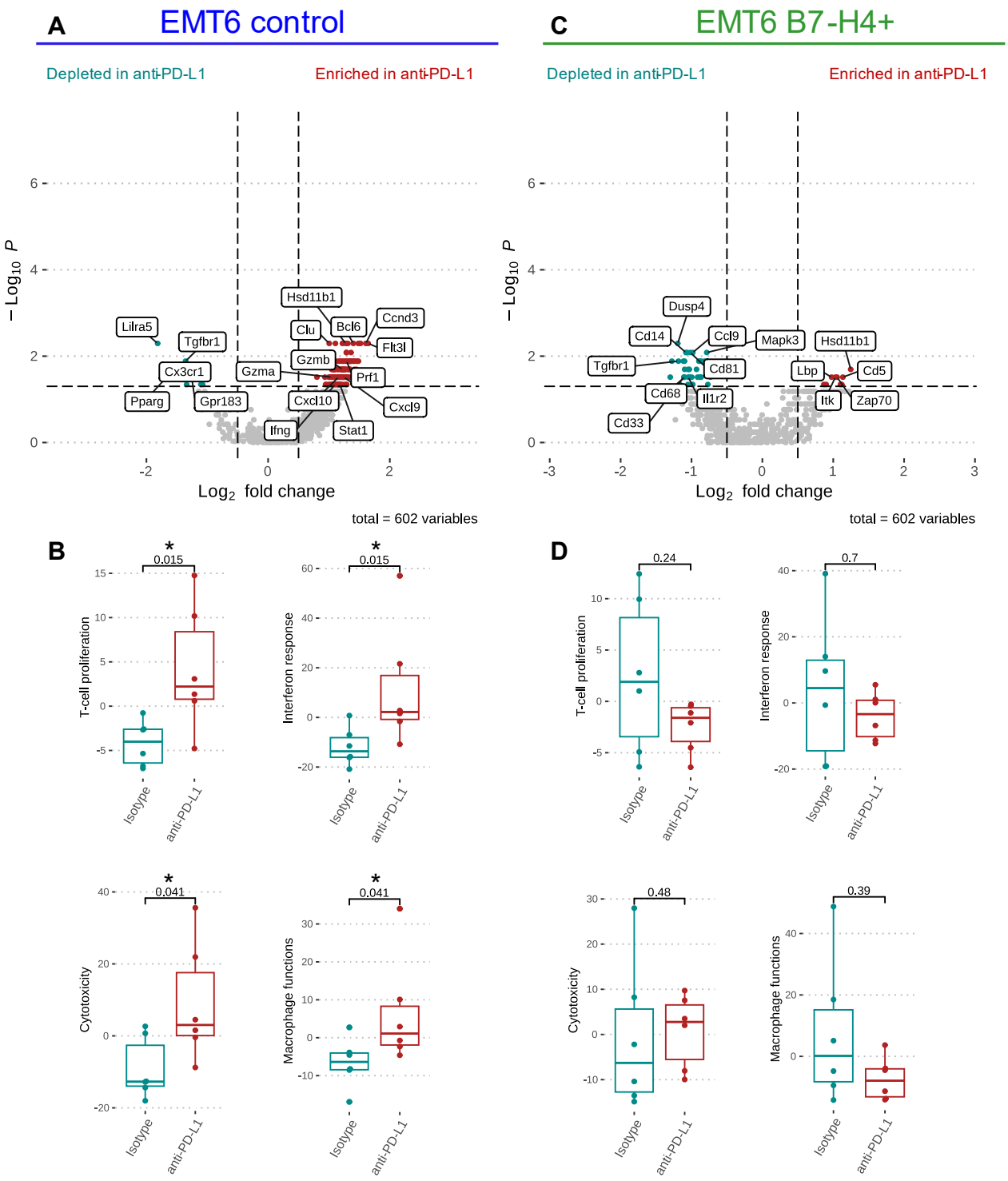

Figure IV.4. **Anti-PD-L1 did not induce a pro-inflammatory immune response in B7-H4+ tumors.** CD45+ cells were sorted from EMT6 tumors ± B7-H4 and subjected to Nanostring gene expression analysis using the Mouse Pan-Cancer Immune Panel. (A) Differentially expressed genes from CD45+ sorted cells from EMT6 control tumors when treated with anti-PD-L1 or isotype control and harvested 7 days post treatment. (B) Changes in immune gene sets between isotype and anti-PD-L1 treated tumors. (C) Differentially expressed genes from CD45+

sorted cells from EMT6 B7-H4+ tumors when treated with anti-PD-L1 or isotype control and harvested 7 days post treatment. (D) Changes in immune gene sets between treatment groups of EMT6 B7-H4+ tumors. Data were analyzed by Wilcoxon rank sum test. Genes with log2 fold change >0.5 or <-0.5 and p-value <0.01 were regarded as significant. n = 6 mice per group for all groups.

(tumor associated macrophage markers). These data suggest B7-H4 is functioning to inhibit full immune activation following ICI and associated with an immunosuppressive gene signature in the EMT6-B7-H4+ model.

We were also interested in whether CD45+ immune cells expressed markers of immune-activated status without ICI treatment. We measured gene expression in the CD45+ cells of early-stage, isotype treated tumors (harvested seven days after treatment). Genes involved in macrophage function were elevated in B7-H4+ tumors, but there were no other significantly different genes (**Figure 4.6A-B**). In CD45+ cells of later stage tumors (harvested at 500mm^3), genes involved in macrophage function were still elevated in B7-H4+ tumors. There was also a trend toward decreased cytotoxicity gene expression in the immune compartment that was not observed at the earlier timepoint (**Figure 4.6D**). *Mrc1*, a marker of M2 macrophages, was more highly expressed in B7-H4+ tumors, suggesting the elevated macrophage function could be immunosuppressive (**Figure 4.6C**). To test this, we further parsed the macrophage function gene set shown in Figure 4.5D into M1 and M2 macrophage genes. When we looked at the gene list overall, it appears EMT6-B7-H4+ tumors have slightly – but insignificantly – elevated expression of M1-related genes but do have significantly upregulated M2-related genes (Supplementary Figure 3). Therefore, B7-H4+ tumors may have a dominant M2-like macrophage phenotype contributing to immunosuppressive functions in the TME. A full list of differentially expressed genes is included (**Supplementary Tables 1-4**). Together, these data suggest B7-H4 is contributing to an immunosuppressive immune microenvironment and is inhibiting immune-activation after treatment with anti-PD-L1.

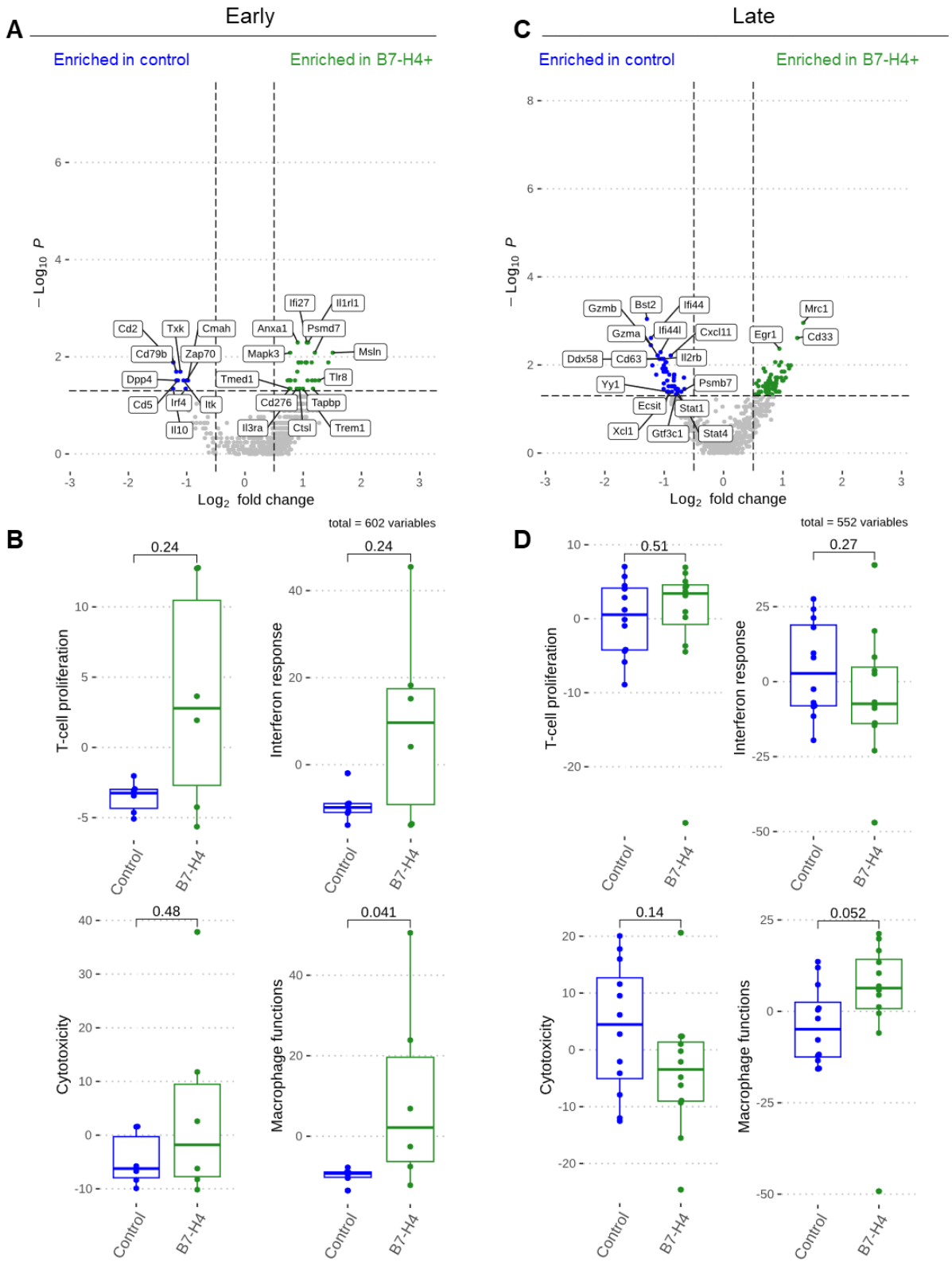

Figure IV.5. **CD45+ gene expression changes from early and later tumor stage between EMT6 control and B7-H4+ tumors.** (A) CD45+ cells were isolated from EMT6 control or B7-

H4+ tumors 7 days post treatment with isotype control antibody. Differentially expressed genes are shown. n = 6 mice per group. (B) Macrophage function was upregulated in B7-H4+ tumors, but minimal other differences were seen. (C) Differentially expressed genes between control and B7-H4+ tumors at a later stage. n = 12 mice per group. CD45+ cells were harvested when tumors reached 500mm3. (D) Macrophage function remains elevated in B7-H4+ tumors, but minimal differences were detected. Data were analyzed by Wilcoxon rank sum test. Genes with log2 fold change >0.5 or <-0.5 and p-value <0.01 were regarded as significant.

B7-H4 expression does not contribute to immunotherapy resistance in human breast cancers

Breast cancer patients with early stage (II-III) and advanced (PD-L1+) TNBC receive chemotherapy with pembrolizumab as standard of care. We tested whether B7-H4 expression in these patient populations also associated with ICI resistance. In the I-SPY2 RPPA cohort (NCT01042379) receiving paclitaxel ± pembrolizumab (followed by doxorubicin and cyclophosphamide), we observed, as others have shown[63,108], that B7-H4 expression was higher in TNBC tumors compared to HR+ tumors, but was expressed in HR+ tumors (**Figure 4.6A**). B7-H4 expression did not correlate with tumor grade (**Figure 4.6B**). We also observed no correlation with B7-H4 expression and pathological complete response (pCR) regardless of treatment with paclitaxel alone or paclitaxel plus pembrolizumab (**Figure 4.6C-D**). We wanted to test for any association with B7-H4 expression and patient survival, to see if the human data recapitulated our pre-clinical murine model. To that end, we analyzed both the patients with early-stage breast cancer (from ISPY2/NCT01042379) and advanced, metastatic TNBC (from NCT03206203). The patients with metastatic TNBC received carboplatin ± atezolizumab (anti-PD-L1) (NCT03206203)[72]. When B7-H4 expression was stratified into high (top 33%) and low (bottom 33%) patient subgroups, high expression was associated with worse event-free survival (EFS) in chemotherapy-alone treated patients with early-stage breast cancer, which appeared to be overcome by anti-PD-1 combination therapy (**Figure 4.6E**). However, when we adjusted for HR-status using a Cox proportional hazard analysis, this finding was no longer significant (p = 0.39). In contrast, we observed no correlation with progression-free survival (PFS) in patients with metastatic TNBC treated with anti-PD-L1 therapy (**Figure 4.6F**). To ask more specifically

whether B7-H4 high or low expressers differentially benefit from ICI, we compared survival by arm in each B7-H4 expression group. Paradoxically, we observed an improved benefit of B7-H4 expression with PFS after ICI in the metastatic setting, and no association with post-surgical EFS in the early setting (**Figure 4.6G-H**). These findings deviate from our observations in the murine model, suggesting that additional complex signaling mechanisms may be altering immunotherapy response. In fact, we found different endogenous B7-H4 expression patterns even between two murine models (**Figure 4.3**).

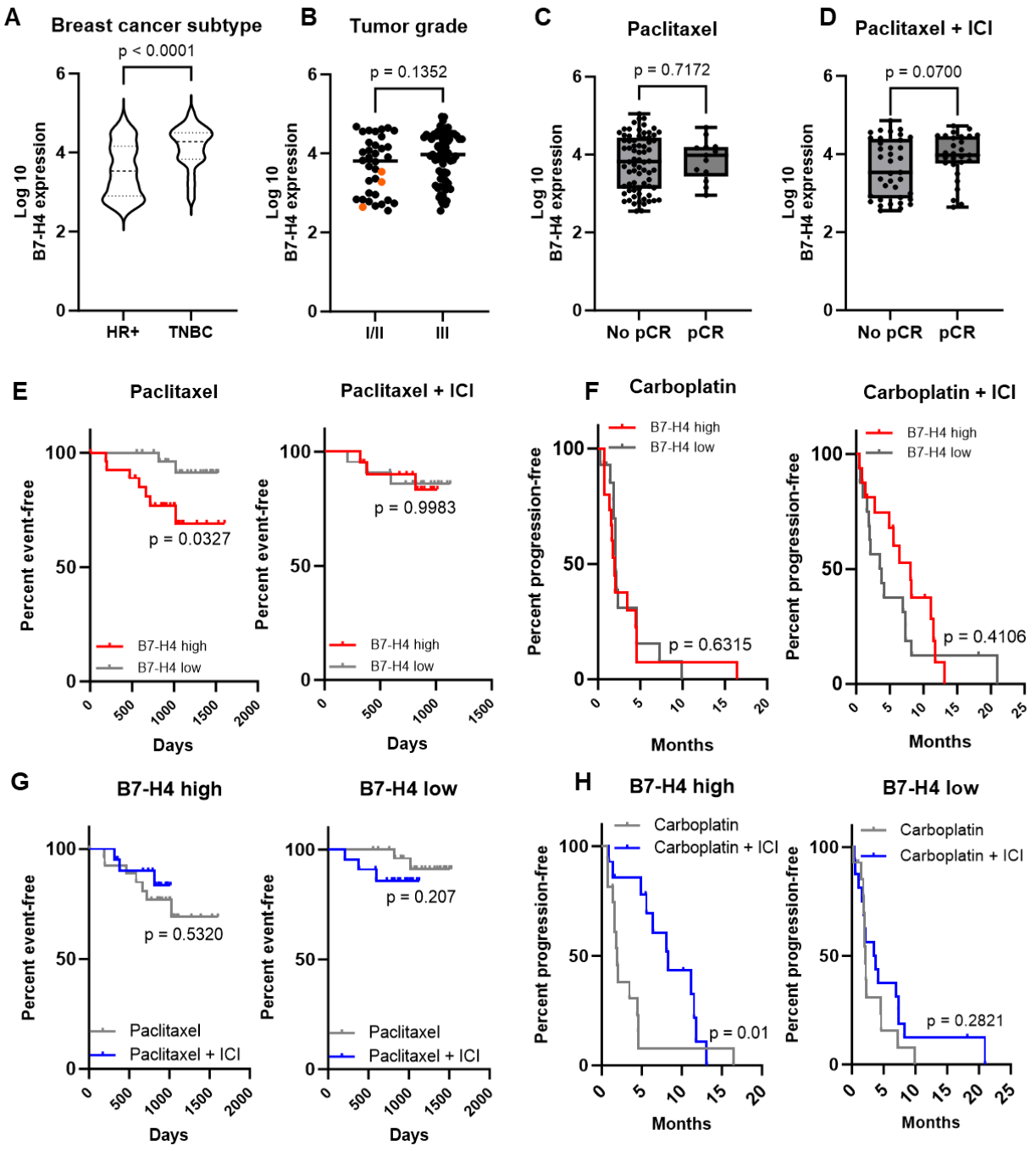

Figure IV.6. **B7-H4 expression does not correlate with resistance to chemotherapy + immunotherapy in human breast tumors.** Patients were from the I-SPY2 clinical trial (paclitaxel control and pembrolizumab arms) or the TBCRC 043 clinical trial (carboplatin control and atezolizumab arms). (A) In breast tumors from the I-SPY2 clinical trial (control and pembrolizumab arms), B7-H4 expression is higher in TNBC tumors compared to HR+ tumors. Data were analyzed by unpaired t-test. (B) In the same patient cohort, B7-H4 expression is not higher in grade III tumors compared to grade I (orange dots) or II. Data analyzed by unpaired t-test. (C-D) B7-H4 expression is not correlated with pathological complete response (pCR) in

tumors regardless of HR status, treated with either paclitaxel or paclitaxel + pembrolizumab (ICI). Data analyzed by unpaired t-test. (E) Event-free survival (EFS) in HR+ and TNBC tumors from the I-SPY2 cohort. Tumors with high B7-H4+ expression (top 33% of patients, expression > 60%) have worse EFS when treated with paclitaxel alone and no survival benefit when treated with paclitaxel + ICI. Data were analyzed by Log-rank Mantel-Cox test. (F) In the metastatic setting, progression-free survival (PFS) stratified by B7-H4 expression (top and bottom 33% of cohort) from primary breast biopsy or metastatic lesion in patients from the TBCRC 043 trial does not correlate with B7-H4 expression in either control or carboplatin + atezolizumab (ICI) groups. Data were analyzed by Log-rank Mantel-Cox test. (G-H) We also assessed survival by treatment status. Metastatic tumors (H) from TBCRC 043 with high B7-H4 expression had significantly improved PFS to ICI, and non-metastatic tumors (I-SPY2) had minimal improvement to ICI (G). Data were analyzed by Log-rank Mantel Cox test. n = 151 patients for A-E and G; n = 91 patients for F and H.

We wanted to test whether a beneficial response to chemotherapy was also observed in our murine EMT6 tumor model ± B7-H4. We treated both parental EMT6 tumors and EMT6-B7-H4+ tumors with paclitaxel, anti-PD-L1, combination, or vehicle following our dosing regimen described above for the EMT6 model. Briefly, mice were treated with first 200ug and subsequently 100ug appropriate therapy once weekly after tumors reached $100mm^3$ for 3 consecutive weeks. Tumors did not respond to single agent paclitaxel regardless of B7-H4 status. We also saw no significant synergistic effect of anti-PD-L1 combined with paclitaxel in tumors regardless of B7-H4 status (**Figure 4.7**). We also tested doxorubicin chemotherapy in our murine EMT6 tumor model and again saw no response to single-agent chemotherapy, whether administered intravenously or intraperitoneal (**Figure 4.8**). Collectively, these data suggest B7-H4 may not be a reliable biomarker for ICI resistance in breast cancer patients and more research is needed to understand its regulation in human and mouse cancers.

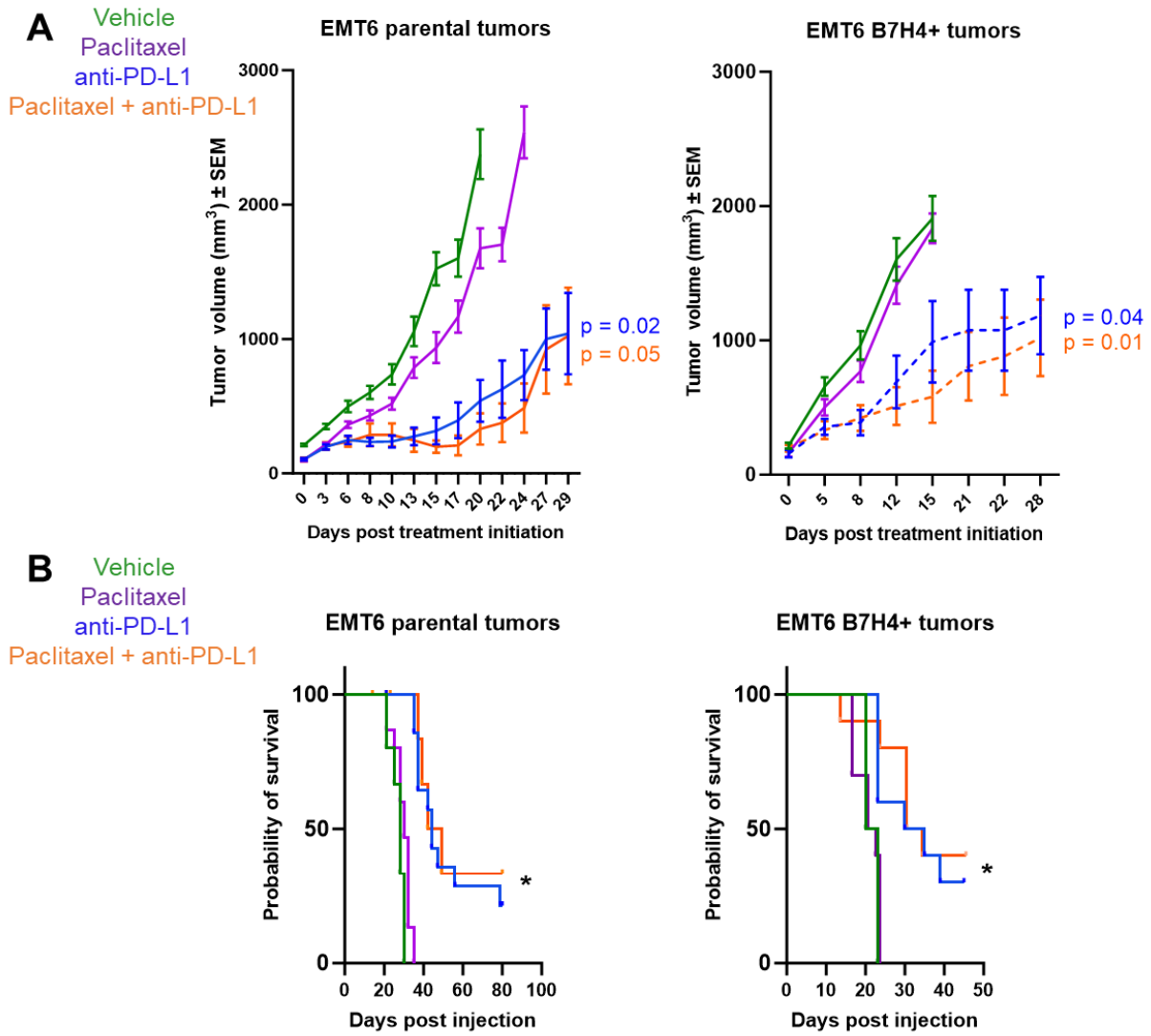

Figure IV.7. **EMT6 tumors do not respond to single-agent chemotherapy. (**A) EMT6 parental or B7-H4+ tumors treated with vehicle (isotype control), anti-PD-L1, paclitaxel chemotherapy, or anti-PD-L1 + paclitaxel (n=15/group parental and n = 10/group B7-H4+). We observed no tumor response to paclitaxel single-agent therapy and thus the response observed in the combination treatment group is driven by anti-PD-L1 effects. (One-way ANOVA with Tukey's post-hoc test for multiple comparisons. P values as shown. (B) Survival of EMT6 parental or B7-H4+ tumors. We observed significant survival of the anti-PD-L1 and combination treatment groups in both tumor types compared to vehicle or paclitaxel treatment groups. (Data were analyzed by Log-rank Mantel-Cox test. Statistics performed in GraphPad Prism v10).

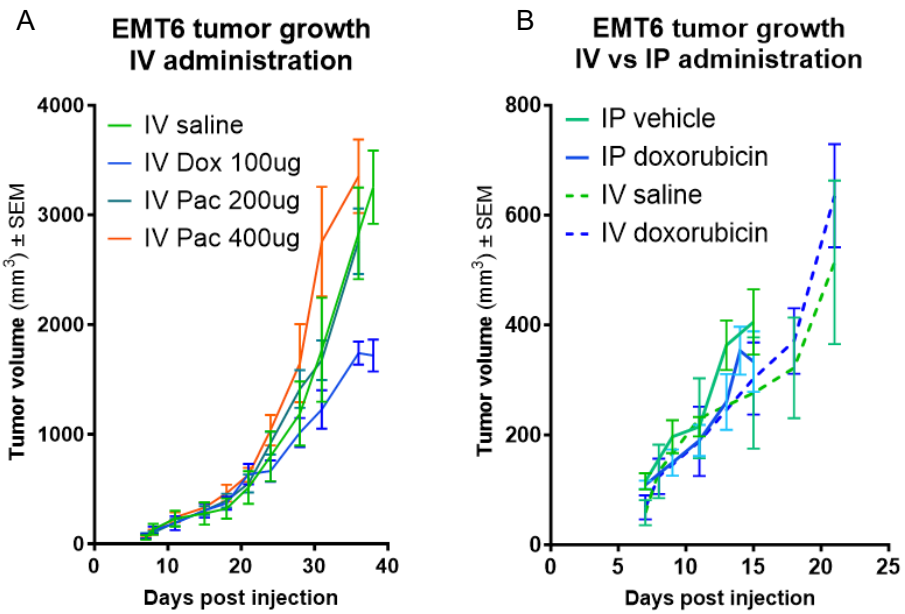

Figure IV.8. **EMT6 tumors do not respond to doxorubicin or paclitaxel regardless of administration route.** (A) EMT6 tumors were intravenously treated with vehicle (saline), paclitaxel, or doxorubicin chemotherapy at the indicated doses, one time weekly for 4 weeks, after tumors reached 100mm^3. Tumors were resistant to chemotherapy regardless of drug and dose. (B) EMT6 tumors were treated with doxorubicin either via intraperitoneal (IP) or intravenous (IV) route of administration at 200ug for the first week, and 100ug once weekly for three additional weeks. Tumors were resistant regardless of treatment administration route.

Discussion

We have shown that B7-H4, which is highly conserved between mice and humans[50] and is strongly associated with epithelial cell status in both murine and human breast cancer cells. However, that may be where the similarities end. In our EMT6 murine model, B7-H4 expression contributed to single-agent immunotherapy resistance and decreased immune cell function (particularly T cell function, as has been previously described)[50,51,62]. Additionally, in a pre-clinical murine C3TAg tumor model, Liu *et al.* described murine B7-H4 KO was sufficient to sensitize tumors to immunotherapy[109]. Surprisingly, when we assessed early-stage and advanced breast cancer patients, we found the opposite phenomenon. B7-H4 expression had minimal effect to ICI response and in one cohort was even associated with improved survival. The biggest difference in study design between the clinical trials and our pre-clinical models was the inclusion of chemotherapy with the immunotherapy regimen. The patients analyzed from

NCT01042379 had early-stage breast cancer and received neoadjuvant paclitaxel with four rounds of pembrolizumab, followed by doxorubicin and cyclophosphamide[43]. The patients as part of NCT03206203 had metastatic TNBC and received carboplatin and atezolizumab together intravenously every 3 weeks until intolerability[45]. When we combined anti-PD-L1 with chemotherapy in our pre-clinical EMT6 model ± B7-H4, we observed no tumor response to paclitaxel chemotherapy alone and no improved tumor response with paclitaxel + anti-PD-L1 over anti-PD-L1 alone. We also observed no response to single-agent paclitaxel or doxorubicin chemotherapy in the EMT6 model. This suggests different mechanisms of action between the human and mouse tumor response to chemotherapy and immunotherapy.

In our pre-clinical model, B7-H4 had a moderate effect on immune cell signaling, most notably in a reduction of cytotoxic T cell function and an increase of immunosuppressive macrophage function, assessed by Nanostring gene expression. Interestingly, B7-H4 expression in treated tumors seems to dampen or inhibit the same induction of immune activation by anti-PD-L1 treatment in the EMT6 controls. It would be interesting to validate these findings by performing a T cell (CD4+ and CD8+) depletion animal study to confirm whether T cell-mediated immunity was a primary mechanism of tumor response or resistance to anti-PD-L1. Identifying the mechanism(s) of B7-H4-mediated immunosuppression within a complex tumor microenvironment, including identifying the receptor and cells expressing the receptor, is an avenue for future experiments.

There are several limitations and caveats to this study. First, we demonstrated B7-H4-induced anti-PD-L1 resistance (gain of function; sufficiency) in a single mouse model. Moreover, we were unable to identify a reciprocal loss of function model (i.e. B7-H4-KO) to test necessity of B7-H4 expression for anti-PD-L1 resistance; however, given that breaks in the tumor immunity cycle can exist at nearly any point in the path, identifying a model that innately expresses B7-H4 in the tumor compartment, and wherein this feature is the sole effector of

resistance to anti-PD-L1 is far less likely given the general paucity of models in the field. Nonetheless, independent and external confirmation was recently published by Liu *et al*, suggesting broader applicability and validity in murine breast tumors, including loss of function leading to enhanced sensitivity to anti-PD-L1[109].

We also observed resistance to chemotherapy in the EMT6 model regardless of B7-H4 status, prohibiting a more direct comparison in study design to the human clinical trial data. Additionally, we observed changes in immune cell gene expression with tumor B7-H4 expression that were not supported by our flow cytometry experiments. These contrasting findings could be due to differences in phenotyping based on gene expression profiling (more quantitative, and reliable but less functional) versus phenotyping by several limited characteristic markers like CD206 expression or granzyme staining. Nonetheless, the combined analysis of both mRNA profiling and immunophenotyping by flow suggest changes in macrophage functionality and generally less T cell activation with B7-H4 expression, particularly in later tumor stages. Future experiments using detailed phenotyping flow cytometry as well as RNA sequencing may shed more light on the mechanism of B7-H4 immunosuppression *in vivo*.

The patients with early-stage breast cancer were also a mixed cohort with HR+ and TNBC and were combined for analysis due to sample size constraints and because both groups demonstrated considerable, but heterogeneous B7-H4 expression. TNBC may have higher expression of B7-H4, but it is not exclusive to that subtype and could be highly expressed in immune-cold tumors regardless of subtype. For example, the MMTV-neu murine model emulates luminal-like HER2+ BC and endogenously expresses B7-H4.

In conclusion, our data show a broad exploration of B7-H4 expression and function in murine and human breast cancer. Based on the difference in tumor progression, or lack thereof, in the human cohorts and mouse models, future understanding of the mechanisms of B7-H4 *in vivo* are essential to rule out or include B7-H4 as a potential biomarker for future breast cancer

patients. Instead of an immune checkpoint, B7-H4 could be a better target for antibody-drug-conjugate (ADC) development, as multiple companies are doing[108,110]. In fact, to our knowledge, there are no B7-H4 blocking antibodies in clinical trials. These ADCs target B7-H4 independent of ICI resistance and may prove a better direction for the field of breast cancer treatment.

Chapter V: FUTURE EXPERIMENTS AND CONSIDERATIONS

Introduction

From the data that have been presented, there remain a number of future experimental directions. Throughout our work, we have strived to identify a mechanism for putative B7-H4 immunosuppressive function in mice that has been suggested throughout the literature[50,51,62]. Dr. Liepeng Chen's group that initially published their discoveries of the checkpoint ligand B7-H4 validated its phenotypic function of suppression of activated T cells *in vitro.* Since then, several groups have identified B7-H4 expression in breast cancer, but there is yet no cancer-specific mechanisms for B7-H4 immunosuppression *in vivo*[57,59,61,65,95,111]. One group studied the effect of host B7-H4 expression on murine tumor growth and found host B7-H4 both dampened antitumor Th1 immune response, but also inhibited pro-tumor myeloid-derived suppressor cells in 4T1 mammary tumors[112]. Another group observed that B7-H4 KO mice had fewer metastatic nodules in the lungs upon 4T1 challenge, suggesting B7-H4 functions primarily as a pro-tumor ligand[113].

As there are still gaps in the field as to the primary functions of B7-H4 in breast tumors and based on our *in vivo* experiments of tumor-specific B7-H4 overexpression, we hypothesized B7-H4 may be acting as an immunosuppressive ligand to tumor-infiltrating T cells as a primary mechanism of resistance to immunotherapy. First, we performed experiments understand the mechanism of B7-H4 protein expression in breast cancer cell lines. We also propose a unique hypothesis involving B7-H4 recruitment of M2 immunosuppressive macrophages that as yet had been unexplored. Finally, one of the biggest unanswered questions in the field of B7-H4 biology is the identity of its receptor binding protein, so we propose two potential experimental strategies to shed light on what protein(s) could be binding to the ligand in the TME.

To that end, the following chapter includes preliminary and/or inconclusive experiments that attempted to validate and test hypotheses for how B7-H4 could suppress ICI induced

immune activation that we saw in the murine EMT6 tumor model. We also introduce and discuss future experiments for unanswered questions surrounding B7-H4 biology. Relevant methods for each set of experiments are included in the figure legends and/or Appendix III.

Additionally, we present some initial work seeking to understand the cell signaling regulation and expression of B7-H4 in some breast cancers but not all. As previously stated, B7-H4 and PD-L1 expression is often mutually exclusively in breast tumors suggesting a different mechanism of regulation[59,61,67]. While we identified the strong correlation between B7-H4 and epithelial cell status, we also sought to identify a mechanism for differential B7-H4 expression on a per cell basis. Below include some initial data suggesting a mechanism of B7-H4 regulation by PI3K signaling, and additional experiments needed to clarify tumor cell signaling of B7-H4.

B7-H4 is regulated by PI3K signaling[3]

Several investigators have observed inverse patterns of expression between B7-H4 and PD-L1 in breast tumors[59,61]. We attempted to associate B7-H4 with epithelial-to-mesenchymal transition in the MMTV-neu cell line, as presented in Chapter III. When we observed no causal mechanism, we attempted to modulate additional signaling pathways in B7-H4+ cancer cells to identify potential regulatory elements.

Because PD-L1 is highly inducible with both alpha and gamma interferon, it has been suggested that B7-H4 is similarly inducible by alpha and/or gamma interferon[50,114–117]. Conversely, we tested whether interferons inhibited B7-H4 expression to explain the phenomenon of PD-L1 and B7-H4 mutually exclusive expression[116,117]. Treatment of MMTV-neu

[3] Some of these data have been published in Wescott, E.C.*, Sun, X., Gonzalez-Ericsson, P.I., Hanna, A., Taylor, B.C., Sanchez, V., Bronzini, J., Opalenik, S.R., Sanders, M.E., Wulfkuhle, J., Gallagher, R.I., Gomez, H., Isaacs, C., Bharti, V., Wilson, J.T., Ballinger, T.J., Santa-Maria, C.A., Shah, P.D., Dees, E.C., Lehmann, B.D., Abramson, V.G., Hirst, G.L., Brown-Swigart, L., van 't Veer, L.J., Esserman, L.J., Petricoin, E.F., Pietenpol, J.A., Balko, J.M. (2024). Epithelial expressed B7-H4 drives differential immunotherapy response in murine and human breast cancer. *Cancer Research Communications*; 4 (4): 1120-1134.

B7-H4+ cells with alpha or gamma interferon did not alter endogenous B7-H4 levels, nor was B7-H4 induced on several B7-H4-negative murine cell lines (**Figure 5.1**). We also tested whether TGFβ, a potent stimulator of EMT, modulated B7-H4 cell surface expression[118]. We saw no change in B7-H4 expression in negative or positive cell lines by treatment with TGFβ.

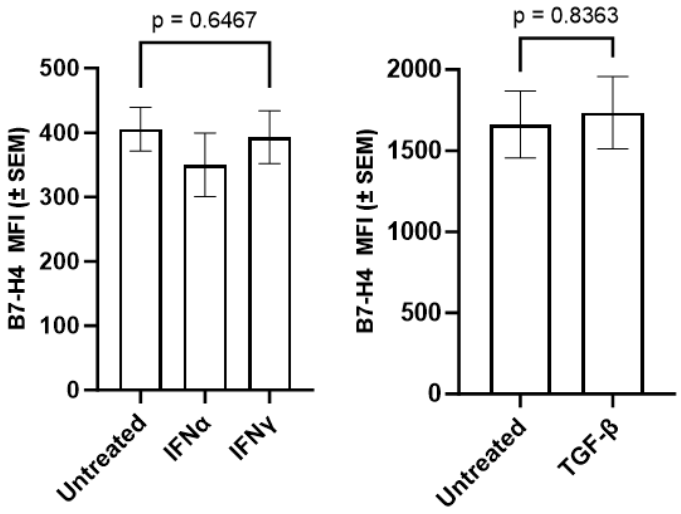

Figure V.1. **B7-H4 expression is not affected by type I or II interferon or TGF-β treatment *in vitro*.** MMTV-neu epithelial cells that have high levels of endogenous B7-H4 were treated for 72 hours with IFNα or IFNγ at 100ng/mL. B7-H4 expression was analyzed by flow cytometry (n=4-5 per group). Similarly, B7-H4 expression was not altered by TGF-β expression (10 ng/mL) *in vitro* after 72 hours. Data were analyzed by One-way ANOVA or unpaired t-test.

To determine other possible pathways regulating B7-H4 expression in tumor cells, we utilized published data from the I-SPY2 neoadjuvant clinical trial of early-stage breast cancer at high risk of recurrence (NCT01042379) that were assayed with reverse phase protein array (RPPA) from laser-capture micro-dissected tumor regions[43,75]. These data include measurements of 121 protein/phosphoproteins in 151 patients treated with neoadjuvant chemotherapy (NAC) alone or NAC + pembrolizumab, with associated clinical outcomes data. For this study, additional RPPA measurements using the same lysates were made for B7-H4 expression in the tumor compartment and compared to the existing phospho-proteomic data. We tested for the existence of significant positive or negative correlations between B7-H4 protein expression and additional tumor proteins from this cohort (**Figure 5.2A**). Interestingly,

we observed strong positive correlations of B7-H4 with PI3K (phosphatidylinositol-3-kinase) and pAKT (as well as EGFR, which can activate PI3K) signaling on tumor cells, but negative correlations between B7-H4 and PTEN expression, a negative regulator of PI3K activity (**Figure 5.2A-B**).

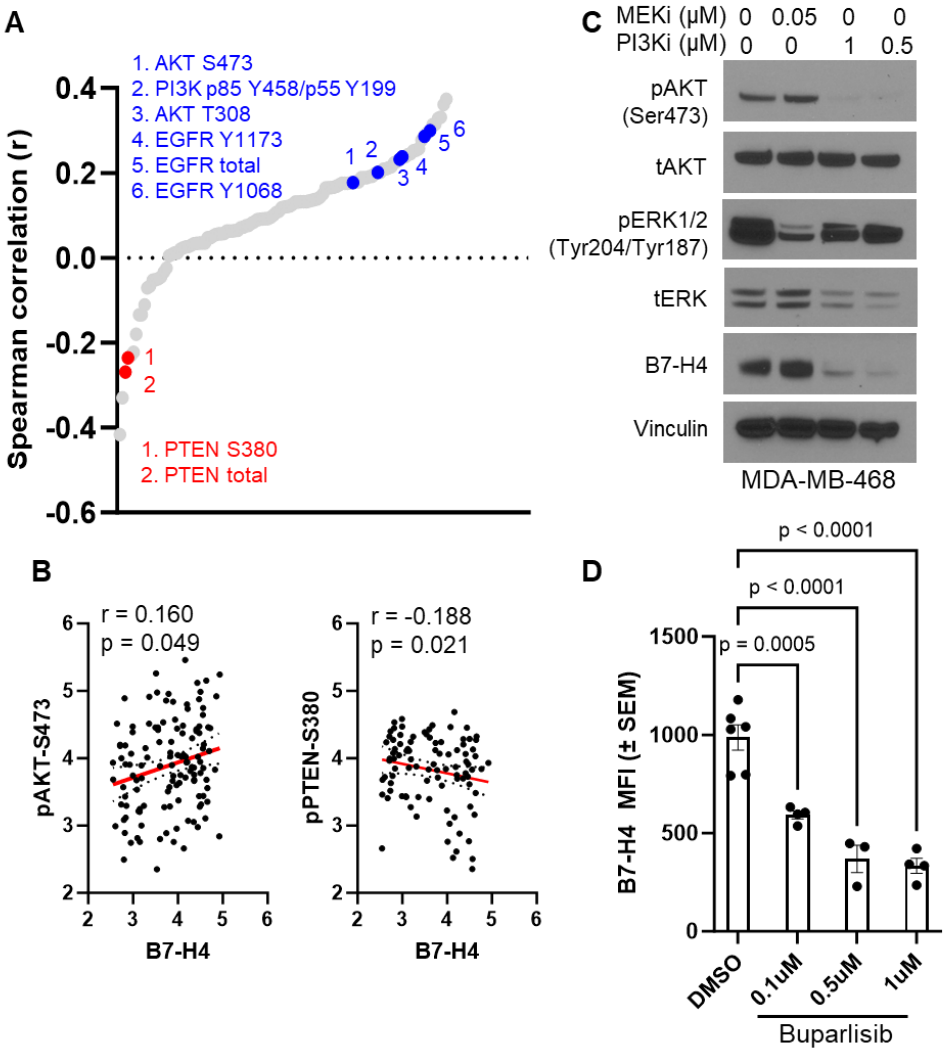

Figure V.2. **B7-H4 expression is regulated by PI3K signaling.** (A) Spearman correlations in protein expression from reverse phase protein array (RPPA) data collected from patients from the ISPY2 trial. Key positive correlations are called out in blue and key negative correlations are called out in red. (B) RPPA data show strong positive correlations between B7-H4 and AKT (pAKT-Ser 473) and strong negative correlations between B7-H4 and PTEN (Ser 380) regardless of tumor hormone receptor status. (C) PI3K inhibitor (buparlisib) treatment for 72 hours robustly decreases B7-H4 expression in human MDA-MB-468 breast cancer cells, while MEK inhibitor (Trametinib) has no effect. (D) Likewise, in MMTV-neu cells, buparlisib reduces B7-H4 expression in dose-dependent manner after 72 hours. Data were analyzed by one-way ANOVA with Dunnet's post-hoc test for multiple comparisons, $p<0.0001$ and $p=0.0005$).

Based on these findings, we tested whether specific inhibition of the PI3K pathway affected B7-H4 expression in breast cancer cells. MDA-MB-468 cells are a basal human TNBC cell line with endogenous B7-H4 expression. When these cells were treated with a pan-PI3K inhibitor (buparlisib) for 72 hours, B7-H4 expression was ablated (**Figure 5.2C**). We also tested the effect of the same pan-PI3K inhibitor in murine MMTV-neu epithelial cells that as shown above also have high levels of endogenous B7-H4. Like MDA-MB-468 cells, surface B7-H4 expression decreased on the MMTV-neu epithelial cells in a concentration-dependent manner when measured by flow cytometry (**Figure 5.2D**).

In addition to these experiments with the buparlisib PI3K inhibitor, we also verified gene expression levels of *VTCN1* in our murine and human cancer cells. Surprisingly, despite seeing a consistent downregulation of B7-H4 protein in both cell lines, we did not see similar differences at the mRNA level (**Figure 5.3**). We also tested the effect of PI3K inhibition on virally transduced EMT6 cancer cells expressing B7-H4 to test whether the effect of buparlisib was specific to protein translated from the endogenous host promoter. The EMT6 cells were virally transduced using the pBabe retroviral vector as described above and thus not under control of the endogenous promoter and transcriptional regulatory elements. The EMT6-B7-H4 cell expression did not change after 72 hours of buparlisib treatment when assessed by flow-cytometry (**Figure 5.4**).

Taken together, these data elucidate a potential mechanism of B7-H4 regulation by PI3K signaling in breast tumors. In both murine and human cancer cells with endogenous B7-H4 expression, PI3K inhibitor treatment reduced and nearly ablated B7-H4 protein. Conversely, in EMT6 cells virally transduced to express B7-H4, no change in expression was observed. Finally, we observed no change in *VTCN1* RNA expression following buparlisib treatment.

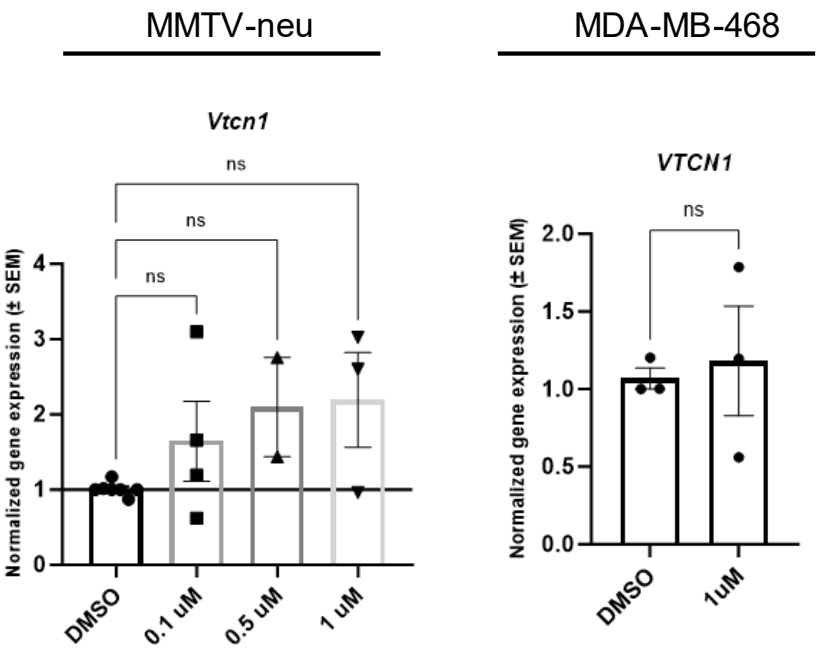

Figure V.3. **PI3K inhibition (buparlisib) did not inhibit *VTCN1* mRNA expression.** MMTV-neu murine or MDA-MB-468 cancer cells were treated with PI3Ki (buparlisib) at the indicated concentrations for 24h and mRNA was quantified by Real Time PCR. Data were analyzed by either One-way ANOVA with Sidak's test for multiple comparisons or unpaired t-test.

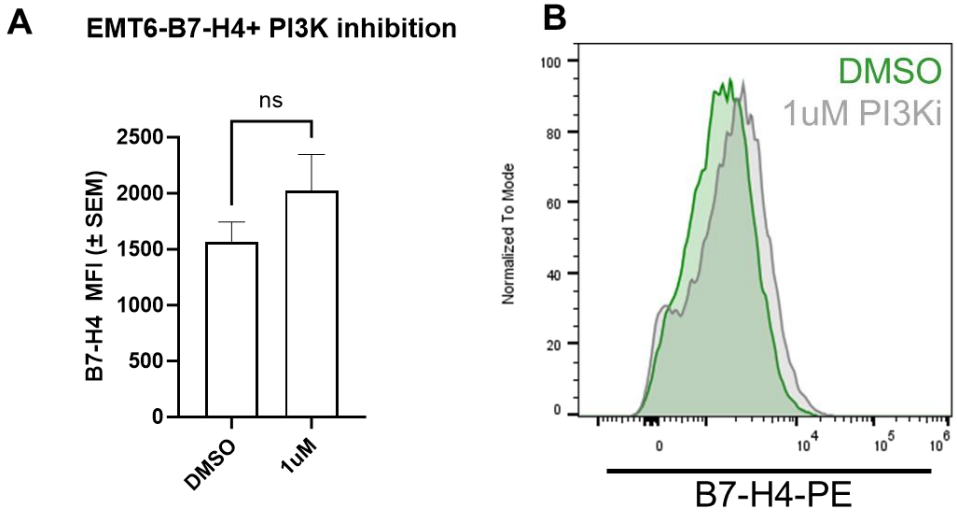

Figure V.4. **PI3K inhibition did not inhibit B7-H4 protein in virally transduced cancer cells.** EMT6 cells with B7-H4 expression via viral transduction were treated with 1uM PI3Ki (buparlisib) for 72 hours before measurement by flow cytometry. Data shown represent 2 independent experiments and were analyzed by unpaired t-test. A representative histogram of the data is shown in (B).

Discussion and future experiments

Phosphatidylinositol-3-kinase (PI3K) mutations are one of the most observed genetic alterations in breast cancer. PI3K phosphorylates membrane phosphatidylinositol and recruits AKT to the cell membrane. Once AKT is phosphorylated by the TORC2 complex, the downstream signaling cascade of cellular growth, proliferation, survival, and angiogenesis occurs[119,120]. As the PI3K signaling pathway is involved in cell growth, survival, and metabolism, its dysregulation is a hallmark of cancer. The tumor suppressor PTEN reverses the effects of PI3K signaling and thus it was expected to observe inverse correlations between PTEN and PI3K signaling proteins in the RPPA breast cancer data set. Many tumor types have activating mutations in *PIK3CA* and inactivating mutations in *PTEN*, thus facilitating tumor progression[119,120].

In luminal breast cancer, which is characterized by estrogen receptor (ER) expression and hormone dependence, PI3K mutations occur at a lower frequency than in basal-like breast cancer. However, these mutations are still observed in up to 30% of luminal breast cancers and are associated with poorer outcomes and resistance to endocrine therapy[121,122]. One common PI3K mutation in cancer is the hotspot mutation E545K in the *PIK3CA* gene, which leads to constitutive activation of the PI3K pathway[123]. Studies have shown that this mutation confers resistance to endocrine therapy by promoting ER phosphorylation and activation[124,125].

Basal-like breast cancer, which is characterized by lack of ER, progesterone receptor (PR), and HER2 amplification or mutation, has a higher frequency of PI3K mutations, with up to 80% of cases harboring these mutations[4,8]. PI3K mutations in basal-like breast cancer include the hotspot mutations H1047R and E545K in the *PIK3CA* gene and are associated with increased cancer cell proliferation and survival[123]. PI3K mutations in basal-like breast cancer, including TNBC, are associated with resistance to chemotherapy, ICI, and overall poor outcomes[122,126,127]. B7-H4 is also highly expressed in TNBC, associated with worse outcomes, and associated with resistance to ICI in mice though not in human TNBC (as shown in Chapter

IV). This suggests the potential correlation between PI3K pathway mutation status and B7-H4 regulation in breast cancer and a proposed combinatorial effect of these pathways in BC. It would be interesting to assess the direct association in B7-H4 expression, PI3K activation, and therapeutic response in TNBC clinical trial cohorts as discussed in Chapter IV.

The data presented above suggest the pan-PI3K inhibitor buparlisib is acting on B7-H4 protein levels at the level of translation or post-translational modification because we see no changes in gene expression. To test this, we can perform a cycloheximide chase assay to measure whether the protein is being degraded or not being translated. Cycloheximide inhibits the elongation step in protein translation, thus preventing protein synthesis[128,129]. We will incubate MMTV-neu and/or MDA-MB-468 cancer cells in media containing cycloheximide for between 2-8 hours to inhibit protein synthesis. After this, we will replace the media with media ± buparlisib for up to 72 hours. We can measure and semi-quantify protein expression via western blotting. If the PI3K inhibition was inhibiting B7-H4 at the protein translation level, we would expect low to no protein following the cycloheximide and buparlisib treatments compared to just cycloheximide treatment. If PI3K inhibition was acting at the post-translational modification level, then we would expect to see some B7-H4 protein being produced.

Several considerations for this experiment include the non-specific effect of cycloheximide on other cellular proteins. We have not yet tested whether PI3K inhibition exerts effects on other B7-family ligand proteins. As it is likely the pan-PI3K inhibitor buparlisib does have off-target effects in the cell, it would be interesting to perform bulk RNA sequencing after treatment to identify any other changes to gene expression in treated cancer cells. As we have observed differences in the effect at the RNA and protein levels, this experiment would need to be followed by an assessment of protein changes. In particular, the biggest caveat to an RNA sequencing experiment was our lack of identifying changes to *VTCN1* gene expression after buparlisib treatment. Nonetheless, RNA sequencing may provide clues to potential other signaling pathways for further study, some of which could be crucial to B7-H4 regulation.

B7-H4 did not significantly suppress T cell activation *in vitro*

One of the predominant hypotheses in the field and one with preliminary published data is that B7-H4 acts as an immunosuppressive ligand by binding to its unknown cognate receptor found on T cells. Thus, we tested both whether purified B7-H4 protein had a suppressive effect on T cells *in vitro* and whether cell-expressed B7-H4 on our EMT6 cell line affected T cell phenotype of syngeneic BALB/c T cells *in vitro* to validate previously published data. We largely found no difference in T cell proliferation when cells were cultured with varying concentrations of B7-H4. Some of these data are shown below (**Figure 5.5**). These results are seemingly contradictory to previously published data, and potential experimental design issues are discussed further below. While slight differences are seen in the number of cells within each numbered cell division peak, more experiments are needed to parse subtle differences that could be representative of experimental variation.

One concern we had was the possibility of unequal coating or inadequate adherence of B7-H4 to the tissue culture plate. Thus, we also tested whether our EMT6 cells expressing murine B7-H4 had an inhibitory effect on syngeneic BALB/c T cells *in vitro* as this could explain the reduction in anti-tumor immunity that we observed in our EMT6 tumor model. Additionally, EMT6 cells could be producing cytokines in cell culture media that could further alter T cell proliferation and/or activation. We cocultured syngeneic BALB/c splenocytes with EMT6 tumors cells ± B7-H4 expression and measured T cell proliferation after 72 hours and cytokine production after 48 hours (**Figure 5.5**). As before, we observed no change in T cell divisions. Data shown are live total splenocytes, however the conclusions are identical when gating on CD4 or CD8 T cells specifically. We also saw no difference in Gzmb cytokine production after 48 hours of co-culture with EMT6-B7-H4 tumor cells. These data suggest that cell-surface B7-H4 did not exert an immunosuppressive effect on activated T cells *in vitro* that was detectable by our experimental methods.

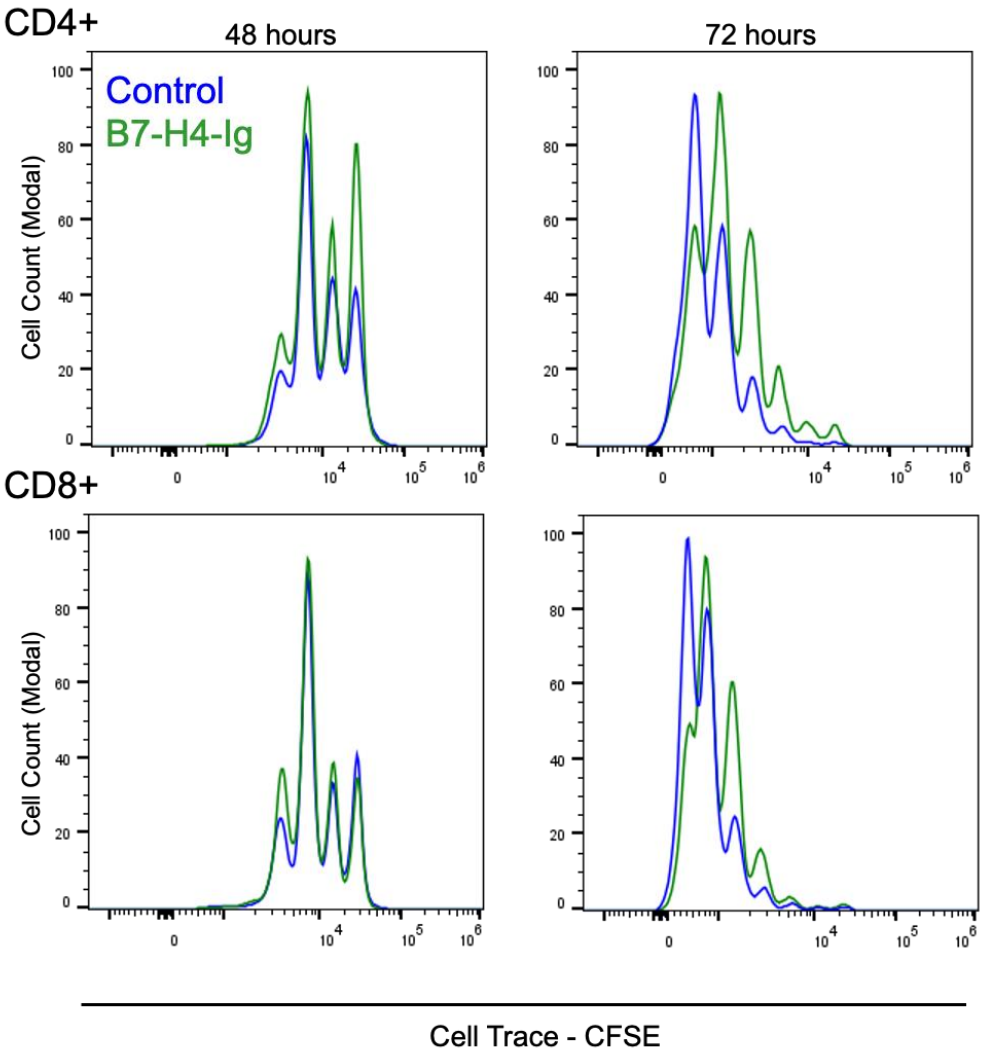

Figure V.5. **B7-H4 protein did not reduce T cell proliferation upon activation *in vitro*.** T cells were isolated from BALB/c mice and sorted using the Miltenyi T cell isolation kit. Cells were plated at 80,000-100,000 cells/well in 96-well plates coated with B7-H4-Ig protein (R&D) at 5ug/mL. Cell proliferation was measured by flow cytometry after 48 and 72 hours gated on CD4+ and CD8+ T cells. Data shown are representative of 2 experimental replicates.

Discussion and future experiments

Many studies have investigated the immunosuppressive role of B7-H4 protein, *in vitro*, in autoimmune conditions such as systemic lupus erythematosus (SLE), and within various cancer types. After the 2003 discovery of this ligand, it was established that B7-H4 exerted inhibitory effects on activated CD4+ murine T cells[50,62]. Additional studies have been conducted in breast

cancers, ovarian cancer, and others. In colorectal cancer and hepatocellular carcinoma, B7-H4 promoted tumor progression, specifically through CD8 T cell exhaustion and promotion of myeloid derived suppressive cells (MDSCs)[130,131]. B7-H4 has also been shown to play an immunosuppressive role in murine SLE[132]. In that study, B7-H4 protein reduced lupus manifestations. B7-H4 has perhaps been most studied in breast cancer above other cancer types, due to its high expression in TNBC that still lacks targeted therapies to match those available to HR+ cancers. Several groups have observed B7-H4 immunosuppressive effects in BC but no direct mechanism has yet been identified[59,61,63,133]. These studies have primarily correlated B7-H4+ tumors with lack of tumor immune cells. However, there are still gaps in the field of specific immunosuppressive mechanisms due to B7-H4 expression, which my experiments have sought to address.

One of the most likely reasons for the lack of inhibitory effect by B7-H4 protein is the presence of strong activation signals in our co-cultures. In the 2003 studies, investigators observed the greatest effect of B7-H4 on T cells in the absence of co-stimulatory CD28. In our experiments, we activated T cells as normal with CD3/CD28 + IL-2 to ensure adequate cell proliferation. Future experiments can titrate the magnitude of stimulus and/or remove CD28 co-stimulation from the assay to see if differences are more significant. Another caveat to these experiments is the differences between human and murine B7-H4 function *in vivo* as presented in Chapter IV. Up to this point, nearly all investigators have relied on pre-clinical murine studies of B7-H4 function to inform therapeutic designs. However, one group has observed similar immunosuppressive effects of human B7-H4 protein on human T cells *in vitro* indicating some translational relevance of B7-H4 function between mice and humans[110]. The extent of these similarities has yet to be determined.

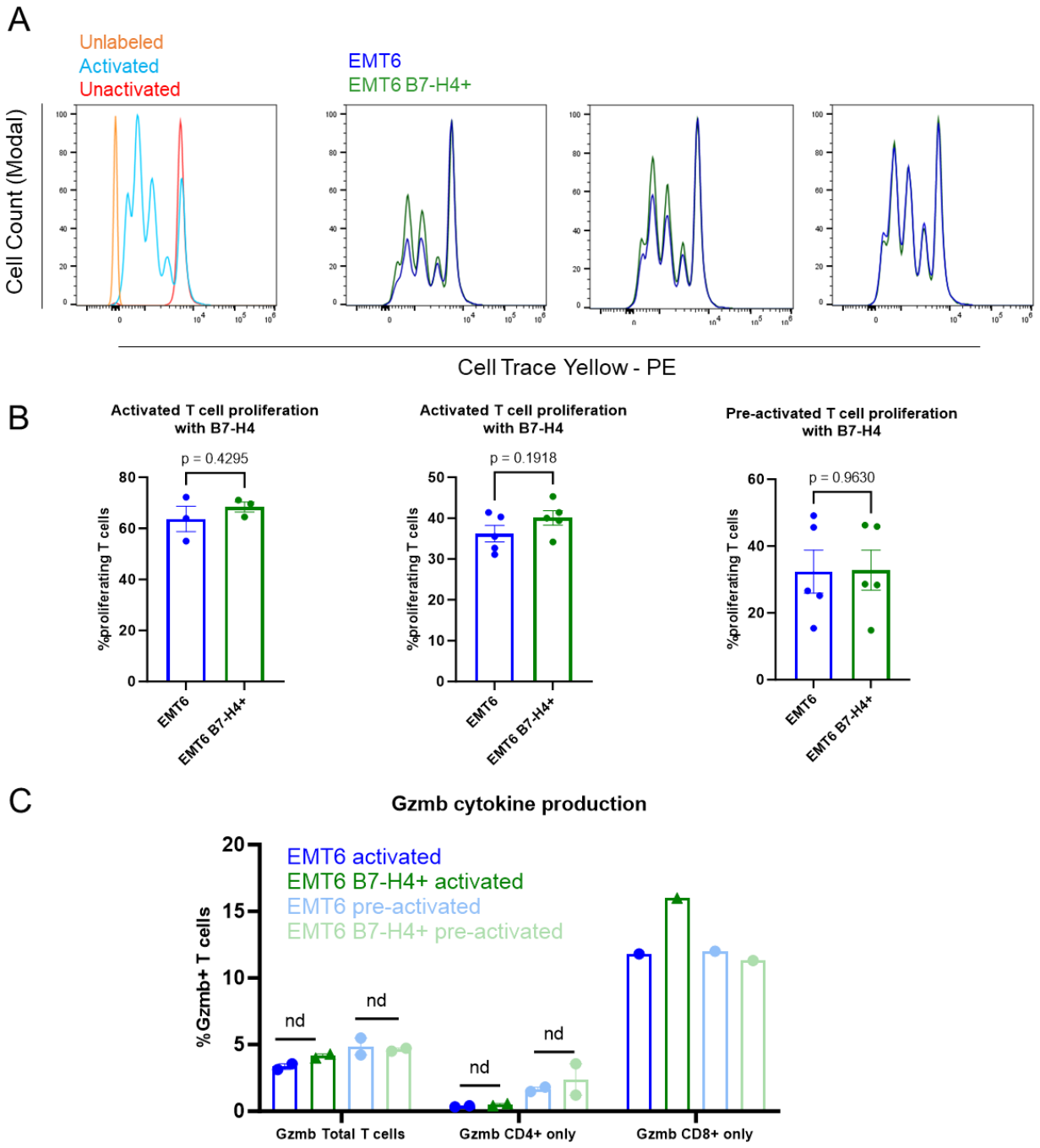

Figure V.6. **Cancer cell surface B7-H4 did not reduce T cell proliferation upon activation *in vitro*.** BALB/c splenocytes were isolated from wildtype animals and co-cultured with EMT6 parent or B7-H4+ cells at a ratio of 10:1. T cells were labeled with Cell Trace Yellow and activated using anti-mouseCD3/CD28 beads and IL-2 (10ng/mL). In two experiments, cells were activated simultaneously with co-culture, in the third cells were pre-activated and then added to co-culture with IL-2 media. Data were collected after 72 hours. (A-B) There was no change observed in T cell division between cells co-cultured with parental or B7-H4+ cells. Data shown represent 3 technical replicates/experiment. Representative histograms are shown in A. (C) We also observed no change in T cell Gzmb cytokine production after co-culture with B7-H4+

cancer cells. Cells were allowed to grow for 48 hours, then subjected to analysis by intracellular flow cytometry staining. Data shown include 2 technical replicates.

B7-H4 glycosylation did not increase macrophage phagocytosis

We developed another hypothesis to explain how B7-H4 may be suppressing pro-inflammatory immune function after our Nanostring gene expression experiments of EMT6 tumors ± B7-H4 expression. One of the most differentially expressed genes in B7-H4+ tumors was *Mrc1*, also known as CD206 or mannose receptor C-type I (**Figure 4.5C**). This C-type lectin can be expressed on macrophages among other cell types. It recognizes mannose, N-acetylglucosamine, and fucose residues on glycosylated proteins[134,135]. Mrc1 is implicated in the uptake of a range of such glycoproteins. In particular, Mrc1 is highly expressed on the surface of M2-like macrophages, which are characterized by their anti-inflammatory or immunosuppressive properties[136,137]. Within the TME, M2 macrophages have been shown to promote tumor growth and metastasis and are considered anti-inflammatory or immunosuppressive[138,139]. B7-H4 is a highly glycosylated protein in its transmembrane and functional conformation, and thus we hypothesized that B7-H4 could be recruiting such M2 macrophages to the TME[133]. Once there, M2 macrophages could be heavily involved in immune cell suppression.

To test the hypothesis of B7-H4 induction of M2 phagocytosis because of its highly glycosylated structure, we performed flow cytometry on labeled BALB/c bone marrow derived macrophages (BMDMs) polarized to M1 or M2 and Cell Trace labeled, killed EMT6 cancer cells ± B7-H4. Appendix III contains detailed methods for this experiment. To assess macrophage phagocytosis of dead cancer cells ± B7-H4 we measured CD11b+ Cell Trace+ cells at varying time points (**Figure 5.4**). At none of the timepoints tested did EMT6 B7-H4+ cancer cells induce significantly greater amounts of macrophage phagocytosis with either M1 or M2 polarized BMDMs.

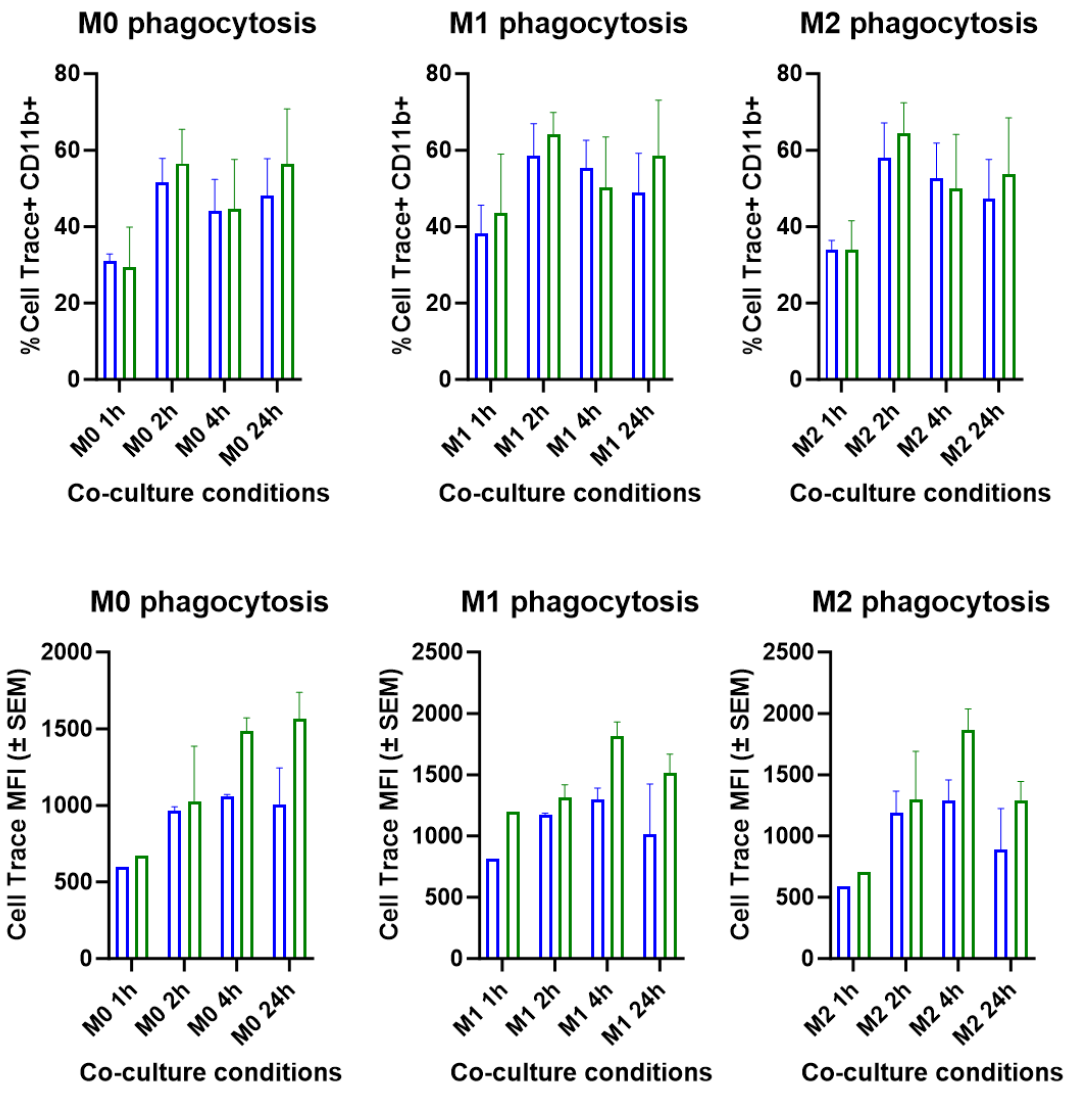

Figure V.7. **EMT6-B7-H4+ cancer cells did not lead to increased phagocytosis by BMDMs.** Bone marrow derived macrophages (BMDMs) from BALB/c mice were isolated, differentiated in M-CSF for 7 days, and polarized with IFNγ to M1 or IL-4 to M2 states. Killed EMT6 cancer cells ± B7-H4 labeled with Cell Trace were co-cultured for the indicated length of time, and double positive CD11b+ Cell Trace+ BMDMs (top) and Cell Trace MFI of CD11b+ cells (bottom) were measured as markers of phagocytosis amount. Data were not statistically significant between groups. Data analyzed by mixed-effects model in GraphPad Prism v10.

Our experiment was difficult to optimize technically, and we tested several iterations before settling on an experimental design (see Appendix III). One caveat to our assessment of BMDM phagocytosis by flow cytometry was large variability in staining between experiments. This variability could be due to fluctuations in staining intensity, different ages of the mice from

which we harvested the BMDMs week to week, and/or differences in actual phagocytosis by the BMDMs week to week. The data from a combined three biological replicates are shown in Figure 5.4 and the variability between replicates suggests there are no significant differences in phagocytosis of B7-H4+ cancer cells compared to control cancer cells.

Discussion and future directions

The data presented do not show a difference in macrophage phagocytosis of B7-H4+ cancer cells *in vitro*. This was an interesting hypothesis due to the significantly higher amount of Mrc1+/CD206+ immune cells within EMT6 B7-H4+ tumors. However, Mrc1+ macrophages can have many alternate functions as M2 macrophages. They are generally pro-tumorigenic and promote tumor progression. They can also promote an immunosuppressive TME through production of anti-inflammatory cytokines like IL-10, TGFβ, and IL-4[140,141]. An interesting follow-up experiment would be to directly measure differences in cytokines in the TME with B7-H4 expression. To confirm the presence and functional status of Mrc1+ M2 macrophages in B7-H4+ tumors, we could inoculate tumors and isolate CD11b+ myeloid cells from dissociated tumors using magnetic bead isolation. Then, these myeloid cells can be plated *ex vivo* for several assays to confirm functional status[142,143].

Arg1+ M2 macrophages produce the enzyme arginase that participates in the urea cycle. Thus, a urea measurement assay can detect the amount and functional status of M2 macrophages within a particular tumor. A kit can detect the concentration of urea in a given solution, such as a cell culture well. We can also perform a standardized phagocytosis assay, in which macrophage phagocytosis of a substrate, typically bacteria (*E. coli*) can be measured and quantified. A broader measure of phagocytosis capability as a measure of M2 functionality would be informative in differentiating B7-H4+ and -ve tumors. Finally, we could perform a macrophage T cell inhibition assay, measuring the ability of tumor associated macrophages (TAMs) to suppress T cell activation *in vitro*. This experiment would also give clues to macrophage function within the TME, through assessing *ex vivo* functionality of TAMs.

In summary, we identified significantly higher Mrc1+ M2 macrophages in untreated EMT6 tumors with B7-H4 expression. The functionality of these myeloid cells is yet unknown. While B7-H4 is proposed to have direct inhibitory effects on T cells within the TME, perhaps the TAMs and additional myeloid cells have perhaps an equally important role in promoting tumor growth and therapeutic resistance.

Future directions: Identifying the receptor for B7-H4

As previously stated, the receptor for B7-H4 is yet uncharacterized but is predicted to be expressed on activated T cells. We propose two strategies in order to identify the receptor. One strategies utilizes a Jurkat T cell triple parameter reporter cell reporter line (TPR cells) that emit fluorescent GFP, CFP, or mCherry upon induction of the NFAT, NF-kB, and AP-1 transcription factors respectively[144,145]. We designed a construct consisting of the murine B7-H4 protein, a glycine-serine linker, and the intracellular signaling domain of CD3ζ and transduced TPR cells via retroviral transduction to generate B7-H4+ TPR cells (See Appendix III). We designed a similar construct with murine PD-L1 protein as a proof-of-concept control. We hypothesized CD3ζ would signal intracellularly as in T cell receptor binding and activation and that the application of force and slight conformational change due to the ligand-receptor binding interaction would signal downstream transcription factors. Methods such as this have been used successfully to identify the MHC-II binding partner[146]. We will culture TPR cells with murine splenocytes from either BALB/c or C57B/6 mice at ratios ranging from 2:1 to 10:1 splenocytes to TPR cells for 24h prior to flow cytometry to detect fluorescence reporter activation. By performing experiments with whole splenocytes (activated or naïve), we can identify the putative receptor on T cells and potentially on other immune cell types.

There are several limitations to this study design. We are assuming that intracellular signaling by CD3ζ will occur from conformational changes to the ligand binding partner when previous studies have attempted this or similar approaches with a known receptor binding

partner. As such, the binding interaction may not be strong enough to activate intracellular signaling within the TPR reporter cells. Our proof-of-concept PD-L1 TPR cells should indicate whether this experimental approach is viable.

We have also designed a bulk RNA sequencing (RNAseq) experiment to identify the B7-H4 receptor protein. We will similarly harvest C57BL/6 splenocytes and activate them using PMA/Ionomycin or CD3/CD28 stimulation for 24-48 hours. We will then co-culture these splenocytes with either recombinant murine B7-H4-Ig purified protein (R&D #4206-B7) or E0771 cancer cells transduced to express cell-surface B7-H4 (as described above for retroviral transduction of EMT6 cancer cells with the pBabe vector). We will use murine PD-L1-Ig (R&D #1019-B7) as a proof-of-concept control. After co-culture for 4 hour and 16 hours, we will harvest the splenocytes and perform bulk RNA sequencing to identify changes in splenocyte gene expression due to interaction with B7-H4 protein. The B7-H4 ligand-receptor binding interaction will likely lead to downstream transcription factor and signaling changes that will be identified by RNAseq. Based on the differentially expressed genes between splenocytes with and without B7-H4 protein co-culture, we can identify first, what cell types are undergoing gene expression changes and second, elicit more information as to what receptor protein classes could be triggering the changes to gene expression.

Discussion

I have presented here several potential experimental avenues to further elucidate B7-H4 biology both at the level of intracellular signaling and immunosuppressive function in breast cancers. The data presented in Chapter IV have shown differential response to ICI between murine and human B7-H4+ tumors. While B7-H4 expression in the EMT6 model was sufficient to induce therapeutic resistance, B7-H4 expression was not associated with therapeutic resistance in human BC. Understanding the functional status of immune cells within the TME may be crucial to uncovering the reason behind these differences. Our data thus far have

shown transcriptional changes in immune cells in B7-H4+ murine tumors. Comparable data from human tumors would be more difficult to obtain and of lower quality (i.e. formalin-fixed biopsy sections). We could explore alternative methods of gene expression such as NanoString GeoMX DSP that allows for whole transcriptome sequencing in isolated regions of interest. This will allow us to highlight immune cell and/or tumor cell regions to identify differentially expressed genes due to the presence of B7-H4 on tumor cells. While the differences in B7-H4+ tumor resistance to ICI therapy suggest B7-H4 may not be the ideal biomarker for therapeutic response in BC patients, understanding the biology of B7-H4 tumor cell expression could elucidate further nuances in signaling within the TME that could uncover additional biomarkers in the future. I've also proposed experiments to uncover the receptor binding partner for B7-H4. As this molecule has yet eluded the field of B7-H4 biology, uncovering its identity could also provide insight into mechanisms of B7-H4 immunosuppressive function *in vivo.*

In summary, we've tested several hypotheses to understand B7-H4 functional and regulation in breast cancers. PI3K inhibition resulted in the most direct reduction in B7-H4 cell-surface expression both in murine and human cell lines, suggesting potential mechanisms for B7-H4 regulation. However, our attempts to measure B7-H4 immunosuppression by T cell inhibition assays and as a target for increased phagocytosis showed no differences between control and treatment samples. Future experiments specifically testing B7-H4 functionality are needed to fill outstanding gaps in knowledge.

Chapter VI: OVERALL DISCUSSION

Breast cancer remains a significant health concern for women globally. Despite advancements in conventional therapies, there is a continuous need for novel therapeutic strategies, particularly for aggressive subtypes. While ICI therapies have been FDA-approved as neoadjuvant therapy in early- and late-stage TNBC, there are still patients that do not respond to ICI and chemotherapy combinations. We have proposed the hypothesis that alternative immune checkpoint ligand B7-H4, which is highly expressed in BC, may be associated with therapeutic resistance in murine and human BCs. We validated previous research associated B7-H4 expression with immune-cold TNBC and increased disease progression in patients. We also identified that epithelial tumor cells, not mesenchymal tumor cells, preferentially express B7-H4 in murine and human cancer cells. These data provide insight into what patients may have high expression of B7-H4 during screening biopsies. Surprisingly, while we did observe B7-H4 induced therapeutic resistance to ICI in a murine model of BC, we did not observe any association of B7-H4 and ICI resistance in two independent human clinical trials (comprised of HR+ and TNBC patients). These data suggest there are yet unobserved differences between murine and human B7-H4 tumor function.

We have proposed several experiments to further assess the functional status of B7-H4 within the TME. While PD-L1 is often expressed in highly immunogenic tumors and is induced by interferons (IFNs), B7-H4 expression was not changed after treatment with Type I and Type II IFN *in vitro*. Instead, we found inhibiting the PI3K signaling pathway in both murine and human BC led to significant reduction to B7-H4 protein expression but not mRNA expression. Our attempts to elucidate B7-H4 immunosuppressive function did not show significant effects. We tested the effect of B7-H4 on inhibiting activated murine T cells. The data show minimal or no effect on T cell proliferation, in contrast to published experiments[50,62,110]. Additionally, we proposed a potential mechanism of B7-H4 immunosuppression by recruiting Mrc1+ M2

macrophages to the TME due to its extensive glycosylation, however found no increase in M2 phagocytosis of B7-H4+ glycosylated cancer cells. Instead, these experiments represent the limitations to studying immune checkpoint ligand function *in vitro* and suggest the need for *in vivo* or *ex vivo* studies involving tumor immune cells. Finally, we have proposed several exciting experimental strategies to identify the elusive receptor binding protein of B7-H4 that has not yet been characterized. Our data open several avenues for continued research in B7-H4 expression and regulation, particularly as it remains a highly sought after target in the field of breast cancer therapeutics.

B7-H4 targeted therapies in breast cancer

B7-H4 has been explored as a target for cancer therapeutics for several years. While initially pre-clinical models focused on monoclonal antibodies with blocking function, in recent years, pharmaceutical companies have focused their efforts on antibody-drug conjugates targeting B7-H4 in clinical trials. Antibody-drug conjugates (ADCs) represent a novel therapeutic approach that combines the specificity of monoclonal antibodies with the cytotoxicity of chemotherapeutic agents. Our data have validated the high yet heterogenous expression of B7-H4 in human breast cancers, including HR+ and TNBC subtypes. However, we have shown from two independent clinical trials, that B7-H4 was not associated with therapeutic resistance, and as such strategies focused on blocking its functions *in vivo* may not elicit the desired improvements to patient outcome. Instead, investigators can take advantage of B7-H4 as a tumor cell marker of BC.

Several companies have explored this avenue by developing ADCs targeting B7-H4 and delivering payload to the TME. I will highlight four ADCs in development and published in the last year with pre-clinical studies and some undergoing early clinical trial testing for safety and efficacy in several cancer types including BC. One study investigated a B7-H4 specific ADC developed by AstraZeneca[147]. A B7-H4 monoclonal antibody (mAb) was conjugated to a DNA-

damaging pyrrolobenzodiazepine (PBD) payload. The effects of the B7-H4-ADC were tested in multiple cell lines *in vitro* and patient derived xenograft (PDX) tumor models. After a single-dose, investigators saw a 60% reduction in breast and ovarian PDX models with B7-H4 expression. Importantly, the B7-H4-ADC had sustained efficacy in models resistant to two other therapy regimens, PARP inhibitors (which are often used in *BRCA* gene mutant BCs) and platinum-based chemotherapy. The investigators propose a mechanism of action encompassing both direct target cell killing and a bystander effect on neighboring cells that may have low or no B7-H4 expression. The ADC was tested in both ovarian and breast cancers.

Another study reports on SGN-B7H4V, a human-specific B7-H4 targeting vedotin ADC[148]. The vedotin payload-linker system consists of a target specific mAb with the payload monomethyl auristatin E (MMAE) via a protease-cleavable linker. These investigators also tested the efficacy of their ADC in ovarian and breast PDX models and *in vitro* studies. *In vitro*, they observed a proposed mechanism including payload-mediated direct cell killing and antibody-mediated effector functions including antibody-dependent cellular cytotoxicity (ADCC) and antibody-dependent cellular phagocytosis (ADCP). In the PDX model, they observed synergy when combined with anti-PD-1 immunotherapy. This ADC has also begun early in-human testing in ovarian and TNBC solid tumors under NCT05194072.

There are two B7-H4 specific ADCs that have reported phase 1 human clinical trials. XMT-1660 was developed by Mersana Therapeutics and consists of a human-specific B7-H4 mAb conjugated to an auristatin hydroxypropylamide payload. Like the previous drug, this ADC also performed well in ovarian and breast PDX models, eliciting tumor regression, and overcame anti-PD-1 resistance in a syngeneic murine tumor model. Their syngeneic model was the mBR9013 MMTV-ERBB2-derived syngeneic tumor in FVB/NJ. Interestingly, like our MMTV-neu model, these cells also have endogenous murine B7-H4 expression and are resistant to anti-PD-1/L1 therapy. They observed complete tumor reduction after a single dose of XMT-

1660. XMT-1660 has recently entered a phase 1 human clinical trial of breast, endometrial, and ovarian cancer tumors under NCT05377996 that has begun enrolling patients[149].

Finally, HS-20089 is a B7-H4 specific ADC developed by Hansoh Pharmaceutical Group that as of mid-2023 had been administered to 44 patients under NCT05263479, including 41 BC patients[150]. The disease control rate was about 60% overall, and about 35% within TNBC specifically. The reported results were from a phase 1 clinical trial, designed to identify dose-limiting toxicities and overall safety. Future studies will evaluate efficacy with broader metrics. The investigators highlight the therapeutic potential specifically for TNBC that is resistant to other chemotherapies and ICI therapies.

These studies highlight the emerging field of B7-H4-specific ADCs that will likely only increase based on such promising pre-clinical and clinical trial data. Based on our paradoxical data of differential therapeutic response between murine and human models of B7-H4+ BC, it will be encouraging to see positive outcomes of B7-H4 targeting ADCs.

Final thoughts

In summary, we have addressed several gaps in knowledge regarding B7-H4 biology in the breast tumor microenvironment. B7-H4 has been a target of interest in cancer therapeutics for nearly two decades, however the literature on its functional applications is still lacking. Our studies have underscored the importance of distinguishing murine and human B7-H4 functionality *in vivo* as we have observed differences in therapeutic response between species. Future experiments may address remaining questions of the functional status and receptor binding protein for this alternate immune checkpoint ligand. While several ADCs show promise in breast cancer therapeutics, there remain unknown but far-reaching implications of B7-H4 expression in breast tumors.

APPENDIX I: SUPPLEMENTARY FIGURES

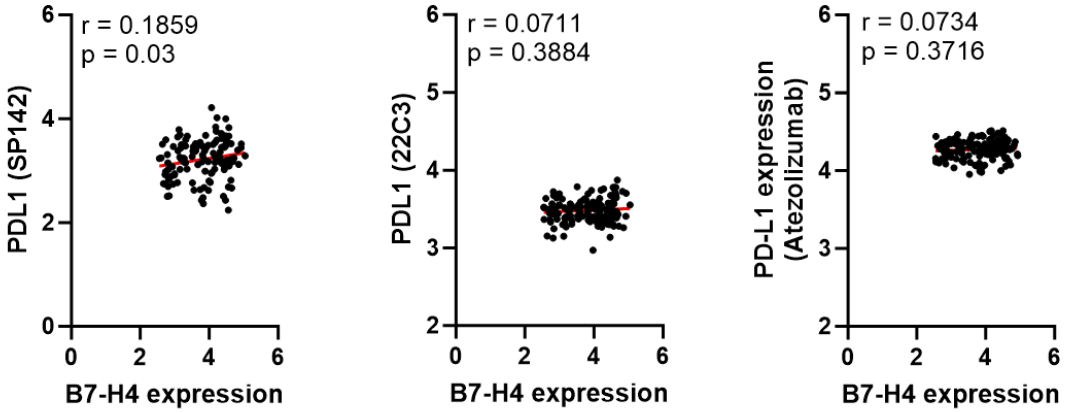

Supplementary Figure 1. **B7-H4 and PD-L1 are not mutually exclusive on tumor cells.** Data shown are reverse phase protein array expression data of B7-H4 and PD-L1 (SP142, 22C3, or Atezolizumab) from the I-SPY2 patient cohort. Samples were a mixture of TNBC and ER+ tumors and were treated with chemotherapy ± anti-PD-1. Depending on the antibody clone selected to detect PD-L1 expression, B7-H4 had no correlation, or a positive correlation to PD-L1 expression in these tumors. Data analyzed by spearman correlation and shown with linear regression best-fit line. n = 151 patients.

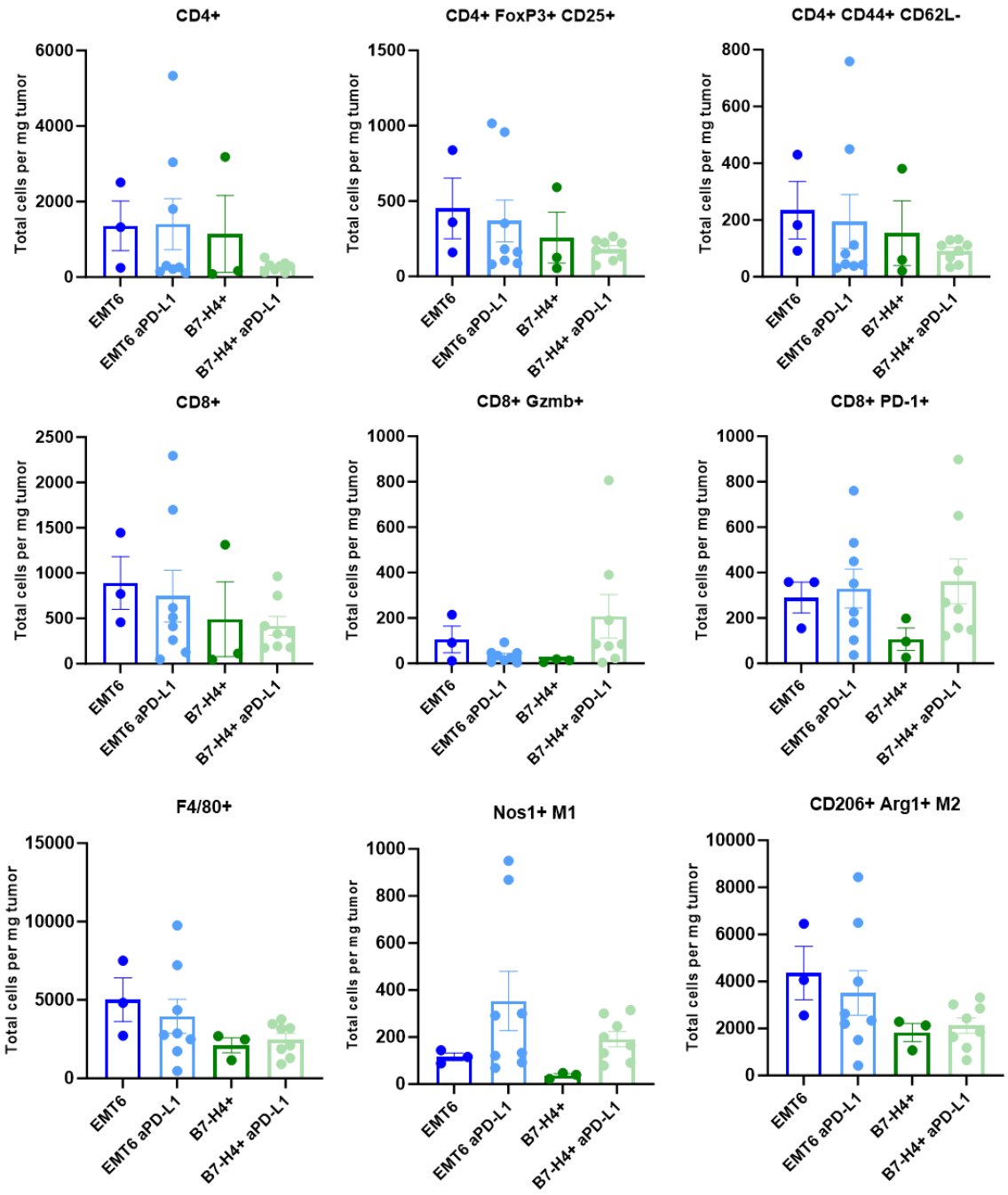

Supplementary Figure 2. **B7-H4 expression did not change quantity of infiltrating tumor immune cells *in vivo* regardless of anti-PD-L1 treatment.** Untreated and anti-PD-L1 treated EMT6 tumors ± B7-H4 were dissociated to single cell suspension and subjected to flow cytometry with a 14 (for myeloid cells) or 17 (for T cells) color panel on a CyTEK Aurora. n = 3/group for control and 8/group for treated samples. Data were analyzed by One-way ANOVA with Sidak's post-hoc test for multiple comparisons between the EMT6 control anti-PD-L1 and EMT6 B7-H4+ anti-PD-L1 treatment groups. One-way ANOVA was not significant between groups. Data were analyzed in GraphPad Prism v10.

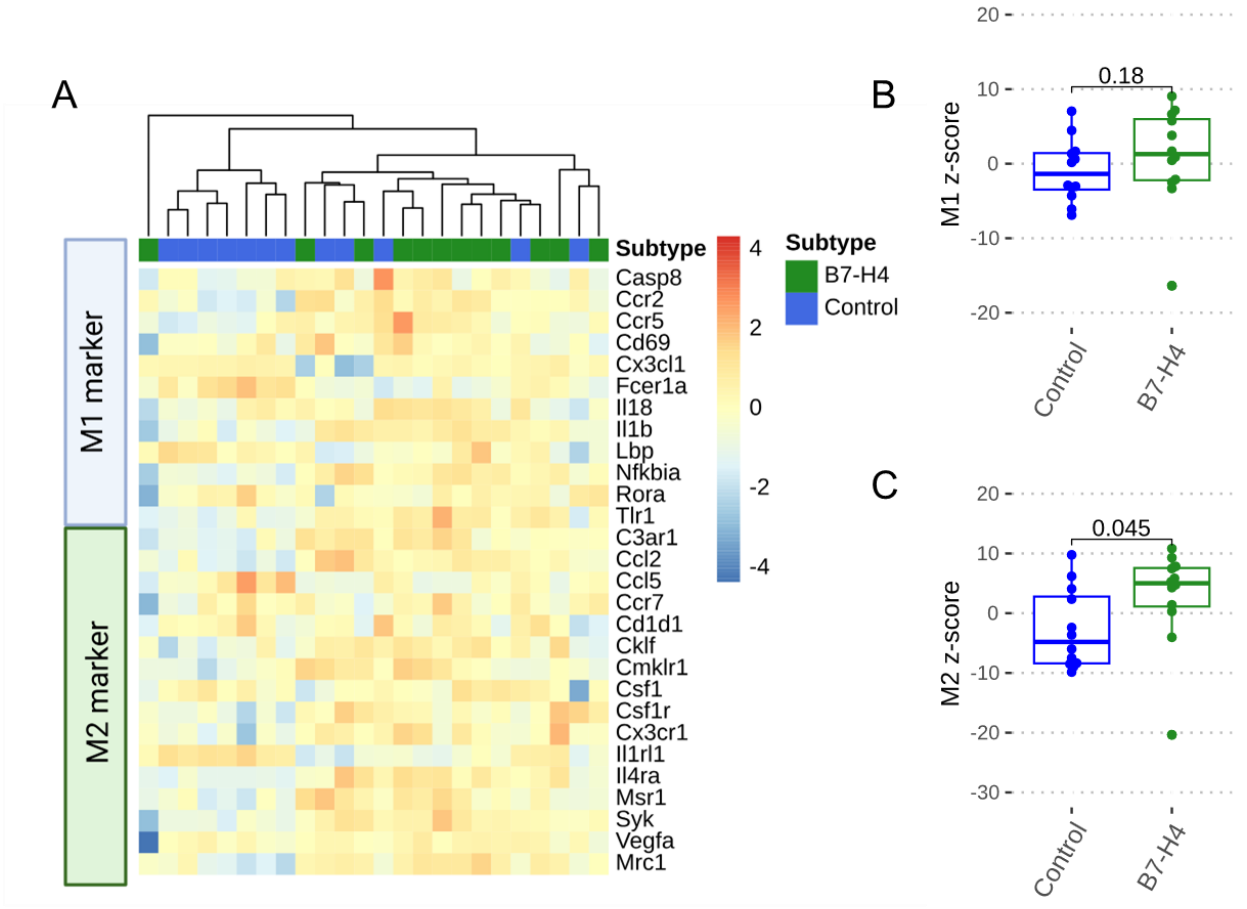

Supplementary Figure 3. **B7-H4+ tumors have higher expression of M2-related macrophage genes compared to control EMT6 tumors.** We compared macrophage gene expression between untreated EMT6 control and EMT6-B7-H4+ tumors and observed overall upregulated expression of macrophage genes, and significantly upregulated expression of M2-related genes in the tumors with B7-H4. Data were analyzed by Wilcoxon rank sum test.

APPENDIX II: SUPPLEMENTARY TABLES FOR CHAPTER IV

feature	avgExpr	logFC	auc	pval	padj	significance
Lilra5	-0.90784	-1.81568	0	0.005075	0.166915	Enriched in Isotype
Bcl6	0.700165	1.400331	1	0.005075	0.166915	Enriched in anti PD-L1
Ccnd3	0.803077	1.606154	1	0.005075	0.166915	Enriched in anti PD-L1
Clu	0.501926	1.003852	1	0.005075	0.166915	Enriched in anti PD-L1
Flt3l	0.82193	1.643861	1	0.005075	0.166915	Enriched in anti PD-L1
Hsd11b1	0.637496	1.274992	1	0.005075	0.166915	Enriched in anti PD-L1
Hspb2	0.552881	1.105761	1	0.005075	0.166915	Enriched in anti PD-L1
Irgm2	0.655248	1.310497	1	0.005075	0.166915	Enriched in anti PD-L1
Mertk	0.610984	1.221968	1	0.005075	0.166915	Enriched in anti PD-L1
Ripk2	0.741284	1.482568	1	0.005075	0.166915	Enriched in anti PD-L1
Traf2	0.759158	1.518317	1	0.005075	0.166915	Enriched in anti PD-L1
C1s1	0.642465	1.284931	0.972222	0.008239	0.166915	Enriched in anti PD-L1
Itga1	0.681039	1.362079	0.972222	0.008239	0.166915	Enriched in anti PD-L1
Pdgfrb	0.644212	1.288423	0.972222	0.008239	0.166915	Enriched in anti PD-L1
Tlr8	0.509443	1.018886	0.972222	0.008239	0.166915	Enriched in anti PD-L1
Tgfbr1	-0.67818	-1.35635	0.055556	0.013065	0.166915	Enriched in Isotype
C1ra	0.65451	1.309021	0.944444	0.013065	0.166915	Enriched in anti PD-L1
Cd200	0.704932	1.409863	0.944444	0.013065	0.166915	Enriched in anti PD-L1
Cfh	0.587555	1.175111	0.944444	0.013065	0.166915	Enriched in anti PD-L1
Dock9	0.677458	1.354915	0.944444	0.013065	0.166915	Enriched in anti PD-L1
Gbp5	0.60317	1.20634	0.944444	0.013065	0.166915	Enriched in anti PD-L1
Gtf3c1	0.67103	1.34206	0.944444	0.013065	0.166915	Enriched in anti PD-L1
Il15ra	0.741902	1.483804	0.944444	0.013065	0.166915	Enriched in anti PD-L1
Il1rl1	0.679315	1.358631	0.944444	0.013065	0.166915	Enriched in anti PD-L1
Irf1	0.638206	1.276412	0.944444	0.013065	0.166915	Enriched in anti PD-L1
Irf2	0.622122	1.244245	0.944444	0.013065	0.166915	Enriched in anti PD-L1
Msln	0.560248	1.120497	0.944444	0.013065	0.166915	Enriched in anti PD-L1
Nos2	0.583593	1.167185	0.944444	0.013065	0.166915	Enriched in anti PD-L1
Pla2g6	0.723939	1.447878	0.944444	0.013065	0.166915	Enriched in anti PD-L1
Prf1	0.644369	1.288739	0.944444	0.013065	0.166915	Enriched in anti PD-L1
Psen2	0.67679	1.35358	0.944444	0.013065	0.166915	Enriched in anti PD-L1
Sigirr	0.61737	1.23474	0.944444	0.013065	0.166915	Enriched in anti PD-L1
Tap1	0.703034	1.406068	0.944444	0.013065	0.166915	Enriched in anti PD-L1
Tnfsf10	0.697634	1.395269	0.944444	0.013065	0.166915	Enriched in anti PD-L1
Trp53	0.669724	1.339448	0.944444	0.013065	0.166915	Enriched in anti PD-L1
Vcam1	0.730375	1.46075	0.944444	0.013065	0.166915	Enriched in anti PD-L1
Cx3cr1	-0.69676	-1.39353	0.083333	0.020241	0.166915	Enriched in Isotype
Pparg	-0.77447	-1.54894	0.083333	0.020241	0.166915	Enriched in Isotype

Angpt1	0.52244	1.04488	0.916667	0.020241	0.166915	Enriched in anti PD-L1
Angpt2	0.572409	1.144818	0.916667	0.020241	0.166915	Enriched in anti PD-L1
Atm	0.725342	1.450684	0.916667	0.020241	0.166915	Enriched in anti PD-L1
Bmi1	0.533631	1.067262	0.916667	0.020241	0.166915	Enriched in anti PD-L1
C3	0.603173	1.206345	0.916667	0.020241	0.166915	Enriched in anti PD-L1
C4b	0.644185	1.28837	0.916667	0.020241	0.166915	Enriched in anti PD-L1
Casp1	0.614344	1.228688	0.916667	0.020241	0.166915	Enriched in anti PD-L1
Casp3	0.604922	1.209844	0.916667	0.020241	0.166915	Enriched in anti PD-L1
Ccl5	0.547809	1.095618	0.916667	0.020241	0.166915	Enriched in anti PD-L1
Cd274	0.542257	1.084515	0.916667	0.020241	0.166915	Enriched in anti PD-L1
Cd38	0.528587	1.057174	0.916667	0.020241	0.166915	Enriched in anti PD-L1
Cd8a	0.659823	1.319646	0.916667	0.020241	0.166915	Enriched in anti PD-L1
Col3a1	0.54969	1.09938	0.916667	0.020241	0.166915	Enriched in anti PD-L1
Cxcl12	0.60892	1.21784	0.916667	0.020241	0.166915	Enriched in anti PD-L1
Cxcr6	0.628773	1.257545	0.916667	0.020241	0.166915	Enriched in anti PD-L1
Cyld	0.569305	1.13861	0.916667	0.020241	0.166915	Enriched in anti PD-L1
Fas	0.630083	1.260167	0.916667	0.020241	0.166915	Enriched in anti PD-L1
Fcgr4	0.533591	1.067182	0.916667	0.020241	0.166915	Enriched in anti PD-L1
Fn1	0.604368	1.208735	0.916667	0.020241	0.166915	Enriched in anti PD-L1
Gbp2b	0.619423	1.238846	0.916667	0.020241	0.166915	Enriched in anti PD-L1
Gzmb	0.61144	1.222881	0.916667	0.020241	0.166915	Enriched in anti PD-L1
Il1r1	0.626041	1.252081	0.916667	0.020241	0.166915	Enriched in anti PD-L1
Irak1	0.674524	1.349048	0.916667	0.020241	0.166915	Enriched in anti PD-L1
Irf3	0.708484	1.416967	0.916667	0.020241	0.166915	Enriched in anti PD-L1
Irf8	0.592471	1.184942	0.916667	0.020241	0.166915	Enriched in anti PD-L1
Lbp	0.620208	1.240416	0.916667	0.020241	0.166915	Enriched in anti PD-L1
Mavs	0.600423	1.200845	0.916667	0.020241	0.166915	Enriched in anti PD-L1
Pdgfc	0.537815	1.07563	0.916667	0.020241	0.166915	Enriched in anti PD-L1
Serping1	0.670015	1.34003	0.916667	0.020241	0.166915	Enriched in anti PD-L1
Smad3	0.661261	1.322521	0.916667	0.020241	0.166915	Enriched in anti PD-L1
Smad4	0.549659	1.099319	0.916667	0.020241	0.166915	Enriched in anti PD-L1
Socs1	0.578124	1.156248	0.916667	0.020241	0.166915	Enriched in anti PD-L1
Tnfrsf9	0.637417	1.274834	0.916667	0.020241	0.166915	Enriched in anti PD-L1
Tnfsf13	0.665614	1.331228	0.916667	0.020241	0.166915	Enriched in anti PD-L1
Zbp1	0.617598	1.235197	0.916667	0.020241	0.166915	Enriched in anti PD-L1
Gpr183	-0.62818	-1.25635	0.111111	0.030639	0.179074	Enriched in Isotype
Tfrc	-0.54533	-1.09066	0.111111	0.030639	0.179074	Enriched in Isotype
Tnfrsf13b	-0.50884	-1.01768	0.111111	0.030639	0.179074	Enriched in Isotype
Amica1	0.648048	1.296096	0.888889	0.030639	0.179074	Enriched in anti PD-L1
Atg12	0.594036	1.188073	0.888889	0.030639	0.179074	Enriched in anti PD-L1
Atg7	0.619649	1.239298	0.888889	0.030639	0.179074	Enriched in anti PD-L1

Bid	0.583676	1.167353	0.888889	0.030639	0.179074	Enriched in anti PD-L1
Bst1	0.593962	1.187924	0.888889	0.030639	0.179074	Enriched in anti PD-L1
Bst2	0.570803	1.141606	0.888889	0.030639	0.179074	Enriched in anti PD-L1
Ccl8	0.56615	1.1323	0.888889	0.030639	0.179074	Enriched in anti PD-L1
Cd40	0.522271	1.044542	0.888889	0.030639	0.179074	Enriched in anti PD-L1
Cd7	0.615732	1.231464	0.888889	0.030639	0.179074	Enriched in anti PD-L1
Cxcl10	0.578662	1.157323	0.888889	0.030639	0.179074	Enriched in anti PD-L1
Cxcl9	0.623568	1.247136	0.888889	0.030639	0.179074	Enriched in anti PD-L1
Egr3	0.695312	1.390624	0.888889	0.030639	0.179074	Enriched in anti PD-L1
Fcer1a	0.466936	0.933872	0.888889	0.030639	0.179074	Enriched in anti PD-L1
Gzma	0.523652	1.047304	0.888889	0.030639	0.179074	Enriched in anti PD-L1
H2-K1	0.612256	1.224513	0.888889	0.030639	0.179074	Enriched in anti PD-L1
H2-M3	0.547351	1.094702	0.888889	0.030639	0.179074	Enriched in anti PD-L1
Il12rb1	0.644959	1.289918	0.888889	0.030639	0.179074	Enriched in anti PD-L1
Ilf3	0.551078	1.102156	0.888889	0.030639	0.179074	Enriched in anti PD-L1
Itgal	0.630469	1.260938	0.888889	0.030639	0.179074	Enriched in anti PD-L1
Kit	0.498099	0.996198	0.888889	0.030639	0.179074	Enriched in anti PD-L1
Ncam1	0.509191	1.018381	0.888889	0.030639	0.179074	Enriched in anti PD-L1
Psmb10	0.641215	1.28243	0.888889	0.030639	0.179074	Enriched in anti PD-L1
Psmb8	0.656588	1.313176	0.888889	0.030639	0.179074	Enriched in anti PD-L1
Psmb9	0.604021	1.208042	0.888889	0.030639	0.179074	Enriched in anti PD-L1
Tapbp	0.672689	1.345377	0.888889	0.030639	0.179074	Enriched in anti PD-L1
Tbk1	0.401018	0.802037	0.888889	0.030639	0.179074	Enriched in anti PD-L1
Tpsab1	0.535281	1.070561	0.888889	0.030639	0.179074	Enriched in anti PD-L1
Cd207	-0.6698	-1.33959	0.138889	0.045328	0.213181	Enriched in Isotype
Cspg4	-0.5385	-1.07699	0.138889	0.045328	0.213181	Enriched in Isotype
Itgax	-0.55258	-1.10516	0.138889	0.045328	0.213181	Enriched in Isotype
Abl1	0.600955	1.20191	0.861111	0.045328	0.213181	Enriched in anti PD-L1
Bax	0.531172	1.062345	0.861111	0.045328	0.213181	Enriched in anti PD-L1
Cd1d1	0.500343	1.000686	0.861111	0.045328	0.213181	Enriched in anti PD-L1
Cma1	0.519864	1.039729	0.861111	0.045328	0.213181	Enriched in anti PD-L1
Cybb	0.528873	1.057747	0.861111	0.045328	0.213181	Enriched in anti PD-L1
Egr2	0.645566	1.291132	0.861111	0.045328	0.213181	Enriched in anti PD-L1
Ifng	0.550883	1.101765	0.861111	0.045328	0.213181	Enriched in anti PD-L1
Igf2r	0.620299	1.240598	0.861111	0.045328	0.213181	Enriched in anti PD-L1
Ikbkg	0.53794	1.07588	0.861111	0.045328	0.213181	Enriched in anti PD-L1
Klrc1	0.507425	1.014851	0.861111	0.045328	0.213181	Enriched in anti PD-L1
Mfge8	0.572522	1.145045	0.861111	0.045328	0.213181	Enriched in anti PD-L1
Mif	0.588398	1.176796	0.861111	0.045328	0.213181	Enriched in anti PD-L1
Reps1	0.55998	1.119959	0.861111	0.045328	0.213181	Enriched in anti PD-L1
Slamf7	0.57654	1.15308	0.861111	0.045328	0.213181	Enriched in anti PD-L1

Snai1	0.597796	1.195593	0.861111	0.045328	0.213181	Enriched in anti PD-L1
Stat1	0.590231	1.180462	0.861111	0.045328	0.213181	Enriched in anti PD-L1
Tie1	0.585324	1.170649	0.861111	0.045328	0.213181	Enriched in anti PD-L1
Tlr3	0.573828	1.147655	0.861111	0.045328	0.213181	Enriched in anti PD-L1
Tnfrsf10b	0.554174	1.108348	0.861111	0.045328	0.213181	Enriched in anti PD-L1
Twist1	0.479049	0.958097	0.861111	0.045328	0.213181	Enriched in anti PD-L1
Vegfc	0.472736	0.945473	0.861111	0.045328	0.213181	Enriched in anti PD-L1
Ythdf2	0.638681	1.277363	0.861111	0.045328	0.213181	Enriched in anti PD-L1

Supplementary Table 1. Differentially expressed genes for figure 4.4A.

feature	avgExpr	logFC	auc	pval	padj	significance
Dusp4	-0.59691	-1.19382	0	0.005075	0.428939	Enriched in Isotype
Ccl9	-0.49089	-0.98179	0.027778	0.008239	0.428939	Enriched in Isotype
Cd14	-0.53943	-1.07886	0.027778	0.008239	0.428939	Enriched in Isotype
Cd81	-0.50884	-1.01768	0.027778	0.008239	0.428939	Enriched in Isotype
Mapk3	-0.39245	-0.7849	0.027778	0.008239	0.428939	Enriched in Isotype
Trem1	-0.53034	-1.06069	0.027778	0.008239	0.428939	Enriched in Isotype
C5ar1	-0.63864	-1.27729	0.055556	0.013065	0.428939	Enriched in Isotype
Cx3cr1	-0.43675	-0.87349	0.055556	0.013065	0.428939	Enriched in Isotype
Osm	-0.55679	-1.11358	0.055556	0.013065	0.428939	Enriched in Isotype
Plaur	-0.39184	-0.78367	0.055556	0.013065	0.428939	Enriched in Isotype
Pvr	-0.54929	-1.09859	0.055556	0.013065	0.428939	Enriched in Isotype
Sh2d1b1	-0.4095	-0.81901	0.055556	0.013065	0.428939	Enriched in Isotype
Tgfbr1	-0.59193	-1.18385	0.055556	0.013065	0.428939	Enriched in Isotype
Tlr2	-0.43235	-0.86471	0.055556	0.013065	0.428939	Enriched in Isotype
Tollip	-0.44775	-0.8955	0.055556	0.013065	0.428939	Enriched in Isotype
Trem2	-0.38899	-0.77798	0.055556	0.013065	0.428939	Enriched in Isotype
Hsd11b1	0.622999	1.245997	0.916667	0.020241	0.428939	Enriched in anti PD-L1
Anxa1	-0.46464	-0.92929	0.083333	0.020241	0.428939	Enriched in Isotype
Cd83	-0.54836	-1.09672	0.083333	0.020241	0.428939	Enriched in Isotype
Csf1r	-0.52332	-1.04663	0.083333	0.020241	0.428939	Enriched in Isotype
Trp53	-0.51571	-1.03142	0.083333	0.020241	0.428939	Enriched in Isotype
Cd5	0.567942	1.135883	0.888889	0.030639	0.428939	Enriched in anti PD-L1
Itk	0.51506	1.030119	0.888889	0.030639	0.428939	Enriched in anti PD-L1
Lbp	0.488371	0.976742	0.888889	0.030639	0.428939	Enriched in anti PD-L1
Zap70	0.526856	1.053711	0.888889	0.030639	0.428939	Enriched in anti PD-L1
Ambp	-0.3663	-0.73261	0.111111	0.030639	0.428939	Enriched in Isotype
Cd33	-0.55388	-1.10775	0.111111	0.030639	0.428939	Enriched in Isotype
Cd68	-0.54932	-1.09865	0.111111	0.030639	0.428939	Enriched in Isotype
Il1r2	-0.52245	-1.0449	0.111111	0.030639	0.428939	Enriched in Isotype
Il3ra	-0.43277	-0.86553	0.111111	0.030639	0.428939	Enriched in Isotype
Il6ra	-0.45702	-0.91404	0.111111	0.030639	0.428939	Enriched in Isotype
Map2k2	-0.51381	-1.02762	0.111111	0.030639	0.428939	Enriched in Isotype
Mcam	-0.43535	-0.8707	0.111111	0.030639	0.428939	Enriched in Isotype
Ncf4	-0.44173	-0.88347	0.111111	0.030639	0.428939	Enriched in Isotype
Psmd7	-0.55156	-1.10313	0.111111	0.030639	0.428939	Enriched in Isotype
Spp1	-0.65005	-1.3001	0.111111	0.030639	0.428939	Enriched in Isotype
Tnfsf14	-0.49818	-0.99637	0.111111	0.030639	0.428939	Enriched in Isotype
C1s1	0.433891	0.867782	0.861111	0.045328	0.428939	Enriched in anti PD-L1
Irf4	0.449907	0.899813	0.861111	0.045328	0.428939	Enriched in anti PD-L1
Lck	0.560193	1.120386	0.861111	0.045328	0.428939	Enriched in anti PD-L1

Txk	0.551047	1.102093	0.861111	0.045328	0.428939	Enriched in anti PD-L1
Btk	-0.49133	-0.98266	0.138889	0.045328	0.428939	Enriched in Isotype
Cdkn1a	-0.52484	-1.04968	0.138889	0.045328	0.428939	Enriched in Isotype
Lyn	-0.38453	-0.76905	0.138889	0.045328	0.428939	Enriched in Isotype
Rel	-0.58178	-1.16356	0.138889	0.045328	0.428939	Enriched in Isotype

Supplementary Table 2. Differentially expressed genes for figure 4.4C.

feature	avgExpr	logFC	auc	pval	padj	significance
Tlr8	0.476633	0.953267	0.826389	0.00726	0.904509	Enriched in B7-H4
Cd2	-0.43354	-0.86708	0.194444	0.012023	0.904509	Enriched in Control
Amica1	0.430141	0.860282	0.805556	0.012023	0.904509	Enriched in B7-H4
Fut7	0.445571	0.891142	0.798611	0.014138	0.904509	Enriched in B7-H4
Ccl6	0.30682	0.61364	0.777778	0.022576	0.904509	Enriched in B7-H4
Cdh1	0.259441	0.518882	0.763889	0.030383	0.904509	Enriched in B7-H4
Irak4	0.304335	0.60867	0.763889	0.030383	0.904509	Enriched in B7-H4
Tfrc	-0.0401	-0.08021	0.236111	0.030383	0.904509	Non-sig
Ewsr1	-0.36512	-0.73024	0.243056	0.035089	0.904509	Enriched in Control
Csf3r	0.420721	0.841443	0.756944	0.035089	0.904509	Enriched in B7-H4
Mpo	0.40698	0.81396	0.75	0.040404	0.904509	Enriched in B7-H4
Msln	0.328274	0.656548	0.75	0.040404	0.904509	Enriched in B7-H4
Cd79b	-0.31048	-0.62097	0.256944	0.046387	0.904509	Enriched in Control
Pax5	-0.28208	-0.56415	0.256944	0.046387	0.904509	Enriched in Control
Ccl8	0.319037	0.638073	0.743056	0.046387	0.904509	Enriched in B7-H4
Cxcr2	0.271868	0.543735	0.743056	0.046387	0.904509	Enriched in B7-H4
Psmd7	0.324559	0.649119	0.743056	0.046387	0.904509	Enriched in B7-H4

Supplementary Table 3. Differentially expressed genes for Figure 4.5A, EMT6 B7-H4+ vs EMT6 control tumor, treated with isotype control and harvest 7 days post treatment.

feature	avgExpr	logFC	auc	pval	padj	significance
Bst2	-0.64575	-1.2915	0.097222	0.000901	0.218658	Enriched in Control
Mrc1	0.670869	1.341738	0.895833	0.001106	0.218658	Enriched in B7-H4
Cd33	0.620628	1.241257	0.868056	0.002437	0.218658	Enriched in B7-H4
Ifi44	-0.61128	-1.22256	0.131944	0.002437	0.218658	Enriched in Control
Gzmb	-0.6122	-1.22439	0.145833	0.00355	0.218658	Enriched in Control
Egr1	0.470177	0.940354	0.847222	0.004265	0.218658	Enriched in B7-H4
Ifi44l	-0.53044	-1.06087	0.159722	0.005108	0.218658	Enriched in Control
Cxcl11	-0.44475	-0.8895	0.166667	0.006099	0.218658	Enriched in Control
Gzma	-0.55551	-1.11102	0.166667	0.006099	0.218658	Enriched in Control
Cd63	-0.52032	-1.04065	0.173611	0.00726	0.218658	Enriched in Control
Ddx58	-0.53937	-1.07874	0.173611	0.00726	0.218658	Enriched in Control
Il2rb	-0.50551	-1.01101	0.173611	0.00726	0.218658	Enriched in Control
Axl	-0.48731	-0.97462	0.180556	0.008616	0.218658	Enriched in Control
Colec12	0.484772	0.969543	0.819444	0.008616	0.218658	Enriched in B7-H4
Il1r2	0.435025	0.87005	0.819444	0.008616	0.218658	Enriched in B7-H4
Map2k2	-0.48318	-0.96635	0.180556	0.008616	0.218658	Enriched in Control
Ewsr1	0.46845	0.9369	0.8125	0.010193	0.218658	Enriched in B7-H4
F13a1	0.543951	1.087902	0.8125	0.010193	0.218658	Enriched in B7-H4
Ifi35	-0.50304	-1.00607	0.1875	0.010193	0.218658	Enriched in Control
Itgam	0.56702	1.134039	0.8125	0.010193	0.218658	Enriched in B7-H4
Tpsab1	-0.59952	-1.19905	0.1875	0.010193	0.218658	Enriched in Control
Ambp	0.552039	1.104078	0.805556	0.012023	0.218658	Enriched in B7-H4
Ccl5	-0.51457	-1.02914	0.194444	0.012023	0.218658	Enriched in Control
H2-T23	-0.48836	-0.97672	0.194444	0.012023	0.218658	Enriched in Control
Tollip	0.337536	0.675072	0.805556	0.012023	0.218658	Enriched in B7-H4
Ctsw	-0.4903	-0.98061	0.201389	0.014138	0.218658	Enriched in Control
Il4ra	0.510837	1.021673	0.798611	0.014138	0.218658	Enriched in B7-H4
Itga2	-0.48806	-0.97612	0.201389	0.014138	0.218658	Enriched in Control
Klrd1	-0.47756	-0.95513	0.201389	0.014138	0.218658	Enriched in Control
Siglec1	0.349824	0.699647	0.798611	0.014138	0.218658	Enriched in B7-H4
Tapbp	-0.50274	-1.00548	0.201389	0.014138	0.218658	Enriched in Control
Tlr1	0.490597	0.981195	0.798611	0.014138	0.218658	Enriched in B7-H4
Zbp1	-0.50508	-1.01016	0.201389	0.014138	0.218658	Enriched in Control
Cma1	-0.56707	-1.13413	0.208333	0.016575	0.218658	Enriched in Control
H60a	0.399703	0.799406	0.791667	0.016575	0.218658	Enriched in B7-H4
Irf7	-0.45658	-0.91316	0.208333	0.016575	0.218658	Enriched in Control
Lag3	-0.41497	-0.82993	0.208333	0.016575	0.218658	Enriched in Control
Txk	-0.41601	-0.83203	0.208333	0.016575	0.218658	Enriched in Control
App	0.439684	0.879369	0.784722	0.019373	0.218658	Enriched in B7-H4
Atg12	0.454494	0.908988	0.784722	0.019373	0.218658	Enriched in B7-H4

Cd7	-0.33338	-0.66677	0.215278	0.019373	0.218658	Enriched in Control
Cxcl10	-0.41811	-0.83623	0.215278	0.019373	0.218658	Enriched in Control
Maf	0.486141	0.972282	0.784722	0.019373	0.218658	Enriched in B7-H4
Tlr5	0.523585	1.04717	0.784722	0.019373	0.218658	Enriched in B7-H4
Tlr6	0.388733	0.777466	0.784722	0.019373	0.218658	Enriched in B7-H4
Atg7	0.494915	0.989831	0.777778	0.022576	0.218658	Enriched in B7-H4
C5ar1	0.502921	1.005841	0.777778	0.022576	0.218658	Enriched in B7-H4
Casp3	-0.41902	-0.83804	0.222222	0.022576	0.218658	Enriched in Control
Ccr1	0.443666	0.887332	0.777778	0.022576	0.218658	Enriched in B7-H4
H2-K1	-0.47482	-0.94965	0.222222	0.022576	0.218658	Enriched in Control
Inpp5d	0.392092	0.784184	0.777778	0.022576	0.218658	Enriched in B7-H4
Map3k1	0.295815	0.591631	0.777778	0.022576	0.218658	Enriched in B7-H4
Nfkbia	0.378385	0.756769	0.777778	0.022576	0.218658	Enriched in B7-H4
Card9	0.436703	0.873407	0.770833	0.026229	0.218658	Enriched in B7-H4
Ccl7	0.418625	0.83725	0.770833	0.026229	0.218658	Enriched in B7-H4
Ccr5	0.412268	0.824537	0.770833	0.026229	0.218658	Enriched in B7-H4
Ccrl2	0.394588	0.789177	0.770833	0.026229	0.218658	Enriched in B7-H4
Cebpb	0.407094	0.814187	0.770833	0.026229	0.218658	Enriched in B7-H4
Cx3cr1	0.424269	0.848537	0.770833	0.026229	0.218658	Enriched in B7-H4
H2-D1	-0.50326	-1.00651	0.229167	0.026229	0.218658	Enriched in Control
Ifitm2	0.378093	0.756186	0.770833	0.026229	0.218658	Enriched in B7-H4
Irak3	0.35582	0.711641	0.770833	0.026229	0.218658	Enriched in B7-H4
Itgax	0.443217	0.886434	0.770833	0.026229	0.218658	Enriched in B7-H4
Sbno2	0.275813	0.551627	0.770833	0.026229	0.218658	Enriched in B7-H4
Trem1	0.392215	0.784431	0.770833	0.026229	0.218658	Enriched in B7-H4
Cd44	0.415423	0.830846	0.763889	0.030383	0.218658	Enriched in B7-H4
Chuk	-0.44049	-0.88098	0.236111	0.030383	0.218658	Enriched in Control
Creb5	0.331879	0.663758	0.763889	0.030383	0.218658	Enriched in B7-H4
Csf3r	0.380162	0.760323	0.763889	0.030383	0.218658	Enriched in B7-H4
Irak2	0.293658	0.587316	0.763889	0.030383	0.218658	Enriched in B7-H4
Itk	-0.42673	-0.85345	0.236111	0.030383	0.218658	Enriched in Control
Jak3	0.439708	0.879416	0.763889	0.030383	0.218658	Enriched in B7-H4
Mfge8	-0.4635	-0.92699	0.236111	0.030383	0.218658	Enriched in Control
Slc7a11	0.361596	0.723191	0.763889	0.030383	0.218658	Enriched in B7-H4
Zap70	-0.41319	-0.82638	0.236111	0.030383	0.218658	Enriched in Control
Akt3	-0.33041	-0.66082	0.243056	0.035089	0.218658	Enriched in Control
C3ar1	0.416323	0.832647	0.756944	0.035089	0.218658	Enriched in B7-H4
Ccr2	0.432471	0.864943	0.756944	0.035089	0.218658	Enriched in B7-H4
Cklf	0.412745	0.82549	0.756944	0.035089	0.218658	Enriched in B7-H4
Cxcr2	0.383716	0.767431	0.756944	0.035089	0.218658	Enriched in B7-H4
Ets1	-0.39514	-0.79027	0.243056	0.035089	0.218658	Enriched in Control

Fos	0.431364	0.862728	0.756944	0.035089	0.218658	Enriched in B7-H4
Il2ra	-0.40424	-0.80849	0.243056	0.035089	0.218658	Enriched in Control
Mapk3	0.417163	0.834327	0.756944	0.035089	0.218658	Enriched in B7-H4
Stat6	0.35788	0.71576	0.756944	0.035089	0.218658	Enriched in B7-H4
Thy1	-0.38423	-0.76846	0.243056	0.035089	0.218658	Enriched in Control
Tnfsf10	-0.50501	-1.01001	0.243056	0.035089	0.218658	Enriched in Control
Tnfsf14	0.355322	0.710644	0.756944	0.035089	0.218658	Enriched in B7-H4
Ccl3	0.439402	0.878804	0.75	0.040404	0.218658	Enriched in B7-H4
Cd163	0.47061	0.94122	0.75	0.040404	0.218658	Enriched in B7-H4
Cxcl2	0.316461	0.632922	0.75	0.040404	0.218658	Enriched in B7-H4
Ecsit	-0.46284	-0.92568	0.25	0.040404	0.218658	Enriched in Control
Egr2	0.379542	0.759084	0.75	0.040404	0.218658	Enriched in B7-H4
Havcr2	0.354749	0.709498	0.75	0.040404	0.218658	Enriched in B7-H4
Lyz2	0.461393	0.922787	0.75	0.040404	0.218658	Enriched in B7-H4
Nlrp3	0.368548	0.737097	0.75	0.040404	0.218658	Enriched in B7-H4
Prkcd	0.297854	0.595708	0.75	0.040404	0.218658	Enriched in B7-H4
Psmb7	-0.3567	-0.71341	0.25	0.040404	0.218658	Enriched in Control
Stat4	-0.38713	-0.77427	0.25	0.040404	0.218658	Enriched in Control
Tlr4	0.377582	0.755163	0.75	0.040404	0.218658	Enriched in B7-H4
Xcl1	-0.43464	-0.86929	0.25	0.040404	0.218658	Enriched in Control
Yy1	-0.47651	-0.95301	0.25	0.040404	0.218658	Enriched in Control
Csf2rb	0.295165	0.590329	0.743056	0.046387	0.230679	Enriched in B7-H4
Cxcl3	0.367071	0.734142	0.743056	0.046387	0.230679	Enriched in B7-H4
Gtf3c1	-0.39922	-0.79843	0.256944	0.046387	0.230679	Enriched in Control
Ikbke	0.268306	0.536612	0.743056	0.046387	0.230679	Enriched in B7-H4
Il17ra	0.403028	0.806057	0.743056	0.046387	0.230679	Enriched in B7-H4
Il1rap	0.289109	0.578217	0.743056	0.046387	0.230679	Enriched in B7-H4
Stat1	-0.39662	-0.79325	0.256944	0.046387	0.230679	Enriched in Control
Tfe3	0.407417	0.814835	0.743056	0.046387	0.230679	Enriched in B7-H4
Ubc	0.373354	0.746708	0.743056	0.046387	0.230679	Enriched in B7-H4

Supplementary Table 4. Differentially expressed genes for Figure 4.5C, EMT6 B7-H4+ vs EMT6 control tumors untreated and harvested at 500mm^3.

T cell proliferation	Interferon response	Cytotoxicity	Macrophage Functions
Casp3	Ccr7	Cd1d2	C3ar1
Ccnd3	Cd3e	Cd8a	Casp8
Cd3e	Ciita	Ctsh	Ccl2
Cxcl12	Cxcl16	Fcgr1	Ccl5
Cxcr4	Ddx58	Fcgr3	Ccr2
Icosl	Eomes	Gzmb	Ccr5
Il15	Fadd	Gzmk	Ccr7
Il1b	Gbp5	Gzmm	Cd1d1
Pdcd1lg2	H2-Aa	H2-D1	Cd69
Ptprc	H2-Ab1	H2-K1	Cklf
Ripk2	H60a	H2-M3	Cmklr1
Spp1	Ifi27	H2-T23	Crp
Tnfrsf13c	Ifi35	H60a	Csf1
Tnfsf13b	Ifi44	Il12a	Csf1r
Tnfsf14	Ifi44l	Il21	Csf2
Traf6	Ifih1	Il23a	Cx3cl1
Trp53	Ifit1	Il7r	Cx3cr1
	Ifit2	Klrb1c	Eng
	Ifit3	Klrk1	Fcer1a
	Ifitm1	Lag3	Fcer2a
	Ifitm2	Prf1	H60a
	Ifna1	Ptprc	Hc
	Ifna2	Pvr	Il13
	Ifna4	Pvrl2	Il17f
	Ifnar1	Sh2d1a	Il18
	Ifnar2	Sh2d1b1	Il1b
	Ifngr1	Stat5b	Il1rl1
	Ifnl2	Tap1	Il23a
	Il12rb2	Ulbp1	Il34
	Irf7	Xcl1	Il4
	Irf8		Il4ra
	Irgm2		Itgb3
	Mavs		Lbp
	Nlrc5		Msr1
	Nos2		Nfkbia
	Runx3		Pparg
	Sh2d1b1		Prkce
	Tbk1		Rora
	Tmem173		Saa1
	Ulbp1		Sbno2

			Syk
			Thbs1
			Tlr1
			Ulbp1
			Vegfa

Supplementary Table 5. Nanostring published gene sets for analysis in figures 4.4 and 4.5.

APPENDIX III: ADDITIONAL METHODS FOR CHAPTER V

Macrophage phagocytosis assays

EMT6-pBabe or EMT6-B7-H4+ cells were cultures in DMEM/F12 media with 10% FBS and 2ug/mL Puromycin to maintain B7-H4 expression. Bone marrow was collected from 8–12-week-old syngeneic (from BALB/c background) mice by flushing tibias and femurs with PBS and passing cells through a 70μM filter before plating cells for 24 hours. After 24 hours, cells were washed and ACK lysed before treatment with media containing M-CSF (20 ng/mL in RPMI with 10% FBS, 1% HEPES, 55μM β-mercaptoethanol) for 7 days. After differentiation, cells were detached and plated on low-attachment tissue culture plates in media containing either IFNy (50 ng/mL) or IL-4 (20 ng/mL) to polarize macrophages to M1 or M2 phenotypes.

EMT6 cancer cells ± B7-H4 were labeled with Cell Trace Far Red (Invitrogen) at 1:5000 dilution following the manufacturer protocol. Cancer cells were killed by freezing in liquid nitrogen for 60-90 seconds, leading to >90-95% cell death. Dead cancer cells were added to polarized macrophages at a ratio of 2:1 macrophages to cancer cells. Cells were incubated for 1, 4, or 24 hours and assessed by flow cytometry including DAPI stain for viability to measure macrophage phagocytosis using the following BioLegend antibodies: CD45 (#103132, 1:400), CD11b (#101215, 1:1000), and B7-H4 (#139405, 1:100).

T cell inhibition assays

For cancer-cell expressed B7-H4 assays, EMT6 cells ± B7-H4 were plated in 96-well plates at a density of 1,000 cells/well and allowed to attach overnight. CD3+, CD4+, or CD8+ T cells were isolated from BALB/c mouse splenocytes using the appropriate Miltenyi kit (130-095-130, 130-104-454, or 130-104-075), allowed to rest overnight, and plated at a density of 80,000-100,000 cells per well after Cell Trace labeling. T cells were stimulated with either CD3/CD28 Mouse T-Activator Dynabeads (ThermoFisher) or CD3 and CD28 antibodies (CD3: Invitrogen at 1ug/mL, CD28: Tonbo Biosciences at 0.5 ug/mL).

For protein inhibition assays, T cells were isolated as above, or whole splenocytes were plated at a density of 80,000 to 100,000 cells per well in a 96-well plate. B7-H4-Ig protein was either immobilized on the plate by coating at 37C for 2-3 hours or at 4C overnight before the cells were added. Cells were plated with CD3/CD28 (CD3: Invitrogen, CD28: Tonbo Biosciences) antibodies in RPMI media containing 10% FBS, 1% HEPES, 55 uM BME, and 10ng/mL IL-2.

For both experiments, the T cells were assessed by flow cytometry for cell proliferation by Cell Trace dilution after 48-72 hours and proliferation was compared between B7-H4+ and control wells.

TPR construct design

Sequences

The following gblock sequences were synthesized by Azenta and cloned into MSCV-Thy1.1-Dest retroviral vector using BglII and SalI restriction enzymes.

mB7-H4-CD3z gblock

BglII – Kozak – mB7-H4 – GS linker – CD3z cytoplasmic – STOP – SalI
GGGAGATCTGCCACC**ATG**GCTTCCTTGGGGCAGATCATCTTTTGGAGTATTATTAACATCA
TCATCATCCTGGCTGGGGCCATCGCACTCATCATTGGCTTTGGCATTTCAGGCAAGCACTT
CATCACGGTCACGACCTTCACCTCAGCTGGAAACATTGGAGAGGACGGGACCCTGAGCTG
CACTTTTGAACCTGACATCAAACTCAACGGCATCGTCATCCAGTGGCTGAAAGAAGGCATC
AAAGGTTTGGTCCACGAGTTCAAAGAAGGCAAAGACGACCTCTCACAGCAGCATGAGATG
TTCAGAGGCCGCACAGCAGTGTTTGCTGATCAGGTGGTAGTTGGCAATGCTTCCCTGAGA
CTGAAAAACGTGCAGCTCACGGATGCTGGCACCTACACATGTTACATCCGCACCTCAAAAG
GCAAAGGGAATGCAAACCTTGAGTATAAGACCGGAGCCTTCAGTATGCCAGAGATAAATGT
GGACTATAATGCCAGTTCAGAGAGTTTACGCTGCGAGGCTCCTCGGTGGTTCCCCCAGCC
CACAGTGGCCTGGGCATCTCAAGTTGACCAAGGAGCCAACTTCTCAGAAGTCTCCAACAC
CAGCTTTGAGTTGAACTCTGAGAATGTGACCATGAAGGTCGTATCTGTGCTCTACAATGTC
ACAATCAACAACACATACTCCTGTATGATTGAAAACGACATTGCCAAAGCCACCGGGGACA
TCAAAGTGACAGATTCAGAGGTCAAAAGGCGGAGTCAGCTGCAGTTGCTGAACTCTGGGC
CTTCCCCGTGTGTTTTTTCTTCTGCCTTTGTGGCTGGCTGGGCACTCCTATCTCTCTCCTGT
TGCCTGATGCTAAGAGGAGGAGGATCACGAGCTAAGTTCTCCCGCTCAGCAGAGACAGCC
GCTAATCTGCAGGACCCCAATCAACTCTATAATGAACTTAATCTCGGTAGACGAGAAGAGT
ACGATGTCCTCGAAAAAAAAAGAGCCCGCGATCCTGAGATGGGCGGTAAACAACAAAGAC
GGCGGAACCCCCAGGAAGGAGTGTATAATGCTCTTCAAAAGGATAAAATGGCTGAGGCCT
ATTCTGAAATAGGCACAAAGGGCGAACGGAGACGCGGCAAGGGGCATGACGGTCTGTATC
AGGGGCTCTCTACCGCCACAAAAGATACATATGACGCCTTGCACATGCAAACTCTCGCACC
AAGGTAGGTCGACGGG

mPD-L1-CD3z gblock

BglII – Kozak – mPD-L1 – GS linker – CD3z cytoplasmic – STOP – SalI

GGGAGATCTGCCACC**ATG**CGCATATTCGCAGGAATCATTTTCACTGCTTGTTGTCACTTGT
TGCGAGCTTTTACCATTACCGCCCCAAAAGACCTTTACGTTGTTGAATACGGGAGTAATGT
GACTATGGAGTGTCGGTTTCCCGTCGAGCGAGAACTGGATCTGCTCGCTCTCGTTGTGTA
CTGGGAAAAGGAAGACGAACAAGTCATACAGTTCGTCGCTGGGGAAGAAGACCTGAAGCC
ACAACATAGTAATTTCCGAGGGCGGGCCTCCCTTCCAAAAGATCAACTTTTGAAAGGCAAT
GCAGCCCTCCAAATAACAGACGTGAAGCTCCAGGACGCCGGAGTGTATTGCTGCATTATTA
GCTACGGCGGGGCTGACTATAAAAGAATCACCTTGAAAGTTAATGCACCCTATAGAAAAAT
TAATCAGCGAATAAGTGTTGACCCCGCAACTTCTGAGCATGAATTGATATGTCAGGCAGAA
GGGTACCCTGAGGCAGAGGTTATTTGGACCAACAGCGATCACCAGCCTGTGAGTGGTAAA
AGGTCTGTGACCACTTCCAGGACTGAGGGTATGCTCCTCAATGTAACAAGCTCACTGCGG
GTAAATGCAACTGCTAACGATGTTTTCTACTGTACTTTCTGGCGGAGCCAACCAGGCCAGA
ATCATACCGCTGAGCTTATAATACCTGAACTTCCCGCTACACATCCCCCCCAGAATCGGAC
TCATTGGGTACTCCTTGGTTCCATTCTTCTTTTCTTGATAGTTGTGAGTACAGTCTTGTTGTT
TCTCCGGAAGCAGGTCAGAATGCTGGATGTCGAGAAATGTGGAGTCGAGGACACATCATC
TAAGAACAGAAATGATACTCAATTCGAAGAGACCGGAGGAGGATCACGAGCTAAGTTCTCC
CGCTCAGCAGAGACAGCCGCTAATCTGCAGGACCCCAATCAACTCTATAATGAACTTAATC
TCGGTAGACGAGAAGAGTACGATGTCCTCGAAAAAAAAAGAGCCCGCGATCCTGAGATGG
GCGGTAAACAACAAAGACGGCGGAACCCCCAGGAAGGAGTGTATAATGCTCTTCAAAAGG
ATAAAATGGCTGAGGCCTATTCTGAAATAGGCACAAAGGGCGAACGGAGACGCGGCAAGG
GGCATGACGGTCTGTATCAGGGGCTCTCTACCGCCACAAAAGATACATATGACGCCTTGC
ACATGCAAACTCTCGCACCAAGGTAGGTCGACGGG

REFERENCES

1. Siegel RL, Miller KD, Wagle NS, Jemal A. Cancer statistics, 2023. *CA Cancer J Clin*. 2023;73(1):17-48. doi:10.3322/caac.21763

2. Prat A, Perou CM. Deconstructing the molecular portraits of breast cancer. *Mol Oncol*. 2011;5(1):5-23. doi:10.1016/j.molonc.2010.11.003

3. Perou CM, Sørlie T, Eisen MB, et al. Molecular portraits of human breast tumours. *Nature*. 2000;406(6797):747-752. doi:10.1038/35021093

4. Koboldt DC, Fulton RS, McLellan MD, et al. Comprehensive molecular portraits of human breast tumours. *Nature*. 2012;490(7418):61-70. doi:10.1038/nature11412

5. Sarvari P, Sarvari P, Ramírez-Díaz I, Mahjoubi F, Rubio K. Advances of Epigenetic Biomarkers and Epigenome Editing for Early Diagnosis in Breast Cancer. *Int J Mol Sci*. 2022;23(17):9521. doi:10.3390/ijms23179521

6. Lee YM, Oh MH, Go JH, Han K, Choi SY. Molecular subtypes of triple-negative breast cancer: understanding of subtype categories and clinical implication. *Genes Genomics*. 2020;42(12):1381-1387. doi:10.1007/s13258-020-01014-7

7. Slamon D, Clark G, Wong S, Levin W, Ullrich A, McGuire W. Human breast cancer: correlation of relapse and survival with amplification of the HER-2/neu oncogene. *Science*. 1987;235(4785):177-182. doi:10.1126/science.3798106

8. Lehmann BD, Bauer JA, Chen X, et al. Identification of human triple-negative breast cancer subtypes and preclinical models for selection of targeted therapies. *J Clin Invest*. 2011;121(7):2750-2767. doi:10.1172/JCI45014

9. Balko JM, Giltnane JM, Wang K, et al. Molecular Profiling of the Residual Disease of Triple-Negative Breast Cancers after Neoadjuvant Chemotherapy Identifies Actionable Therapeutic Targets. *Cancer Discov*. 2014;4(2):232-245. doi:10.1158/2159-8290.CD-13-0286

10. Rakha EA, Reis-Filho JS, Ellis IO. Basal-Like Breast Cancer: A Critical Review. *J Clin Oncol*. 2008;26(15):2568-2581. doi:10.1200/JCO.2007.13.1748

11. Ali S, Coombes RC. Estrogen Receptor Alpha in Human Breast Cancer: Occurrence and Significance. *J Mammary Gland Biol Neoplasia*. 2000;5(3):271-281. doi:10.1023/A:1009594727358

12. Yarden Y, Sliwkowski MX. Untangling the ErbB signalling network. *Nat Rev Mol Cell Biol*. 2001;2(2):127-137. doi:10.1038/35052073

13. Turner NC, Reis-Filho JS. Basal-like breast cancer and the BRCA1 phenotype. *Oncogene*. 2006;25(43):5846-5853. doi:10.1038/sj.onc.1209876

14. Mersch J, Jackson MA, Park M, et al. Cancers associated with BRCA1 and BRCA2 mutations other than breast and ovarian. *Cancer*. 2015;121(2):269-275. doi:10.1002/cncr.29041

15. Harbeck N, Penault-Llorca F, Cortes J, et al. Breast cancer. *Nat Rev Dis Primer*. 2019;5(1):1-31. doi:10.1038/s41572-019-0111-2

16. Genetics of Breast and Gynecologic Cancers (PDQ®) - NCI. Published December 22, 2023. Accessed January 30, 2024. https://www.cancer.gov/types/breast/hp/breast-ovarian-genetics-pdq

17. Chen DS, Mellman I. Oncology Meets Immunology: The Cancer-Immunity Cycle. *Immunity*. 2013;39(1):1-10. doi:10.1016/j.immuni.2013.07.012

18. Denkert C, von Minckwitz G, Darb-Esfahani S, et al. Tumour-infiltrating lymphocytes and prognosis in different subtypes of breast cancer: a pooled analysis of 3771 patients treated with neoadjuvant therapy. *Lancet Oncol*. 2018;19(1):40-50. doi:10.1016/S1470-2045(17)30904-X

19. Adams S, Gray RJ, Demaria S, et al. Prognostic Value of Tumor-Infiltrating Lymphocytes in Triple-Negative Breast Cancers From Two Phase III Randomized Adjuvant Breast Cancer Trials: ECOG 2197 and ECOG 1199. *J Clin Oncol*. 2014;32(27):2959-2966. doi:10.1200/JCO.2013.55.0491

20. Loi S, Michiels S, Salgado R, et al. Tumor infiltrating lymphocytes are prognostic in triple negative breast cancer and predictive for trastuzumab benefit in early breast cancer: results from the FinHER trial. *Ann Oncol*. 2014;25(8):1544-1550. doi:10.1093/annonc/mdu112

21. Loi S, Sirtaine N, Piette F, et al. Prognostic and Predictive Value of Tumor-Infiltrating Lymphocytes in a Phase III Randomized Adjuvant Breast Cancer Trial in Node-Positive Breast Cancer Comparing the Addition of Docetaxel to Doxorubicin With Doxorubicin-Based Chemotherapy: BIG 02-98. *J Clin Oncol*. 2013;31(7):860-867. doi:10.1200/JCO.2011.41.0902

22. El Bairi K, Haynes HR, Blackley E, et al. The tale of TILs in breast cancer: A report from The International Immuno-Oncology Biomarker Working Group. *Npj Breast Cancer*. 2021;7(1):1-17. doi:10.1038/s41523-021-00346-1

23. Valenza C, Taurelli Salimbeni B, Santoro C, Trapani D, Antonarelli G, Curigliano G. Tumor Infiltrating Lymphocytes across Breast Cancer Subtypes: Current Issues for Biomarker Assessment. *Cancers*. 2023;15(3):767. doi:10.3390/cancers15030767

24. Emens LA, Molinero L, Loi S, et al. Atezolizumab and nab-Paclitaxel in Advanced Triple-Negative Breast Cancer: Biomarker Evaluation of the IMpassion130 Study. *JNCI J Natl Cancer Inst*. 2021;113(8):1005-1016. doi:10.1093/jnci/djab004

25. Gaynor N, Crown J, Collins DM. Immune checkpoint inhibitors: Key trials and an emerging role in breast cancer. *Semin Cancer Biol*. 2022;79:44-57. doi:10.1016/j.semcancer.2020.06.016

26. Sharma P, Allison JP. Immune Checkpoint Targeting in Cancer Therapy: Toward Combination Strategies with Curative Potential. *Cell*. 2015;161(2):205-214. doi:10.1016/j.cell.2015.03.030

27. Disis ML, Stanton SE. Immunotherapy in breast cancer: An introduction. *The Breast*. 2018;37:196-199. doi:10.1016/j.breast.2017.01.013

28. Planes-Laine G, Rochigneux P, Bertucci F, et al. PD-1/PD-L1 Targeting in Breast Cancer: The First Clinical Evidences are Emerging—A Literature Review. *Cancers*. 2019;11(7):1033. doi:10.3390/cancers11071033

29. Sadreddini S, Baradaran B, Aghebati-Maleki A, et al. Immune checkpoint blockade opens a new way to cancer immunotherapy. *J Cell Physiol*. 2019;234(6):8541-8549. doi:10.1002/jcp.27816

30. Pardoll DM. The blockade of immune checkpoints in cancer immunotherapy. *Nat Rev Cancer*. 2012;12(4):252-264. doi:10.1038/nrc3239

31. Ribas A, Wolchok JD. Cancer immunotherapy using checkpoint blockade. *Science*. 2018;359(6382):1350-1355. doi:10.1126/science.aar4060

32. Schmid P, Cortes J, Dent R, et al. Event-free Survival with Pembrolizumab in Early Triple-Negative Breast Cancer. *N Engl J Med*. 2022;386(6):556-567. doi:10.1056/NEJMoa2112651

33. Robert C. A decade of immune-checkpoint inhibitors in cancer therapy. *Nat Commun*. 2020;11(1):3801. doi:10.1038/s41467-020-17670-y

34. Siegel RL, Miller KD, Fuchs HE, Jemal A. Cancer Statistics, 2021. *CA Cancer J Clin*. 2021;71(1):7-33. doi:10.3322/caac.21654

35. Loibl S, Poortmans P, Morrow M, Denkert C, Curigliano G. Breast cancer. *The Lancet*. 2021;397(10286):1750-1769. doi:10.1016/S0140-6736(20)32381-3

36. Schmid P, Adams S, Rugo HS, et al. Atezolizumab and Nab-Paclitaxel in Advanced Triple-Negative Breast Cancer. *N Engl J Med*. 2018;379(22):2108-2121. doi:10.1056/NEJMoa1809615

37. Schmid P, Cortes J, Pusztai L, et al. Pembrolizumab for Early Triple-Negative Breast Cancer. *N Engl J Med*. 2020;382(9):810-821. doi:10.1056/NEJMoa1910549

38. O'Meara TA, Tolaney SM. Tumor mutational burden as a predictor of immunotherapy response in breast cancer. *Oncotarget*. 2021;12(5):394-400. doi:10.18632/oncotarget.27877

39. Tarantino P, Corti C, Schmid P, et al. Immunotherapy for early triple negative breast cancer: research agenda for the next decade. *Npj Breast Cancer*. 2022;8(1):1-7. doi:10.1038/s41523-022-00386-1

40. Stanton SE, Adams S, Disis ML. Variation in the Incidence and Magnitude of Tumor-Infiltrating Lymphocytes in Breast Cancer Subtypes: A Systematic Review. *JAMA Oncol*. 2016;2(10):1354-1360. doi:10.1001/jamaoncol.2016.1061

41. Mittendorf EA, Zhang H, Barrios CH, et al. Neoadjuvant atezolizumab in combination with sequential nab-paclitaxel and anthracycline-based chemotherapy versus placebo and chemotherapy in patients with early-stage triple-negative breast cancer (IMpassion031): a

randomised, double-blind, phase 3 trial. *The Lancet*. 2020;396(10257):1090-1100. doi:10.1016/S0140-6736(20)31953-X

42. Schmid P, Rugo HS, Adams S, et al. Atezolizumab plus nab-paclitaxel as first-line treatment for unresectable, locally advanced or metastatic triple-negative breast cancer (IMpassion130): updated efficacy results from a randomised, double-blind, placebo-controlled, phase 3 trial. *Lancet Oncol*. 2020;21(1):44-59. doi:10.1016/S1470-2045(19)30689-8

43. Nanda R, Liu MC, Yau C, et al. Effect of Pembrolizumab Plus Neoadjuvant Chemotherapy on Pathologic Complete Response in Women With Early-Stage Breast Cancer: An Analysis of the Ongoing Phase 2 Adaptively Randomized I-SPY2 Trial. *JAMA Oncol*. Published online February 13, 2020. doi:10.1001/jamaoncol.2019.6650

44. Cortes J, Cescon DW, Rugo HS, et al. Pembrolizumab plus chemotherapy versus placebo plus chemotherapy for previously untreated locally recurrent inoperable or metastatic triple-negative breast cancer (KEYNOTE-355): a randomised, placebo-controlled, double-blind, phase 3 clinical trial. *The Lancet*. 2020;396(10265):1817-1828. doi:10.1016/S0140-6736(20)32531-9

45. Lander EM, Lehmann BD, Shah PD, et al. A phase II trial of atezolizumab (anti-PD-L1) with carboplatin in patients with metastatic triple-negative breast cancer (mTNBC). *J Clin Oncol*. 2020;38(15_suppl):TPS1112-TPS1112. doi:10.1200/JCO.2020.38.15_suppl.TPS1112

46. Ademuyiwa FO, Gao F, Street CR, et al. A randomized phase 2 study of neoadjuvant carboplatin and paclitaxel with or without atezolizumab in triple negative breast cancer (TNBC) - NCI 10013. *NPJ Breast Cancer*. 2022;8:134. doi:10.1038/s41523-022-00500-3

47. James JL, Balko JM. Biomarker Predictors for Immunotherapy Benefit in Breast: Beyond PD-L1. *Curr Breast Cancer Rep*. 2019;11(4):217-227. doi:10.1007/s12609-019-00331-5

48. Dong P, Xiong Y, Yue J, Hanley SJB, Watari H. B7H3 As a Promoter of Metastasis and Promising Therapeutic Target. *Front Oncol*. 2018;8. Accessed February 19, 2024. https://www.frontiersin.org/journals/oncology/articles/10.3389/fonc.2018.00264

49. Jiang Y, Liu J, Chen L, Qian Z, Zhang Y. A promising target for breast cancer: B7-H3. *BMC Cancer*. 2024;24(1):182. doi:10.1186/s12885-024-11933-3

50. Sica GL, Choi IH, Zhu G, et al. B7-H4, a Molecule of the B7 Family, Negatively Regulates T Cell Immunity. *Immunity*. 2003;18(6):849-861. doi:10.1016/S1074-7613(03)00152-3

51. Zang X, Loke P, Kim J, Murphy K, Waitz R, Allison JP. B7x: A widely expressed B7 family member that inhibits T cell activation. *Proc Natl Acad Sci*. 2003;100(18):10388-10392. doi:10.1073/pnas.1434299100

52. Podojil JR, Miller SD. Potential targeting of B7-H4 for the treatment of cancer. *Immunol Rev*. 2017;276(1):40-51. doi:10.1111/imr.12530

53. Salceda S, Tang T, Kmet M, et al. The immunomodulatory protein B7-H4 is overexpressed in breast and ovarian cancers and promotes epithelial cell transformation. *Exp Cell Res*. 2005;306(1):128-141. doi:10.1016/j.yexcr.2005.01.018

54. Wang L, Rubinstein R, Lines JL, et al. VISTA, a novel mouse Ig superfamily ligand that negatively regulates T cell responses. *J Exp Med*. 2011;208(3):577-592. doi:10.1084/jem.20100619

55. Ni L, Dong C. New B7 Family Checkpoints in Human Cancers. *Mol Cancer Ther*. 2017;16(7):1203-1211. doi:10.1158/1535-7163.MCT-16-0761

56. Kobayashi Y, Lim SO, Yamaguchi H. Oncogenic signaling pathways associated with immune evasion and resistance to immune checkpoint inhibitors in cancer. *Semin Cancer Biol*. 2020;65:51-64. doi:10.1016/j.semcancer.2019.11.011

57. Kim NI, Park MH, Kweon SS, Lee JS. B7-H3 and B7-H4 Expression in Breast Cancer and Their Association with Clinicopathological Variables and T Cell Infiltration. *Pathobiology*. Published online February 21, 2020:1-14. doi:10.1159/000505756

58. Wang JY, Wang WP. B7-H4, a promising target for immunotherapy. *Cell Immunol*. 2020;347:104008. doi:10.1016/j.cellimm.2019.104008

59. Altan M, Kidwell KM, Pelekanou V, et al. Association of B7-H4, PD-L1, and tumor infiltrating lymphocytes with outcomes in breast cancer. *Npj Breast Cancer*. 2018;4(1):40. doi:10.1038/s41523-018-0095-1

60. Choi IH, Zhu G, Sica GL, et al. Genomic Organization and Expression Analysis of B7-H4, an Immune Inhibitory Molecule of the B7 Family. *J Immunol*. 2003;171(9):4650-4654. doi:10.4049/jimmunol.171.9.4650

61. Gruosso T, Gigoux M, Manem VSK, et al. Spatially distinct tumor immune microenvironments stratify triple-negative breast cancers. *J Clin Invest*. 2019;129(4):1785-1800. doi:10.1172/JCI96313

62. Prasad DVR, Richards S, Mai XM, Dong C. B7S1, a Novel B7 Family Member that Negatively Regulates T Cell Activation. *Immunity*. 2003;18(6):863-873. doi:10.1016/S1074-7613(03)00147-X

63. Wang L, Yang C, Liu X bo, Wang L, Kang F biao. B7-H4 overexpression contributes to poor prognosis and drug-resistance in triple-negative breast cancer. *Cancer Cell Int*. 2018;18(1):100. doi:10.1186/s12935-018-0597-9

64. Escors D, Gato-Cañas M, Zuazo M, et al. The intracellular signalosome of PD-L1 in cancer cells. *Signal Transduct Target Ther*. 2018;3(1):26. doi:10.1038/s41392-018-0022-9

65. Zhou L, Ruan M, Liu Y, et al. B7H4 expression in tumor cells impairs CD8 T cell responses and tumor immunity. *Cancer Immunol Immunother*. 2020;69(2):163-174. doi:10.1007/s00262-019-02451-4

66. MacGregor HL, Ohashi PS. Molecular Pathways: Evaluating the Potential for B7-H4 as an Immunoregulatory Target. *Clin Cancer Res*. 2017;23(12):2934-2941. doi:10.1158/1078-0432.CCR-15-2440

67. Song X, Zhou Z, Li H, et al. Pharmacological suppression of B7-H4 glycosylation restores antitumor immunity in immune-cold breast cancers. *Cancer Discov*. Published online January 1, 2020. doi:10.1158/2159-8290.CD-20-0402

68. Sousa LG, McGrail DJ, Lazar Neto F, et al. Spatial Immunoprofiling of Adenoid Cystic Carcinoma Reveals B7-H4 Is a Therapeutic Target for Aggressive Tumors. *Clin Cancer Res*. 2023;29(16):3162-3171. doi:10.1158/1078-0432.CCR-23-0514

69. Wimberly H, Brown JR, Schalper K, et al. PD-L1 Expression Correlates with Tumor-Infiltrating Lymphocytes and Response to Neoadjuvant Chemotherapy in Breast Cancer. *Cancer Immunol Res*. 2015;3(4):326-332. doi:10.1158/2326-6066.CIR-14-0133

70. Ali HR, Glont SE, Blows FM, et al. PD-L1 protein expression in breast cancer is rare, enriched in basal-like tumours and associated with infiltrating lymphocytes. *Ann Oncol*. 2015;26(7):1488-1493. doi:10.1093/annonc/mdv192

71. Schalper KA, Velcheti V, Carvajal D, et al. In Situ Tumor PD-L1 mRNA Expression Is Associated with Increased TILs and Better Outcome in Breast Carcinomas. *Clin Cancer Res*. 2014;20(10):2773-2782. doi:10.1158/1078-0432.CCR-13-2702

72. Lehmann BD, Abramson VG, Dees EC, et al. Atezolizumab in Combination With Carboplatin and Survival Outcomes in Patients With Metastatic Triple-Negative Breast Cancer: The TBCRC 043 Phase 2 Randomized Clinical Trial. *JAMA Oncol*. Published online December 14, 2023. doi:10.1001/jamaoncol.2023.5424

73. Morgenstern JP, Land H. Advanced mammalian gene transfer: high titre retroviral vectors with multiple drug selection markers and a complementary helper-free packaging cell line. *Nucleic Acids Res*. 1990;18(12):3587-3596.

74. Bankhead P, Loughrey MB, Fernández JA, et al. QuPath: Open source software for digital pathology image analysis. *Sci Rep*. 2017;7(1):16878. doi:10.1038/s41598-017-17204-5

75. Wolf DM, Yau C, Wulfkuhle J, et al. Redefining breast cancer subtypes to guide treatment prioritization and maximize response: Predictive biomarkers across 10 cancer therapies. *Cancer Cell*. 2022;40(6):609-623.e6. doi:10.1016/j.ccell.2022.05.005

76. Paweletz CP, Charboneau L, Bichsel VE, et al. Reverse phase protein microarrays which capture disease progression show activation of pro-survival pathways at the cancer invasion front. *Oncogene*. 2001;20(16):1981-1989. doi:10.1038/sj.onc.1204265

77. Abu-Khalaf MM, Alex Hodge K, Hatzis C, et al. AKT/mTOR signaling modulates resistance to endocrine therapy and CDK4/6 inhibition in metastatic breast cancers. *Npj Precis Oncol*. 2023;7(1):1-12. doi:10.1038/s41698-023-00360-5

78. Cortes J, Rugo HS, Cescon DW, et al. Pembrolizumab plus Chemotherapy in Advanced Triple-Negative Breast Cancer. *N Engl J Med*. 2022;387(3):217-226. doi:10.1056/NEJMoa2202809

79. Emens LA, Adams S, Barrios CH, et al. First-line atezolizumab plus nab-paclitaxel for unresectable, locally advanced, or metastatic triple-negative breast cancer: IMpassion130

final overall survival analysis. *Ann Oncol*. 2021;32(8):983-993. doi:10.1016/j.annonc.2021.05.355

80. Emens LA, Goldstein LD, Schmid P, et al. The tumor microenvironment (TME) and atezolizumab + nab-paclitaxel (A+nP) activity in metastatic triple-negative breast cancer (mTNBC): IMpassion130. *J Clin Oncol*. 2021;39(15_suppl):1006-1006. doi:10.1200/JCO.2021.39.15_suppl.1006

81. Sørlie T. Molecular portraits of breast cancer: tumour subtypes as distinct disease entities. *Eur J Cancer*. 2004;40(18):2667-2675. doi:10.1016/j.ejca.2004.08.021

82. Elenbaas B, Spirio L, Koerner F, et al. Human breast cancer cells generated by oncogenic transformation of primary mammary epithelial cells. *Genes Dev*. 2001;15(1):50-65. doi:10.1101/gad.828901

83. Dongre A, Weinberg RA. New insights into the mechanisms of epithelial–mesenchymal transition and implications for cancer. *Nat Rev Mol Cell Biol*. 2019;20(2):69-84. doi:10.1038/s41580-018-0080-4

84. Dongre A, Rashidian M, Eaton EN, et al. Direct and Indirect Regulators of Epithelial–Mesenchymal Transition–Mediated Immunosuppression in Breast Carcinomas. *Cancer Discov*. 2021;11(5):1286-1305. doi:10.1158/2159-8290.CD-20-0603

85. Dongre A, Rashidian M, Reinhardt F, et al. Epithelial-to-Mesenchymal Transition Contributes to Immunosuppression in Breast Carcinomas. *Cancer Res*. 2017;77(15):3982-3989. doi:10.1158/0008-5472.CAN-16-3292

86. Koliaraki V, Prados A, Armaka M, Kollias G. The mesenchymal context in inflammation, immunity and cancer. *Nat Immunol*. Published online August 3, 2020:1-9. doi:10.1038/s41590-020-0741-2

87. Lamouille S, Xu J, Derynck R. Molecular mechanisms of epithelial–mesenchymal transition. *Nat Rev Mol Cell Biol*. 2014;15(3):178-196. doi:10.1038/nrm3758

88. Zeisberg M, Neilson EG. Biomarkers for epithelial-mesenchymal transitions. *J Clin Invest*. 2009;119(6):1429-1437. doi:10.1172/JCI36183

89. Ye X, Weinberg RA. Epithelial–Mesenchymal Plasticity: A Central Regulator of Cancer Progression. *Trends Cell Biol*. 2015;25(11):675-686. doi:10.1016/j.tcb.2015.07.012

90. Kalluri R, Weinberg RA. The basics of epithelial-mesenchymal transition. *J Clin Invest*. 2009;119(6):1420-1428. doi:10.1172/JCI39104

91. Lv W, He X, Wang Y, et al. A novel immune score model predicting the prognosis and immunotherapy response of breast cancer. *Sci Rep*. 2023;13(1):6403. doi:10.1038/s41598-023-31153-2

92. Lv Y, Lv D, Lv X, Xing P, Zhang J, Zhang Y. Immune Cell Infiltration-Based Characterization of Triple-Negative Breast Cancer Predicts Prognosis and Chemotherapy Response Markers. *Front Genet*. 2021;12. Accessed February 26, 2024. https://www.frontiersin.org/journals/genetics/articles/10.3389/fgene.2021.616469

93. Stanton SE, Disis ML. Clinical significance of tumor-infiltrating lymphocytes in breast cancer. *J Immunother Cancer*. 2016;4(1):59. doi:10.1186/s40425-016-0165-6

94. Salgado R, Denkert C, Demaria S, et al. The evaluation of tumor-infiltrating lymphocytes (TILs) in breast cancer: recommendations by an International TILs Working Group 2014. *Ann Oncol*. 2015;26(2):259-271. doi:10.1093/annonc/mdu450

95. Mugler KC, Singh M, Tringler B, et al. B7-H4 Expression in a Range of Breast Pathology: Correlation With Tumor T-cell Infiltration: *Appl Immunohistochem Mol Morphol*. 2007;15(4):363-370. doi:10.1097/01.pai.0000213159.79557.71

96. Cerami E, Gao J, Dogrusoz U, et al. The cBio Cancer Genomics Portal: An Open Platform for Exploring Multidimensional Cancer Genomics Data. *Cancer Discov*. 2012;2(5):401-404. doi:10.1158/2159-8290.CD-12-0095

97. Gao J, Aksoy BA, Dogrusoz U, et al. Integrative analysis of complex cancer genomics and clinical profiles using the cBioPortal. *Sci Signal*. 2013;6(269):pl1. doi:10.1126/scisignal.2004088

98. Guy CT, Webster MA, Schaller M, Parsons TJ, Cardiff RD, Muller WJ. Expression of the neu protooncogene in the mammary epithelium of transgenic mice induces metastatic disease. *Proc Natl Acad Sci*. 1992;89(22):10578-10582. doi:10.1073/pnas.89.22.10578

99. Muller WJ, Arteaga CL, Muthuswamy SK, et al. Synergistic interaction of the Neu proto-oncogene product and transforming growth factor alpha in the mammary epithelium of transgenic mice. *Mol Cell Biol*. 1996;16(10):5726-5736. doi:10.1128/MCB.16.10.5726

100. Ursini-Siegel J, Hardy WR, Zuo D, et al. ShcA signalling is essential for tumour progression in mouse models of human breast cancer. *EMBO J*. 2008;27(6):910-920. doi:10.1038/emboj.2008.22

101. Creedon H, Balderstone LA, Muir M, et al. Use of a genetically engineered mouse model as a preclinical tool for HER2 breast cancer. *Dis Model Mech*. 2016;9(2):131-140. doi:10.1242/dmm.023143

102. Nanda R, Liu MC, Yau C, et al. Effect of Pembrolizumab Plus Neoadjuvant Chemotherapy on Pathologic Complete Response in Women With Early-Stage Breast Cancer: An Analysis of the Ongoing Phase 2 Adaptively Randomized I-SPY2 Trial. *JAMA Oncol*. 2020;6(5):676-684. doi:10.1001/jamaoncol.2019.6650

103. Taylor BC, Sun X, Gonzalez-Ericsson PI, et al. NKG2A is a Therapeutic Vulnerability in Immunotherapy Resistant MHC-I Heterogeneous Triple Negative Breast Cancer. *Cancer Discov*. Published online October 4, 2023. doi:10.1158/2159-8290.CD-23-0519

104. Yao Y, Ye H, Qi Z, et al. B7-H4(B7x)–Mediated Cross-talk between Glioma-Initiating Cells and Macrophages via the IL6/JAK/STAT3 Pathway Lead to Poor Prognosis in Glioma Patients. *Clin Cancer Res*. 2016;22(11):2778-2790. doi:10.1158/1078-0432.CCR-15-0858

105. Kryczek I, Zou L, Rodriguez P, et al. B7-H4 expression identifies a novel suppressive macrophage population in human ovarian carcinoma. *J Exp Med*. 2006;203(4):871-881. doi:10.1084/jem.20050930

106. Cao Q, Wang Y, Zheng D, et al. IL-10/TGF-β–Modified Macrophages Induce Regulatory T Cells and Protect against Adriamycin Nephrosis. *J Am Soc Nephrol JASN*. 2010;21(6):933-942. doi:10.1681/ASN.2009060592

107. Kryczek I, Wei S, Zhu G, et al. Relationship between B7-H4, Regulatory T Cells, and Patient Outcome in Human Ovarian Carcinoma. *Cancer Res*. 2007;67(18):8900-8905. doi:10.1158/0008-5472.CAN-07-1866

108. Kinneer K, Wortmann P, Cooper ZA, et al. Design and Preclinical Evaluation of a Novel B7-H4–Directed Antibody–Drug Conjugate, AZD8205, Alone and in Combination with the PARP1-Selective Inhibitor AZD5305. *Clin Cancer Res*. 2023;29(6):1086-1101. doi:10.1158/1078-0432.CCR-22-2630

109. Liu Y, John P, Nishitani K, et al. A SOX9-B7x axis safeguards dedifferentiated tumor cells from immune surveillance to drive breast cancer progression. *Dev Cell*. Published online November 13, 2023. doi:10.1016/j.devcel.2023.10.010

110. Toader D, Fessler SP, Collins SD, et al. Discovery and Preclinical Characterization of XMT-1660, an Optimized B7-H4-Targeted Antibody-Drug Conjugate for the Treatment of Cancer. *Mol Cancer Ther*. Published online June 9, 2023:MCT-22-0786. doi:10.1158/1535-7163.MCT-22-0786

111. Tringler B, Zhuo S, Pilkington G, et al. B7-H4 Is Highly Expressed in Ductal and Lobular Breast Cancer. *Clin Cancer Res*. 2005;11(5):1842-1848. doi:10.1158/1078-0432.CCR-04-1658

112. Leung J, Suh WK. Host B7-H4 Regulates Antitumor T Cell Responses through Inhibition of Myeloid-Derived Suppressor Cells in a 4T1 Tumor Transplantation Model. *J Immunol*. 2013;190(12):6651-6661. doi:10.4049/jimmunol.1201242

113. Abadi YM, Jeon H, Ohaegbulam KC, et al. Host B7x Promotes Pulmonary Metastasis of Breast Cancer. *J Immunol*. 2013;190(7):3806-3814. doi:10.4049/jimmunol.1202439

114. Mandai M, Hamanishi J, Abiko K, Matsumura N, Baba T, Konishi I. Dual Faces of IFNγ in Cancer Progression: A Role of PD-L1 Induction in the Determination of Pro- and Antitumor Immunity. *Clin Cancer Res*. 2016;22(10):2329-2334. doi:10.1158/1078-0432.CCR-16-0224

115. Yi M, Niu M, Xu L, Luo S, Wu K. Regulation of PD-L1 expression in the tumor microenvironment. *J Hematol OncolJ Hematol Oncol*. 2021;14(1):10. doi:10.1186/s13045-020-01027-5

116. Xu Y, Zhu S, Song M, et al. B7-H4 expression and its role in interleukin-2/interferon treatment of clear cell renal cell carcinoma. *Oncol Lett*. 2014;7(5):1474-1478. doi:10.3892/ol.2014.1961

117. Chen C, Qu QX, Shen Y, et al. Induced expression of B7-H4 on the surface of lung cancer cell by the tumor-associated macrophages: A potential mechanism of immune escape. *Cancer Lett*. 2012;317(1):99-105. doi:10.1016/j.canlet.2011.11.017

118. Pang MF, Georgoudaki AM, Lambut L, et al. TGF-β1-induced EMT promotes targeted migration of breast cancer cells through the lymphatic system by the activation of CCR7/CCL21-mediated chemotaxis. *Oncogene*. 2016;35(6):748-760. doi:10.1038/onc.2015.133

119. Hennessy BT, Smith DL, Ram PT, Lu Y, Mills GB. Exploiting the PI3K/AKT Pathway for Cancer Drug Discovery. *Nat Rev Drug Discov*. 2005;4(12):988-1004. doi:10.1038/nrd1902

120. Stemke-Hale K, Gonzalez-Angulo AM, Lluch A, et al. An Integrative Genomic and Proteomic Analysis of PIK3CA, PTEN, and AKT Mutations in Breast Cancer. *Cancer Res*. 2008;68(15):6084-6091. doi:10.1158/0008-5472.CAN-07-6854

121. Miller TW, Balko JM, Arteaga CL. Phosphatidylinositol 3-Kinase and Antiestrogen Resistance in Breast Cancer. *J Clin Oncol*. 2011;29(33):4452-4461. doi:10.1200/JCO.2010.34.4879

122. Baselga J. Targeting the Phosphoinositide-3 (PI3) Kinase Pathway in Breast Cancer. *The Oncologist*. 2011;16(S1):12-19. doi:10.1634/theoncologist.2011-S1-12

123. Shimoi T, Hamada A, Yamagishi M, et al. PIK3CA mutation profiling in patients with breast cancer, using a highly sensitive detection system. *Cancer Sci*. 2018;109(8):2558-2566. doi:10.1111/cas.13696

124. Razavi P, Chang MT, Xu G, et al. The Genomic Landscape of Endocrine-Resistant Advanced Breast Cancers. *Cancer Cell*. 2018;34(3):427-438.e6. doi:10.1016/j.ccell.2018.08.008

125. Miller TW, Hennessy BT, González-Angulo AM, et al. Hyperactivation of phosphatidylinositol-3 kinase promotes escape from hormone dependence in estrogen receptor–positive human breast cancer. *J Clin Invest*. 2010;120(7):2406-2413. doi:10.1172/JCI41680

126. Bullock KK, Shattuck-Brandt R, Scalise C, et al. Endogenous pAKT activity is associated with response to AKT inhibition alone and in combination with immune checkpoint inhibition in murine models of TNBC. *Cancer Lett*. 2024;586:216681. doi:10.1016/j.canlet.2024.216681

127. Hu H, Zhu J, Zhong Y, et al. PIK3CA mutation confers resistance to chemotherapy in triple-negative breast cancer by inhibiting apoptosis and activating the PI3K/AKT/mTOR signaling pathway. *Ann Transl Med*. 2021;9(5):410. doi:10.21037/atm-21-698

128. Schneider-Poetsch T, Ju J, Eyler DE, et al. Inhibition of Eukaryotic Translation Elongation by Cycloheximide and Lactimidomycin. *Nat Chem Biol*. 2010;6(3):209-217. doi:10.1038/nchembio.304

129. Buchanan BW, Lloyd ME, Engle SM, Rubenstein EM. Cycloheximide Chase Analysis of Protein Degradation in Saccharomyces cerevisiae. *J Vis Exp JoVE*. 2016;(110):53975. doi:10.3791/53975

130. Ohaegbulam KC, Liu W, Jeon H, Almo SC, Zang X. Tumor-expressed immune checkpoint B7x promotes cancer progression and antigen-specific CD8 T cell exhaustion

and suppressive innate immune cells. *Oncotarget*. 2017;8(47):82740-82753. doi:10.18632/oncotarget.21098

131. Dong L, Xie L, Li M, et al. Downregulation of B7-H4 suppresses tumor progression of hepatocellular carcinoma. *Sci Rep*. 2019;9(1):14854. doi:10.1038/s41598-019-51253-2

132. Xiao ZX, Zheng X, Hu L, Wang J, Olsen N, Zheng SG. Immunosuppressive Effect of B7-H4 Pathway in a Murine Systemic Lupus Erythematosus Model. *Front Immunol*. 2017;8. doi:10.3389/fimmu.2017.01765

133. Song X, Zhou Z, Li H, et al. Pharmacologic Suppression of B7-H4 Glycosylation Restores Antitumor Immunity in Immune-Cold Breast Cancers. *Cancer Discov*. 2020;10(12):1872-1893. doi:10.1158/2159-8290.CD-20-0402

134. Schlesinger PH, Doebber TW, Mandell BF, et al. Plasma clearance of glycoproteins with terminal mannose and N-acetylglucosamine by liver non-parenchymal cells. Studies with β-glucuronidase, N-acetyl-β-d-glucosaminidase, ribonuclease B and agalacto-orosomucoid. *Biochem J*. 1978;176(1):103-109. doi:10.1042/bj1760103

135. Harris N, Peters LL, Eicher EM, et al. The Exon-Intron Structure and Chromosomal Localization of the Mouse Macrophage Mannose Receptor Gene *Mrcl*: Identification of a Ricin-like Domain at the N-Terminus of the Receptor. *Biochem Biophys Res Commun*. 1994;198(2):682-692. doi:10.1006/bbrc.1994.1099

136. Orecchioni M, Ghosheh Y, Pramod AB, Ley K. Macrophage Polarization: Different Gene Signatures in M1(LPS+) vs. Classically and M2(LPS–) vs. Alternatively Activated Macrophages. *Front Immunol*. 2019;10. Accessed February 27, 2024. https://www.frontiersin.org/journals/immunology/articles/10.3389/fimmu.2019.01084

137. Viktoriia K, Polina V, Andrey E, Timur F, Gennady S. Biochemical and molecular inducers and modulators of M2 macrophage polarization in clinical perspective. *Int Immunopharmacol*. 2023;122:110583. doi:10.1016/j.intimp.2023.110583

138. Mantovani A, Allavena P, Marchesi F, Garlanda C. Macrophages as tools and targets in cancer therapy. *Nat Rev Drug Discov*. 2022;21(11):799-820. doi:10.1038/s41573-022-00520-5

139. Wang S, Wang J, Chen Z, et al. Targeting M2-like tumor-associated macrophages is a potential therapeutic approach to overcome antitumor drug resistance. *Npj Precis Oncol*. 2024;8(1):1-19. doi:10.1038/s41698-024-00522-z

140. Biswas SK, Mantovani A. Macrophage plasticity and interaction with lymphocyte subsets: cancer as a paradigm. *Nat Immunol*. 2010;11(10):889-896. doi:10.1038/ni.1937

141. Ruffell B, Coussens LM. Macrophages and Therapeutic Resistance in Cancer. *Cancer Cell*. 2015;27(4):462-472. doi:10.1016/j.ccell.2015.02.015

142. Chen S, Saeed AFUH, Liu Q, et al. Macrophages in immunoregulation and therapeutics. *Signal Transduct Target Ther*. 2023;8(1):1-35. doi:10.1038/s41392-023-01452-1

143. Wynn TA, Barron L, Thompson RW, et al. Quantitative Assessment of Macrophage Functions in Repair and Fibrosis. *Curr Protoc Immunol*. 2011;93(1):14.22.1-14.22.12. doi:10.1002/0471142735.im1422s93

144. Jutz S, Leitner J, Schmetterer K, et al. Assessment of costimulation and coinhibition in a triple parameter T cell reporter line: Simultaneous measurement of NF-κB, NFAT and AP-1. *J Immunol Methods*. 2016;430:10-20. doi:10.1016/j.jim.2016.01.007

145. Rosskopf S, Leitner J, Paster W, et al. A Jurkat 76 based triple parameter reporter system to evaluate TCR functions and adoptive T cell strategies. *Oncotarget*. 2018;9(25):17608-17619. doi:10.18632/oncotarget.24807

146. Schreeder DM, Cannon JP, Wu J, Li R, Shakhmatov MA, Davis RS. Cutting Edge: FcR-Like 6 Is an MHC Class II Receptor. *J Immunol*. 2010;185(1):23-27. doi:10.4049/jimmunol.1000832

147. Gitto SB, Whicker M, Davies G, et al. A B7-H4–Targeting Antibody–Drug Conjugate Shows Antitumor Activity in PARPi and Platinum-Resistant Cancers with B7-H4 Expression. *Clin Cancer Res*. Published online November 15, 2023:OF1-OF15. doi:10.1158/1078-0432.CCR-23-1079

148. Gray E, Ulrich M, Epp A, et al. SGN-B7H4V, an investigational vedotin ADC directed to the immune checkpoint ligand B7-H4, shows promising activity in preclinical models. *J Immunother Cancer*. 2023;11(10):e007572. doi:10.1136/jitc-2023-007572

149. Hamilton EP, Chaudhry A, Spira AI, et al. XMT-1660: A phase 1b trial of a B7-H4 targeted antibody drug conjugate (ADC) in breast, endometrial, and ovarian cancers. *J Clin Oncol*. 2023;41(16_suppl):TPS3154-TPS3154. doi:10.1200/JCO.2023.41.16_suppl.TPS3154

150. Wu J, Zhang J, Li H, et al. 381O First-in-human/phase I trial of HS-20089, a B7-H4 ADC, in patients with advanced solid tumors. *Ann Oncol*. 2023;34:S336. doi:10.1016/j.annonc.2023.09.558